Defective branched chain amino acid catabolism impairs exercise capacity and glucose homeostasis in the mouse

Lauren E Abell

A Dissertation

submitted in partial fulfillment of the

requirements for the degree of

Doctor of Philosophy

University of Washington

2019

Reading Committee:

Rong Tian, Chair

Daniel Raftery

Stephen Hauschka

Program Authorized to Offer Degree:

Pathology

©Copyright 2019
Lauren E Abell

University of Washington

Abstract

Defective branched chain amino acid catabolism impairs exercise capacity and glucose homeostasis in the mouse

Lauren E Abell

Chair of Supervisory Committee:

Professor Rong Tian

Department of Bioengineering

The branched-chain amino acids (BCAAs) leucine, isoleucine and valine, play a central role in substrate metabolism, energetics, and protein synthesis. Although BCAA supplementation is widely used to improve exercise capacity and physical fitness, elevated levels of the BCAAs have been implicated in the development of obesity and metabolic diseases, and the mechanisms governing these conflicting outcomes are still unknown. This work explored the effects of systemically elevated BCAA levels in a mouse model of defective BCAA catabolism (knockout [KO]) on exercise capacity and performance. We studied the impact of BCAAs on three factors of exercise metabolism; the role of BCAAs in regulating glucose and fatty acid utilization in skeletal muscle, the role of downstream intermediates on tricarboxylic acid (TCA) cycle flux during exercise, and the impact of elevated BCAAs on gluconeogenesis during exhaustive exercise.

We found that defective BCAA catabolism significantly decreased endurance exercise capacity in the mouse, and this impairment may be due to disruption of glucose homeostasis. Although elevated BCAAs did not significantly impact substrate utilization in the skeletal muscle, increasing glucose utilization in the skeletal muscle through activation of pyruvate dehudrogenase (PDH) caused a further decrease in exercise capacity in KO mice. Exhaustive

exercise and prolonged fasting caused a further elevation in systemic BCAA levels in KO mice, and caused a similar depletion in liver and skeletal muscle glycogen levels. Fasted KO mice were unable to increase their blood glucose levels from the glucogenic precursors pyruvate and glutamine, suggesting that elevated BCAAs suppress gluconeogenesis and impair whole body glucose homeostasis. However, elevating blood glucose levels in mice during exercise did not impact exercise performance. These results provide insights on the efficacy of BCAA supplementation on improved exercise performance, however, whether BCAA catabolism is an instigator or merely a symptom of impaired exercise performance, metabolic health, and weight management.

Table of Contents

List of abbreviations……..……..……ii
List of figures……..…..iv
Acknowledgements……..…v
Chapter 1. Introduction…….…….1
1.1. Introduction……..…1
1.2. Figures……..……....……11
1.1. References……....……14
Chapter 2. Defective BCAA catabolism impairs exercise capacity and glucose homeostasis in the mice……20
2.1. Introduction…….....20
2.2. Methods……..……22
2.3. Results……...……..26
2.4. Discussion……..……29
2.5. Figures……....……34
2.6. References……..……45
Chapter 3. Determining the role of elevated branched chain amino acids in the perfused heart using stable isotope tracing and gas chromatography mass spectrometry……...49
3.1. Introduction……..49
3.2. Methods……51
3.3. Results……..54
3.4. Discussion……56
3.5. Figures…….....……61
3.6. References……....…67
Chapter 4. Simultaneous analysis of major coenzymes of cellular redox reactions and energy using *ex vivo* ^{1}H NMR spectroscopy……70
4.1. Abstract……..……...…70
4.2. Introduction……..……71
4.3. Methods……72
4.4. Results and discussion……..……73
4.5. Figures……..…84
4.6.
References……....……..……91
CV and publications……..……94

List of Abbreviations

4EB-P1 - eukaryotic translation initiation factor 4E-binding protein 1

α-KG – alpha-ketoglutarate

ADP - adenosine diphosphate

AMP - adenosine monophosphate

ATP - adenosine triphosphate

BCAA - Branched chain amino acids

BCAT – Branched chain ketoacid dehydrogenase

BC-CoA - branched chain CoAs

BCKA – Branched chain keto acids

BCKDH - branched-chain ketoacid dehydrogenase

BDK - branched-chain ketoacid dehydrogenase kinase

BMRB - biological magnetic resonance data bank

D_2O - Deuterium oxide

DCA - dichloroacetate

DI – dionized

DQF-COSY - ^{1}H-^{1}H double quantum filtered correlation spectroscopy

EDP - end diastolic pressure

F1,6BPase - fructose 1,6-bisphosphatase

G6Pase - glucose 6-phosphatase

GCMS – gas chromatography mass spectrometry

HMDB - human metabolome database

IMTG - Intramuscular triglycerides

IR – ischemia reperfusion

KIC - α-ketoisocaproate (ketolucine)

KIV - α-ketoisovalerate (ketovaline)

KMV - α-keto-A-methylvalerate (ketoisoleucine)

KO – knock out

LCMS – liquid chromatography mass spectrometry

MPT1 - via mitochondrial pyruvate transporter

MS – mass spectrometry

MSUD – maple syrup urine disease

MTBSTFA - N-methy-N-tert-butyldimethylsilyl trifluoroacetamide

mTOR – mammalian target of rapamycin

NAD - nicotinamide adenine dinucleotide, oxidized

NADH - nicotinamide adenine dinucleotide, reduced

NADP - nicotinamide adenine dinucleotide phosphate, oxidized

NADPH - nicotinamide adenine dinucleotide phosphate, reduced

NaH_2PO_4 - monosodium phosphate

NAMPT - nicotinamide phosphoribosyltransferase

NMR – nuclear magnetic resonance

OAA - oxaloacetate

PBS – phosphate buffered saline

PC - pyruvate carboxylation

PDH – pyruvate dehydrogenase

PEPCK – phosphoenolpyruvate carboxykinase

PP2Cm – mitochondrial protein phosphatase 2C

RER – respiratory exchange ratio

SIT – stable isotope tracer

SPF - specific pathogen free

T2D – type II diabetes

TCA – tricarboxylic acid

TCOSY - ^{1}H-^{1}H total correlation spectroscopy

TSP - 3-(trimethylsilyl)propionic acid-2,2,3,3-d_4

WT – wild type

List of Figures

Figure 1.1 The BCAA catabolic pathway

Figure 1.2 Interaction of liver and skeletal muscle BCAA catabolism

Figure 1.3 The gluconeogenesis pathway

Figure 2.1 Treadmill testing scheme

Figure 2.2 The PP2Cm-KO mouse has reduced endurance exercise capacity

Figure 2.3 Chronic accumulation of BCAAs has no effect on anaplerosis in skeletal muscle

Figure 2.4 Chronic accumulation of BCAAs has no effect on substrate utilization in skeletal muscle

Figure 2.5 Activation of PDH decreases exercise capacity in the $PP2Cm^{-/-}$

Figure 2.6 $PP2Cm^{-/-}$ mice have impaired liver glucose homeostasis

Figure 2.7 Blood glucose levels are not altered in the $PP2Cm^{-/-}$ mouse during exercise

Figure 3.1 Isolated heart perfusion protocol

Figure 3.2 Mass isotopomer positons

Figure 3.3 BCAA concentration in the perfusate directly alters BCAA concentration in the perfused heart

Figure 3.4 BCAAs deplete TCA cycle intermediate pool size

Figure 3.5 BCAAs alter the labeling pattern of TCA cycle intermediates from glucose

Figure 4.1 NMR spectrum of a mouse liver tissue

Figure 4.2. Characteristic annotated fingerprint regions of NMR spectra

Figure 4.3 Coenzyme levels are sensitive to tissue harvesting/extraction protocols

Figure 4.4 Absolute concentrations for ATP, ADP, AMP, NAD^+, NADH, $NADP^+$ and NADPH in heart tissue

Figure 4.5 NAD^+ and NADH peak intensity in WT, cKO, cNAMPT and cKO/cNAMPT mice

Acknowledgements

I am extremely grateful to my thesis advisor, Dr. Rong Tian, for her mentorship and guidance throughout my research. I would also like to thank my co-mentor, Dr. Dan Raftery, for his support and encouragement. I would like to thank our collaborators at the Northwest Metabolomics Center, Drs. Greg Barding and Haiwei Gu for their support with running the GCMS and LCMS experiments, as well as Dr. Nagana Gowda for running the NMR experiments. I am grateful to my committee members Drs. Chuck Murry and Stephen Hauschka. I would especially like to thank Drs Rong Tian, Dan Raftery and Stephen Hauschka for reading my dissertation. I am extremely thankful for my graduate cohort and all the supporting members of the Pathology Department, especially Drs. Jean Campbell and Bill Mahoney for their incredible mentorship and guidance. Finally, I am forever grateful to my wonderful family, Jim, Chris and Sarah, for all of their support and encouragement throughout this journey.

Chapter 1

1.1 Introduction

The branched-chain amino acids (BCAAs) leucine, isoleucine and valine are three of the nine essential amino acids and are defined by their branched carbon functional group. They account for ~35% of the indispensable amino acids in muscle protein and make up approximately 40% of the amino acids found in dietary protein[1]. Due to their high abundance in the diet BCAA deficiencies do not occur naturally, and mammalian cells have a tightly controlled enzymatic system for BCAA degradation. When this catabolism is disrupted (elevated systemic BCAAs), it can lead to metabolic disease, and some intermediates formed in their catabolism [such as the branched-chain keto acids (BCKA)] can be toxic at high concentrations[2]. The studies described in this thesis focus on the consequences of excessive intake and systemically elevated levels of the BCAAs and their impact on substrate utilization and metabolic homeostasis.

Regulation of BCAA Catabolism

The rate of protein turnover, BCAA catabolism, and BCAA intake are key mechanisms that govern BCAA homeostasis. The first, reversible step of catabolism is catalyzed by mitochondrial branched-chain aminotransferase (BCATm) and produces the branched chain α-ketoacids (BCKA). This transamination reaction is coupled with the conversion of alpha-ketoglutarate (α-KG) to glutamate. The three BCKAs (i.e. α-ketoisocaproate from leucine, α-ketoisovalerate from valine, and α-keto-A- methylvalerate from isoleucine) undergo irreversible decarboxylation by the branched-chain ketoacid dehydrogenase (BCKDH) complex[3]. BCKDH is the rate-limiting enzyme in the pathway and the main target for regulation of BCAA catabolism. This enzyme is activated by increased availability of leucine and valine, and allosterically inhibited by NADH and CoA esters derived from BCAA catabolism[1]. BCKDH is also inhibited by phosphorylation by BCKDH kinase (BDK), and activated by dephosphorylation via a mitochondrial localized 2C-type serine-threonine protein phosphatase (PP2Cm)[4]. Thereafter, the pathways resemble fatty acid oxidation yielding end products (acetyl-CoA from leucine, acetyl-CoA and

succinyl-CoA from isoleucine, and succinyl-CoA from valine) that can enter the tricarboxylic acid (TCA) cycle as anaplerotic substrates[1]. (Fig 1.1)

Genetic disorders of BCAA metabolism typically target the function of BCKDH and can have severe clinical consequences[5]. Traditionally, defective BCAA catabolism has been known in the context of Maple Syrup Urine Disease (MSUD). The disease is named from the presence of sweet-smelling urine, similar to maple syrup, when the patient is in metabolic crisis. MSUD is caused by an inherited deficiency in the BCKDH complex[6], which causes a buildup of the BCAAs and their downstream intermediates, the BCKAs. High levels of these metabolites are toxic to the brain, and accumulation can lead to severe neurological, respiratory and hepatic defects. If caught early, careful monitoring and strict diet control can manage the disease, but left untreated infants usually die within 7-10 days from central respiratory failure[7].

In contrast with other essential amino acids, which are oxidized primarily in the liver, the BCAAs largely bypass first pass of liver degradation due to a lack of hepatic BCATm[1]. This allows BCAA levels to increase in the circulation after consumption of a protein-containing meal[8]. Although a large number of tissues can oxidize the BCAAs, skeletal muscle, because of its size, is the principle site of BCAA catabolism[9]. Depending on the energy status of the skeletal muscle, BCAAs can either be used as building blocks in muscle protein synthesis, or undergo the first step of catabolism to form the BCKAs. The liver has extremely low levels of BCATm but expresses high levels of the second enzyme in the BCAA catabolic pathway, BCKDH, and the reverse is true in the skeletal muscle. BCATm expression is high in skeletal muscle, but at rest, the percentage of active BCKDH in the skeletal muscle is only 4-6% of the total BCKDH pool[3]. BCKAs generated in the skeletal muscle are secreted back into the blood and taken up by the liver to be catabolized into glucogenic and ketogenic precursors[1]. (Fig 1.2) This unique catabolism gives the BCAAs, particularly leucine, an important role in metabolic control and nutrient signaling.

The role of BCAA catabolism in exercise

Dietary BCAA supplementation has been shown to play a positive role in muscle hypertrophy, exercise capacity and prevention of fatigue[8,10]. Leucine is known to be a potent stimulator of protein synthesis in muscle cells, and consumption of dietary BCAAs before or immediately after an exercise bout significantly increases the rate of protein synthesis during exercise and reduces muscle breakdown during the recovery period compared to fasting individuals[2-3,11-12]. Supplementation with leucine has been shown to activate mammalian target of rapamycin (mTOR) activity as well as its downstream targets S6 kinase (S6K) and eukaryotic translation initiation factor 4E-binding protein 1 (4EB-P1)[13], that stimulate transcription initiation. Additionally, oral BCAA administration suppresses the rise in serum creatine kinase post-exercise, indicating that supplementation reduced the levels of muscle damage[11-12,14]. For this reason, high protein foods and BCAA supplements, especially whey, are popular in competitive sports and high intensity resistance training.

High levels of BCAAs also regulate oxidative metabolism by reducing utilization of glucose and increasing capacity for fatty acid oxidation[15]. Adequate dietary intake of BCAAs during exercise promotes fatty acid oxidation by increasing the release of fatty acids from adipocytes[16] and increasing cellular fatty acid uptake[17], while preserving lean muscle mass[12]. Muscle contraction increases the rate of BCAA catabolism in skeletal muscle[3], increasing the availability of downstream intermediates. 3-HIB, a downstream intermediate of valine catabolism, has been shown to directly stimulate fatty acid uptake in endothelial cells and leads to triglyceride accumulation in skeletal muscle[17]. BCAAs also promote mitochondrial biogenesis, which increases oxidative capacity resulting in improved muscle function, increased running capacity, and increased lifespan[8,18]. Rats fed BCAAs before exhaustive exercise had increased liver and gastrocnemius glycogen stores, and suppression of the pyruvate dehydrogenase (PDH) complex, suggesting that BCAA suppresses glucose utilization and oxidation in skeletal muscle[15]. Mice with systemic deletion of PP2Cm (PP2Cm-KO) had reduced PDH activity in the heart and

demonstrated a shift in substrate preference from glucose to fatty acids[19]. Conversely, ingestion of glucose rapidly reduces the oxidation of leucine during exercise[20], suggesting that carbohydrates and BCAAs compete with each other as alternative substrate sources at high workload.

The role of elevated serum BCAAs in metabolic disease

In the past ten years, studies involving comprehensive metabolic profiling have highlighted the importance of essential amino acid metabolism in the cause of obesity-associated metabolic diseases. Circulating levels of the three BCAAs and their related metabolites tend to be increased in obese individuals[21]. Additionally, serum BCAA levels strongly and positively correlate with the risk of developing Type II Diabetes (T2D) [22], coronary artery disease[23-4], and metabolic syndrome[25]. In a 12-year follow-up study of individuals from the Framingham Offspring Study, normoglycemic, healthy-weight individuals with elevated serum BCAA levels were more likely to develop T2D in the future[26]. Additionally, serum BCAA levels in obese individuals correlates with severity of baseline insulin resistance (IR) and predicted improvement of IR post-weight loss[27]. Individuals with low levels of physical activity and elevated adiposity have decreased expression of genes involved in the catabolism of BCAA, which increases serum BCAA levels[28]. These findings suggest that the association between this BCAA metabolic signature and the development of T2D and obesity is not only due to elevated BCAA levels, but with suppressed flux through the BCAA catabolic pathway. Whether the elevation in circulating BCAAs is a cause or a consequence of metabolic disorders remains unclear.

Substrate metabolism during exercise: potential impact of BCAA

Sustained exercise is powered by several energy sources, including glucose from glycogen degradation, fatty acids from lipolysis, and anaplerotic amino acids (e.g. BCAAs, glutamate, aspartate, alanine) from protein breakdown. Substrate utilization during an exercise bout is governed by the absolute power output, which controls the rate of ATP expenditure, and the exercise intensity, which determines the relative contributions of carbohydrate and fatty acid

oxidation[29]. The initiation of exercise causes a spike in carbohydrate oxidation, generated primarily from glucose produced by hepatic glycogenolysis. During prolonged moderate-intensity exercise (>60 min), increasing energy demand is met through increasing lipid oxidation, and the reliance on hepatic and muscle glycogen declines and is replaced by plasma FFA oxidation. Intramuscular triglycerides (IMTGs) also act as an important fuel source in prolonged (>90 min) moderate-intensity exercise[29-30]. Depending on the duration and intensity, amino acid oxidation can provide up to 10% of the total energy for sustained exercise[30].

During exercise, flux through the TCA cycle and ATP turnover rate within working skeletal muscle can be more that 100-fold greater compared to at rest[31]. Metabolic homeostasis in exercising muscle requires a balance between anaplerotic and cataplerotic reactions to keep up with the increased carbon demand of the TCA cycle[32]. Anaplerosis refers to metabolic pathways that replenish citric acid cycle intermediates in order to keep up with the increased metabolic demands of the cell, while cataplerosis refers to the removal of intermediates to prevent accumulation in the mitochondrial matrix. BCAA catabolism in the skeletal muscle is tightly regulated at rest and during exercise by the activity of BCKDH[2]. Exercise activates BCKDH in contracting muscle, and the downstream intermediates of BCAA catabolism, acetyl-CoA and succinyl-CoA, are used as anaplerotic substrates by the TCA cycle[2]. Amino acids secreted from contracting muscle can be converted to glutamate (via glutamate dehydrogenase) then to alanine (via glutamate-pyruvate transaminase). Alanine, along with the glucogenic precursors lactate and pyruvate, is taken up by the liver, where it undergoes gluconeogenesis to produce glucose. This glucose is released into the bloodstream and taken up by the skeletal muscle to fuel contraction in a process known as the Cori Cycle[33].

A single bout of exercise elicits a rapid, but transient increase in relative mRNA expression of genes that regulate CHO metabolism, lipid mobilization, transport and oxidation, mitochondrial metabolism and oxidative phosphorylation, and mitochondrial biogenesis[29]. Long-term effects of exercise training are due to the cumulative effects of each exercise bout, resulting in changes in

enzyme function and altered metabolic responses over time that lead to improved exercise performance. These adaptations begin to occur within as little as one week and continue over several months, and collectively contribute towards maximizing substrate utilization, mitochondrial respiratory capacity, and contractile function during exercise[29]. Muscle adaptations to endurance exercise training include increases in mitochondrial density and expression of oxidative enzymes, increased GLUT4 expression, improved insulin action and greater glycogen storage, as well as increased fat oxidation during exercise paired with reduced carbohydrate oxidation and lactate production[29]. Additionally, regular exercise increased enzyme activity of the rate-limiting steps of BCAA catabolism, and leucine oxidation is significantly increased in trained vs untrained individuals[20].

Crosstalk between skeletal muscle and liver metabolism during exercise

The accelerated metabolic demands of exercising muscle cannot be met without a robust response from the liver. Exercise increases glucose uptake in working muscle, which is matched by an increase in hepatic glycogenolysis and gluconeogenesis to maintain glucose homeostasis[34]. The liver stores, releases and recycles potential energy as glucose[35], and without this response sustained exercise would result in hypoglycemia and lead to exhaustion. During exercise, glucose homeostasis is maintained by the liver in a process dubbed the Cori Cycle[33], which converts glucogenic precursors derived from the byproducts of glycolysis in contracting skeletal muscle (lactate, pyruvate and alanine), cataplerosis from the TCA cycle (glutamine) and lipolysis (glycerol) to glucose via gluconeogenesis. Gluconeogenesis is essential for maintaining blood glucose levels during exercise and during fasting[34]. There are three rate limiting steps in the gluconeogenic pathway; the conversion of oxaloacetate to phosphoenolpyruvate via phosphoenolpyruvate carboxykinase (PEPCK), the conversion of fructose 1,6-bisphosphate to fructose-6-phosphate via fructose 1,6-bisphosphatase (F1,6BPase), and the conversion of fructose-6-phosphate to glucose-6-phosphate via glucose 6-phosphatase

(G6Pase) [35]. The other steps in this pathway are governed by reversible reactions that are shared with glycolysis (Fig 1.3).

Just as skeletal muscle adapts to exercise training through repeated exercise bouts, the liver undergoes a dynamic remodeling in response to training. The mechanisms that influence hepatic glycogen turnover during high workload are mainly governed by changes in the hormonal response to exercise[35]. Hepatic glucose homeostasis is under the control of circulating insulin and glucagon concentrations[34]. Glycogen synthesis is stimulated by insulin and inhibited by glucagon, while glycogenolysis and gluconeogenesis is stimulated by glucagon and inhibited by insulin, glucose, and nonesterified fatty acids[36]. Glucagon also facilitates the transport of glucogenic amino acids to the liver for gluconeogenesis[35]. Endurance exercise training blunts the rise in glucagon and lessens the decline in plasma insulin during moderate-intensity exercise[37]. This reduces both liver and muscle glycogen use during exercise, which likely contributes to greater endurance performance and exercise capacity by maintaining the rates of carbohydrate oxidation and blood glucose homeostasis during the later stages of exercise[36].

Animal models of altered BCAA catabolism

Several animal models have been developed to study the effect of decreased BCAA catabolism on total body metabolism. BCAT-knock out mice ($BCAT^{-/-}$) have a systemic deletion of the first step in the BCAA catabolic pathway (Fig 1.1). $BCAT^{-/-}$ mice have a 20-30 fold increase in the three BCAAs, and have to be maintained on a low-BCAA diet in order to prevent toxic accumulation of the BCAAs. Deletion of BCAT increased energy expenditure due to an active futile cycle of increased protein degradation and synthesis[38]. These mice are exercise intolerant, with a ~70% decrease in treadmill running time compared to WT controls[39]. BCAT converts BCAAs to BCKAs in a transamination reaction paired to the conversion of a-KG to glutamate, which is paired with the conversion of oxaloacetate to aspartate to promote the malate-aspartate shuttle and with the conversion of pyruvate to alanine to supply glucogenic precursors to the liver for gluconeogenesis (Fig 1.2). These studies highlight the importance of muscle transaminases

in regulating anaplerotic mechanisms that govern amino acid balance across the mitochondria, and their role in generating gluconeogenic substrates for the liver. Overexpression of BCAT in hepatic tissue reduces liver BCAA concentrations while increasing the concentration of other nonessential amino acids. When paired with a high-fat diet, these animals had decreased mTOR activity and impaired blood glucose homeostasis[4]. These results suggest the importance of liver-skeletal muscle cooperation in regulating BCAA catabolism, and highlight the importance of hepatic BCAA levels on the regulation of glucose homeostasis.

BCKDH is the rate-limiting enzyme in the BCAA catabolic pathway, and is inhibited by phosphorylation by BDK (decreased BCAA levels) and activated by dephosphorylation via PP2Cm (elevated BCAA levels) (Fig 1.1). BDK-knock out mice have increased BCKDH activity, systemically decreased BCAA levels, and suffer from neurological abnormalities and low body weight that can be rescued with a high-protein diet[41]. Muscle-specific deletion of BDK reduced mTOR activity and protein content in mice, suggesting that BCAAs are essential for maintaining protein synthesis in skeletal muscle[42], and liver-specific deletion of BDK activated de novo lipogenesis, suggesting the link between BCAA catabolism and fatty acid oxidation[43].

PP2Cm is responsible for the dephosphorylation of the E1a subunit (Ser293) of the BCKDH, and activation of the complex[44]. Loss of PP2Cm in genetic models impaired BCAA catabolism, resulting in a 3-4 fold increase of circulating and tissue BCAAs and a 5-10 fold increase in BCKAs in liver and serum. Cells isolated from PP2Cm-KO mice display changes frequently linked to obesity, insulin resistance and T2DM, such as increased lipotoxicity and lipid peroxidation, increased oxidative stress, increased apoptosis and stress kinase activation[45]. Previous studies in the Tian Laboratory have shown that chronic accumulation of BCAAs due to PP2Cm deletion significantly remodeled substrate metabolism in the heart by shifting oxidative metabolism away from glucose towards fatty acid oxidation through inhibition of PDH [19]. Taken together, these mouse models demonstrate that the BCAAs act as signaling molecules that

regulate glucose, lipid and amino acid homeostasis in the cell, and dysregulation of BCAA catabolism negatively impacts substrate utilization and energy metabolism.

Mass spectrometry as a tool to explore substrate metabolism

Mass spectrometry (MS) is a sensitive, reliable, and highly accurate method for the measurement of isotopic labeling, making it particularly useful for the detection of mass isotopomers of low concentration metabolites[46]. Gas-chromatography mass spectrometry (GC/MS) is particularly effective in the analysis of primary metabolites, specifically those involved in central carbon metabolism. TCA cycle intermediates are present in very low concentrations, usual <2 μmol of total intermediates per gram tissue, with oxaloacetate (OAA) being present in miniscule concentrations (5-10 nmol/g)[32]. While the measurement of metabolite concentrations can be very informative regarding metabolism and metabolic changes in cells, this information is incomplete. Steady-state concentrations of metabolite levels provide relatively little insight into the dynamics of cellular metabolism. Many metabolites can be found in a number of different metabolic pathways, with different metabolic precursors and products. Quantitative analysis of such metabolites does not distinguish the same metabolites derived from multiple pathways[47].

To circumvent this problem, stable isotope tracer (SIT) based metabolite profiling provides insights into the functions and dynamics of specific anaplerotic and cataplerotic pathways[48]. In SIT studies, cells or tissues are supplied with single or multiple isotope tracers such as uniformly or site specific ^{13}C-labeled glucose, which enable measurements of its consumption as well as concentrations of the fractions of the downstream metabolites of the isotope tracer. Tracing the number and distribution of ^{13}C carbons in downstream intermediates can be crucial for unambiguously distinguishing different pathways involving the same metabolite (for example pyruvate entering TCA cycle through pyruvate carboxylase or pyruvate dehydrogenase)[32].

Nuclear magnetic resonance (NMR) spectroscopy is a powerful tool for determining the structure, dynamics and interactions of metabolic molecules. NMR offers the ability to reliably identify and simultaneously quantify many compounds in complex biological mixtures with high

reproducibility and quantification accuracy[47]. This is particularly useful for determining the quantities and identities of metabolites with very similar structures and mass, such as the redox coenzymes NAD+ (nicotinamide adenine dinucleotide, oxidized) and NADH (nicotinamide adenine dinucleotide, reduced) as well as NADP+ (nicotinamide adenine dinucleotide phosphate, oxidized) and NADPH (nicotinamide adenine dinucleotide phosphate, reduced)[49].

The role of BCAA catabolism in substrate utilization and glucose homeostasis

Given its central role in substrate metabolism and protein homeostasis, it is clear that the BCAAs and their catabolism play an important role in exercise capacity, substrate utilization, and metabolic homeostasis. Despite many studies investigating the role of BCAA catabolism in metabolic health and disease, more work is necessary to elucidate the mechanisms connecting these phenomena. Below, we describe two studies that investigate the role of decreased BCAA catabolism on the regulation of glucose homeostasis and gluconeogenesis, as well as the impact of elevated BCAA levels on substrate utilization in the perfused heart. Lastly, we review a collaborative publication detailing a novel method for quantitative measurement of redox coenzymes in tissue using NMR, with an emphasis on the importance of rigorous biological sample preparation.

1.2 Figures

Figure 1.1

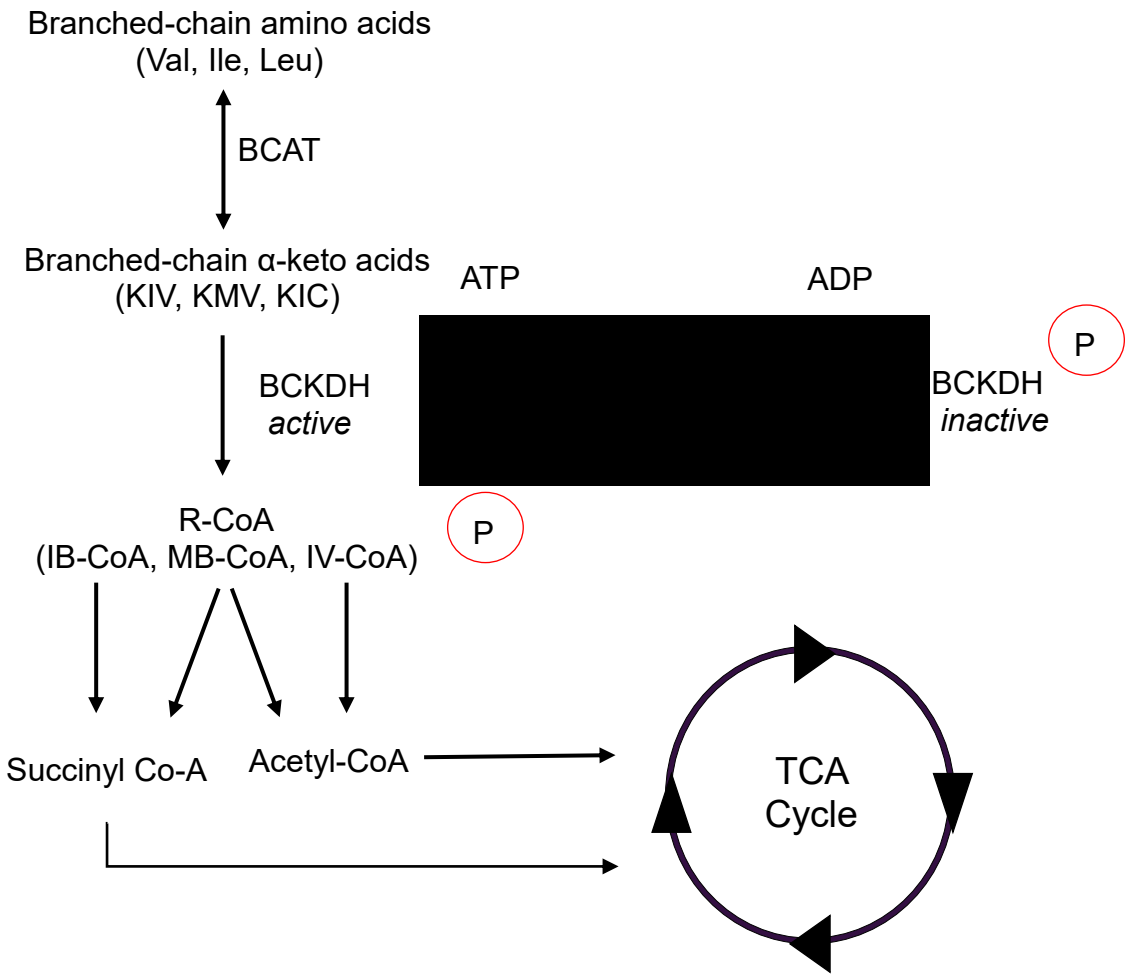

The BCAA catabolic pathway. The three BCAAs undergo a series of catabolic steps to produce acetyl- and succinyl-CoA for the TCA cycle. BCKDH, the rate-limiting step of the pathway, is regulated by phosphorylation states.

Figure 1.2

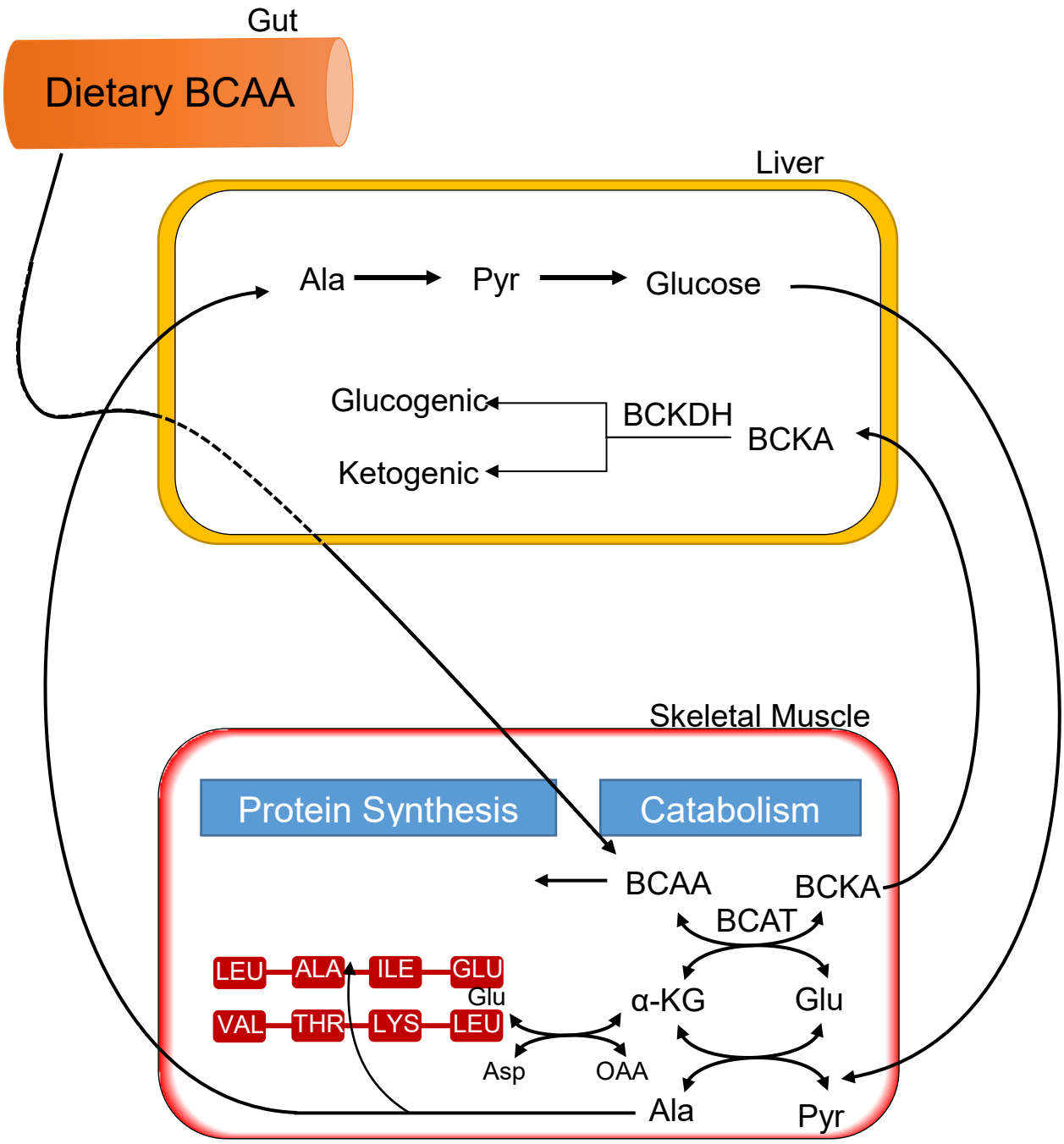

Interaction of liver and skeletal muscle BCAA catabolism. The three BCAAs bypass the liver and are taken up by the skeletal muscle.

Figure 1.3

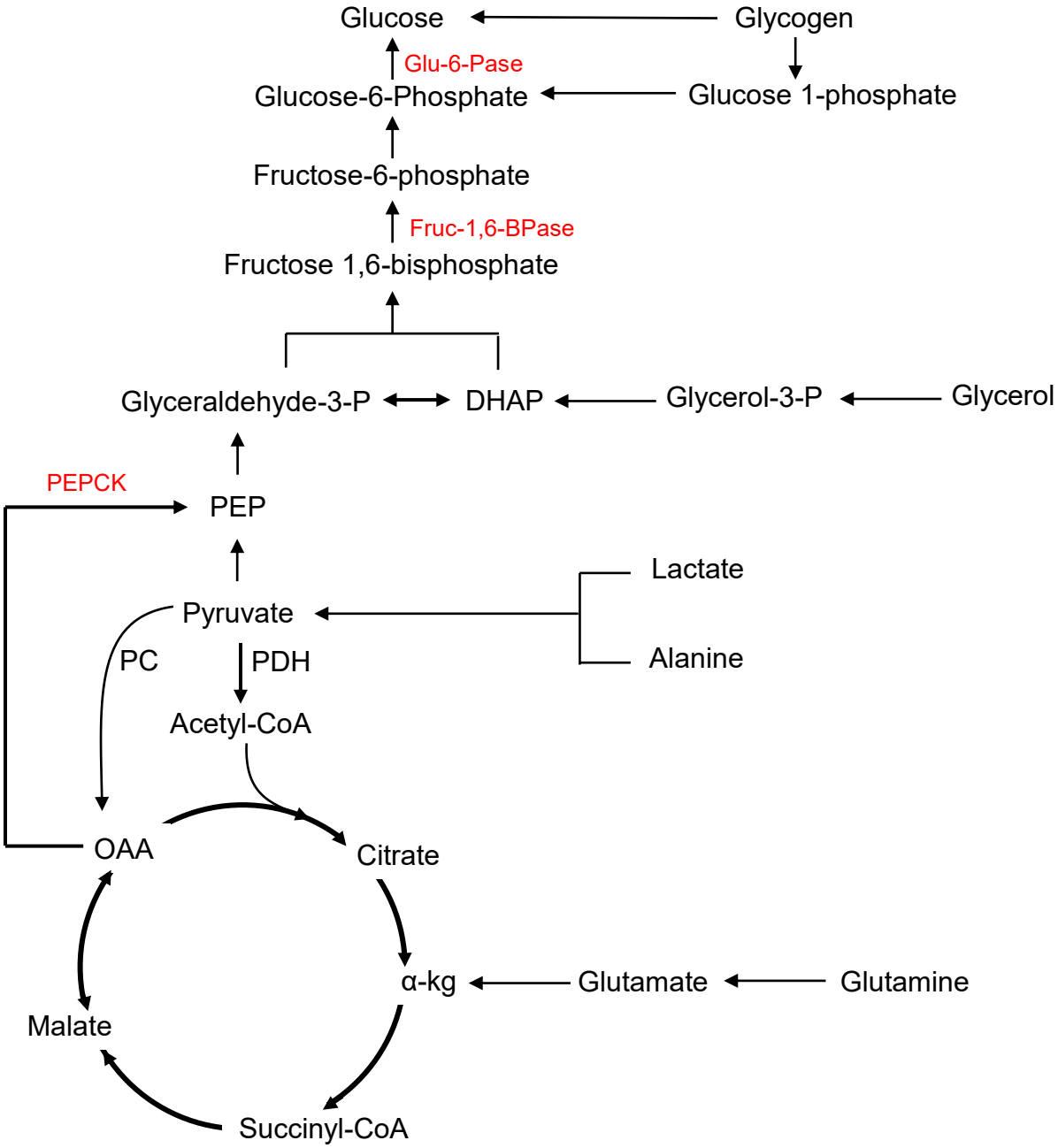

The gluconeogenesis pathway. Rate limiting enzymes are highlighted in red.

1.3 References

1) Harper, A.E., R.H. Miller, and K.P. Block, *Branched-chain amino acid metabolism.* Annu Rev Nutr, 1984. 4: p. 409-54.
2) Shimomura, Y., Murakami T, Makai N, Magasaki M, Harris R, *Exercise promotes BCAA catabolism: effects of BCAA supplimentation on skeletal muscle during exercise*. The Journal of Nutrition, 2004
3) Shimomura, Y, Honda T, Shiraki M, Murakami T, Sato J, Kobayashi H, Mawatari K, Obayashi M, Harris RA. *Branched-Chain Amino Acid catabolism in excercise and liver disease.* The Journal of Nutrition, 2006.
4) Lu, G., Sun H, She P, Youn JY, Warburton S, Ping P, Vondriska TM, Cai H, Lynch CJ, Wang Y. l., *Protein phosphatase 2Cm is a critical regulator of branched-chain amino acid catabolism in mice and cultured cells.* J Clin Invest, 2009. **119**(6): p. 1678-87.
5) Chuang D, Chuang J, Wynn R. *Lessons from genetic disorders of branched-chain amino acid metabolism*. J Nutr, 2006, Jan;136(1 Suppl):243S-9S
6) Harris, R.A., et al., *Regulation of the branched-chain alpha-ketoacid dehydrogenase and elucidation of a molecular basis for maple syrup urine disease.* Adv Enzyme Regul, 1990. **30**: p. 245-63.
7) Strauss, K.A., E.G. Puffenberger, and D.H. Morton, *Maple Syrup Urine Disease*, Gene Reviews, 1993
8) Crowe, M.J., J.N. Weatherson, and B.F. Bowden, *Effects of dietary leucine supplementation on exercise performance.* Eur J Appl Physiol, 2006. **97**(6): p. 664-72.
9) Neinast MD, Jang C, Hui S, Murashige DS, Chu Q, Morscher RJ, Li X, Zhan L, White E, Anthony TG, Rabinowitz JD, Arany Z. *Quantitative Analysis of the Whole-Body Metabolic Fate of Branched-Chain Amino Acids*, Cell Metabolism. 2019 Feb 5;29(2):417-429.e4

10) Mero, A., *Leucine supplementation and intensive training.* Sports Med, 1999. **27**(6): p. 347-58.

11) Shimomura Y, Yamamoto Y, Bajotto G, Sato J, Murakami T, Shimomura N, Kobayashi H, Mawatari K, *Nutraceutical effects of BCAA on skeletal muscle.* The Journal of Nutrition, 2006.

12) Hulmi, J.J., C.M. Lockwood, and J.R. Stout, *Effect of protein/essential amino acids and resistance training on skeletal muscle hypertrophy: A case for whey protein.* Nutr Metab (Lond), 2010. **7**: p. 51.

13) Stipanuk, M.H., *Leucine and Protein Synthesis: mTOR and Beyond.* Nutrition Reviews, 2007. **65**(3): p. 122-129.

14) Coombes, J.S. and L.R. McNaughton, *Effects of branched-chain amino acid supplementation on serum creatine kinase and lactate dehydrogenase after prolonged exercise.* J Sports Med Phys Fitness, 2000. **40**(3): p. 240-6.

15) Shimomura, Y., Murakami T, Nakai N, Obayyashi M, Li Z, Xu M, Sato Y, Kato T, Shimomura N, Fujitsuka N, Tanaka K, Sato M, *Suppression of glycogen consumption during acute exercise by dietary branched-chain amino acids in rats.* J Nutr Sci Vitaminol (Tokyo), 2000. **46**(2): p. 71-7

16) Balage, M. and D. Dardevet, *Long-term effects of leucine supplementation on body composition.* Curr Opin Clin Nutr Metab Care, 2010. **13**(3): p. 265-70.

17) Jang, C., et al., *A branched-chain amino acid metabolite drives vascular fatty acid transport and causes insulin resistance.* Nat Med, 2016. **22**(4): p. 421-6.

18) D'Antona, G., et al., *Branched-chain amino acid supplementation promotes survival and supports cardiac and skeletal muscle mitochondrial biogenesis in middle-aged mice.* Cell Metab, 2010. **12**(4): p. 362-72.

19) Li, T., et al., *Defective Branched-Chain Amino Acid Catabolism Disrupts Glucose Metabolism and Sensitizes the Heart to Ischemia-Reperfusion Injury.* Cell Metab, 2017. **25**(2): p. 374-385.

20) Brooks GA, *Amino acid and protein metabolism during exercise and recovery*. Med Sci Sports Exerc. 1987 Oct;19(5 Suppl):S150-6.

21) Newgard, C.B., et al., *A branched-chain amino acid-related metabolic signature that differentiates obese and lean humans and contributes to insulin resistance.* Cell Metab, 2009. **9**(4): p. 311-26.

22) Huffman, K.M., et al., *Relationships between circulating metabolic intermediates and insulin action in overweight to obese, inactive men and women.* Diabetes Care, 2009. **32**(9): p. 1678-83.

23) Tai, E.S., et al., *Insulin resistance is associated with a metabolic profile of altered protein metabolism in Chinese and Asian-Indian men.* Diabetologia, 2010. **53**(4): p. 757-67.

24) Shah, S.H., et al., *Association of a peripheral blood metabolic profile with coronary artery disease and risk of subsequent cardiovascular events.* Circ Cardiovasc Genet, 2010. **3**(2): p. 207-14.

25) Newgard CB, *Interplay between lipids and branched-chain amino acids in development of insulin resistance*. Cell Metab. 2012 May 2;15(5):606-14.

26) Wang, T.J., et al., *Metabolite profiles and the risk of developing diabetes.* Nat Med, 2011. **17**(4): p. 448-53.

27) Shah, S.H., et al., *Branched-chain amino acid levels are associated with improvement in insulin resistance with weight loss.* Diabetologia, 2012. **55**(2): p. 321-30.

28) Lee S, Gulseth H, Refsum H, Langleite T, Holen T, Jensen J, Drevon C, Birkeland K, *Branched-Chain Amino Acid (BCAA) Metabolism, Insulin Sensitivity (IS), and Liver Fat*

Response to Exercise Training in Sedentary Prediabetic and Normoglycemic Men, Diabetes 2018

29) Egan B, Zierath JR. *Exercise metabolism and the molecular regulation of skeletal muscle adaptation*. Cell Metabolism. 2013 Feb 5;17(2):162-84.

30) Brooks GA. *Anaerobic threshold: review of the concept and directions for future research*. Med Sci Sports Exerc. 1985 Feb;17(1):22-34.

31) Gibala MJ, MacLean DA, Graham TE, Saltin B. *Tricarboxylic acid cycle intermediate pool size and estimated cycle flux in human muscle during exercise*. Am J Physiol. 1998 Aug; 275(2): E235-42.

32) Des Rosiers, Labarthe F, Lloyd S, Chatham C, *Cardiac anaplerosis in health and disease: food for thought*, Cardiovascular Research (2011) 90, 210–219

33) Brooks GA, *The lactate shuttle during exercise and recovery*. Med Sci Sports Exerc. 1986 Jun 18(3):360-8.

34) Trefts E, Williams A, Wasserman D. *Exercise and the Regulation of Hepatic Metabolism*, Prog Mol Biol Transl Sci. 2015 ; 135: 203–225.

35) Rui L. *Energy metabolism in the liver*. Compr Physiol. 2014 January ; 4(1): 177–197.

36) Gonzalez JT, Fuchs CJ, Betts JA, van Loon LJ, *Liver glycogen metabolism during and after prolonged endurance-type exercise*. Am J Physiol Endocrinol Metab. 2016 Sep 1;311(3):E543-53.

37) Coggan AR, Raguso CA, Williams BD, Sidossis LS, Gastaldelli A, *Glucose kinetics during high-intensity exercise in endurance-trained and untrained humans*. J Appl Physiol (1985). 1995 Mar;78(3):1203-7.

38) She P, Reid TM, Bronson SK, Vary TC, Hajnal A, Lynch CJ, Hutson SM. *Disruption of BCATm in mice leads to increased energy expenditure associated with the activation of a futile protein turnover cycle*. Cell Metabolism. 2007 Sep;6(3):181-94

39) She, P., Zhou Y, Zhang Z, Griffin K, Gowda K, Lynch CJ. *Disruption of BCAA metabolism in mice impairs exercise metabolism and endurance.* J Appl Physiol (1985), 2010. **108**(4): p. 941-9.

40) Ananieva E, Van Horn C, Jones M, Hutson S. *Liver BCATm transgenic mouse model reveals the important role of the liver in maintaining BCAA homeostasis.* J Nutr Biochem. 2017 Feb; 40: 132–140.

41) Joshi, M.A., Jeoung NH, Obayashi M, Hattab EM, Brocken EG, Liechty EA, Kubek MJ, Vattem KM, Wek RC, Harris RA.., *Impaired growth and neurological abnormalities in branched-chain alpha-keto acid dehydrogenase kinase-deficient mice.* Biochem J, 2006. **400**(1): p. 153-62.

42) Ishikawa T, Kitaura Y, Kadota Y, Morishita Y, Ota M, Yamanaka F, Xu M, Ikawa M, Inoue N, Kawano F, Nakai N, Murakami T, Miura S, Hatazawa Y, Kamei Y, Shimomura Y. *Muscle-specific deletion of BDK amplifies loss of myofibrillar protein during protein undernutrition*. Sci Rep. 2017 Jan 4;7:39825.

43) White PJ, McGarrah RW, Grimsrud PA, Tso SC, Yang WH, Haldeman JM, Grenier-Larouche T, An J, Lapworth AL, Astapova I, Hannou SA, George T, Arlotto M, Olson LB, Lai M, Zhang GF, Ilkayeva O, Herman MA, Wynn RM, Chuang DT, Newgard CB. *The BCKDH Kinase and Phosphatase Integrate BCAA and Lipid Metabolism via Regulation of ATP-Citrate Lyase*. Cell Metabolism. 2018 Jun 5;27(6):1281-1293.e7.

44) Lu, G., Sun H, She P, Youn JY, Warburton S, Ping P, Vondriska TM, Cai H, Lynch CJ, Wang Y. l., *Protein phosphatase 2Cm is a critical regulator of branched-chain amino acid catabolism in mice and cultured cells.* J Clin Invest, 2009. **119**(6): p. 1678-87.

45) Lynch, C.J. and S.H. Adams, *Branched-chain amino acids in metabolic signalling and insulin resistance.* Nat Rev Endocrinol, 2014. **10**(12): p. 723-36.

46) Ruiz M, Gelinast R, Vaillant F, Lauzier B, Des Rosiers C. *Metabolic tracing using stable isotope-labeled substrates and mass spectrometry in the perfused mouse heart*. Methods in Enzymology, 2015, Volume 561

47) Des Rosairs C, Lloyd S, Comte B, Chatham J. *A critical perspective of the use of 13C-isotopomer analysis of GCMS and NMR as applied to cardiac metabolism*, Metabolic Engineering, 2004, 44-58

48) Zamboni N, Fendt SM, Rühl M, Sauer U. *(13)C-based metabolic flux analysis*. Nat Protoc. 2009;4(6):878-92.

49) Gowda N, Abell L, Lee CF, Tian R, Raftery D. *Simultaneous analysis of major coenzymes of cellular redox reactions and energy using ex vivo 1H NMR spectroscopy*. Anal. Chem. 2016, 88, 4817−4824

Chapter 2

Defective BCAA catabolism impairs exercise capacity and glucose homeostasis

2.1 Introduction

The three branched-chain amino acids (BCAAs) leucine, isoleucine and valine are essential amino acids that have been associated with positive effects on the regulation of body weight[1-2], muscle protein synthesis[3-4] and glucose homeostasis[5-6]. In contrast with other essential amino acids, which are oxidized primarily in the liver, the BCAAs bypass hepatic oxidation allowing levels to increase in the circulation after consumption of a protein-containing meal[7-8]. This gives the BCAAs, particularly leucine, and important role in metabolic control and nutrient signaling.

The catabolic pathways of the three BCAAs have several features in common. The initial step of the pathway is a reversible transamination reaction is catalyzed by mitochondrial branched-chain aminotransferase (BCATm) and produces the branched chain α-ketoacids (BCKA). The second rate-limiting, irreversible step of the pathway is catalyzed by the branched-chain ketoacid dehydrogenase (BCKD) complex[9], which catalyzes the oxidative decarboxylation of α-ketoisocaproate (ketoleucine, KIC), α-ketoisovalerate (ketovaline, KIV), and α-keto-A-methylvalerate (ketoisoleucine, KMV) to form isovaleryl-CoA, 3-methylbutyryl-CoA, and isobutyryl-CoA, respectively. BCKD is inhibited by phosphorylation of its E1α subunit (Ser 293) by BCKD kinase (BDK), and activated by dephosphorylation via a mitochondrial localized 2C-type serine-threonine protein phosphatase (PP2Cm)[10] (Fig 1). Thereafter, the pathways resemble fatty acid oxidation yielding end products (acetyl-CoA from leucine, acetyl-CoA and succinyl-CoA from isoleucine, and succinyl-CoA from valine) that can enter the tricarboxylic acid (TCA) cycle[7]. Loss of PP2Cm in genetic models impairs BCAA catabolism through suppression of BCKDH activity and leads to a modest increase in systemic BCAA levels.

The liver lacks BCATm, so the first step of BCAA catabolism occurs in the skeletal muscle and other peripheral tissues[11]. After a protein-containing meal, dietary BCAAs appear in the bloodstream and are taken up by the skeletal muscle, which has high levels of BCAT, and either used as a building block for protein synthesis or undergo the first step in their catabolism to form the branched chain keto-acids[7]. Non-contracting skeletal muscle has BCKDH in the inactive form[9], so at rest BCKAs are exported to the liver to be catabolized into their glucogenic or ketogenic precursors. During exercise, BCKDH is activated[9], increasing BCAA catabolism in the skeletal muscle and allowing BCAAs to act as a carbon substrate for TCA cycle metabolism.

During exercise, the liver takes up glucogenic precursors and releases glucose in an effort to keep up with the metabolic demands of the skeletal muscle[12]. During muscular activity the ATP demand increases, which is provided by the breakdown of glycogen to feed glycolysis[13]. During strenuous activity pyruvate is converted to lactate, which is exported to the liver where it is converted to pyruvate, then to glucose through gluconeogenesis. This glucose is then secreted from the liver to maintain blood glucose homeostasis and supply contracting muscle with glucose in a process called the Cori Cycle[14]. Other gluconeogenic substrates include glucogenic amino acids (such as glutamine) produced by protein degradation and glycerol from lipolysis[15].

Increasing evidence links low serum BCAA levels and elevated BCAA catabolism with elevated physical activity and better metabolic health[8]. For this reason, BCAA supplementation is often used pre-workout to promote exercise capacity in athletes. Conversely, circulating levels of the three BCAAs and their related metabolites tend to be increased in obese individuals[16]. Serum BCAA levels are strongly and positively correlated with the development of insulin resistance[2,17], coronary heart disease[18-19], and type II diabetes[20] (T2D), and are predictive of patient responses to therapeutics and intervention outcomes[2]. These findings suggest that the association between this BCAA metabolic signature and the development of T2D and obesity is not only due to elevated BCAA levels, but with suppressed flux through the BCAA catabolic pathway. Therefore, it is important to understand the mechanisms regulating BCAA catabolism

and their effect on metabolic homeostasis within the body. In the present study, we sought to elucidate the impact of impaired BCAA catabolism on exercise capacity and metabolic homeostasis using PP2Cm-deficient mice. Loss of PP2Cm in genetic models impairs BCAA catabolism through suppression of BCKDH activity and leads to a modest increase in systemic BCAA levels. When compared to other KO Because the majority of BCAA catabolic disorders target the activity of BCKDH, the PP2Cm-knock out model most closely reflects the phenotypes found in human disease. Our results show a link between BCAA catabolism, exercise capacity, and glucose homeostasis.

2.2 Materials and Methods

2.2.1 Animal Model

Homozygous PP2Cm-knock out (KO) mice were developed by Dr. Wang as previously described[10]. In brief, a LacZ-expression cassette was inserted into the translational initiation site of the PP2Cm allele, while replacing the major portion of exon 2 of the mouse PP2Cm gene on a C57/BL6 background. Wild-type (WT) littermates were used as controls. Mice were purchased from Charles River and maintained as an inbred line. All mice were housed in specific pathogen free (SPF) conditions on a 12:12 light/dark cycle with free access to standard chow and water. All animal experiments were approved by the UW Institutional Animal Care and Use Committee. Animals were euthanized with either an overdose of injectable anesthesia or by cervical dislocation.

2.2.2 Exercise Testing and Treatment Strategies

Mice between 12-16 weeks of age were exercised on motorized treadmills (Columbus Instruments) and encouraged to run as long as possible with the use of an electric grid located at the back of the treadmill (1.6 mA, 1Hz). Mice were defined as exhausted if they remained on the shock grid for 5 continuous seconds. Prior to the test, all mice were provided a 3-day

familiarization period consisting of 10 min of running at a speed of 10m/min at 10% incline for two days, and 10 min of running at a speed of 10meter/min (m/min) at 10% incline with the shock grid activated on the final day (Fig 2.1a-b). Any animal that refused to exercise by the end of the 3rd session was excluded from the cohort.

Two tests were performed, one for evaluation of maximal running capacity (MAX Test) and one for endurance capacity (Endurance Test) as previously described[21]. The MAX test started at a fixed inclination of 10° and a 10.2m/min belt speed for 2 min followed by 2 min intervals of 14.4 m/ min, 18.6 m/min, 23.8 m/min, 25.2 m/min, 27.6 m/min, 30 m/min, 32.4 m/min, 34.8m/min, 37.2 m/min, and a final interval of 2 min at 42 m/min (Fig 2.1c). Shock grid is activated (1Hz, 0.5-1.0mA) immediately upon beginning the test. The test was stopped at exhaustion (defined as the mouse remaining on the shock grid for more than 5 seconds) of after the final step at 42 m/min if the mouse completed the test. The Endurance Test started at a fixed inclination of 10° and a 10.2m/min belt speed for 30 min followed by 15 min intervals at 12.6m/min, 15m/min, 17.4m/min, 19.8m/min, and a final step of 90 min at 22.2m/min (Fig 2.1d). Shock grid is activated at 45 min. The Endurance Test concluded once the mouse reached exhaustion or completes the final stage. For metabolite analysis, quadriceps, liver and blood glucose was taken from sedentary mice (T = 0 min), from exercising mice at intermediate timepoints (T = 30, 45 min), and immediately upon exhaustion. A group of control mice had blood samples collected at the average time the KO mice were exhausted (85 min).

To determine the effect of increased skeletal muscle pyruvate utilization on exercise capacity, 3-4 month old KO and WT mice were divided into control and treatment groups and received an IP injection of dichloroacetate (DCA) (25mg/mL, 125mg/kg) or an equivalent volume of saline 15 min before completing either MAX Capacity Test or Endurance Capacity Test. DCA is a PDH kinase inhibitor, which activates PDH and increases glucose utilization in skeletal muscle. Blood glucose was measured with a glucometer via tail prick at rest and immediately

following exhaustion. To determine the effect of increased availability of gluconeogenic substrate on exercise capacity, 3-4 month old KO and WT mice were divided into control and treatment groups and received an IP injection of glycerol (0.5-2 g/kg/bw) or an equivalent volume of saline 15 min before completing either MAX Capacity Test or Endurance Capacity Test. Glycerol is a glucogenic precursor which can be used as a substrate for glucose production in the liver. Blood glucose was measured with a glucometer via tail prick at rest and immediately following exhaustion.

2.2.3 Biochemical assays

Glycogen content in quadriceps and liver tissue was measured with a colorimetric assay kit (Sigma). Triglyceride levels in quadriceps and liver tissue were measured with a colorimetric assay kit (Cayman). Total RNA was isolated from frozen tissue using the RNeasy Kit (Qiagen), and cDNA was synthesized using Maxima First Strand cDNA kit according to manufacturers' guidelines. Real-time PCR was performed using SYBR green (Bio-Rad). The primers are described in Table 1. Results of mRNA levels were normalized to 18S mRNA levels in skeletal muscle and cardiac tissue and L32 mRNA levels in liver and reported as fold-change over WT. Blood glucose measurements were measured via tail prick using Contour glucometer. PEPCK activity in liver was measured with a colorimetric assay kit (Biovision).

2.2.4 Metabolomics

For metabolomics analysis, frozen mouse tissue (20-25mg) specimens were mixed with a 1.2mL mixture of cold methanol/chloroform (1:2 v/v; 4^{o}C) and homogenized using a *Tissue Tearor* homogenizer (Biospec) and sonicated for 20 seconds. A further 800µL cold chloroform/distilled water solution (1:1 v/v) was added, the sample was then vortexed and set aside for 30 min on ice to separate the solvent layers. After centrifugation at 2000 rpm for 20 min, the aqueous (top) layer was separated and filtered using a 1.5mL 0.2µm syringe filter and 150µL was evaporated to dryness using a Vacufuge Plus (Eppendorf) and used for each analysis.

Blood was collected via retrorbital bleeding. Blood samples were spun down at 10,000rpm and top serum layer was collected for analysis. Blood serum samples (10μL) were precipitated by the addition of 100 μL methanol. The mixture was briefly vortexed and placed in -20 °C freezer for 30 min. While still cold, samples were centrifuged for 10 min at 13000 rpm. The 100 μL supernatant liquid was transferred to a new tube. Samples were evaporated to dryness.

To prepare the samples for GC/MS analysis, 30μL of 20mg/mL methoxyamine hydrochloride dissolved in pyridine was added to the dried sample and incubated at 37°C for 90 min. After that, samples were derivatized with 70μL of N-methy-N-tert-butyldimethylsilyl trifluoroacetamide (MTBSTFA) was added and incubated at 37°C for 30 min. Samples were run on an Agilent 5977A Series GC/MSD system.

To prepare the samples for LCMS analysis, 40μL of 1:1 MeOH:H_2O and 60μL of ACN were added to a tube, vortexed and spun down. Samples were run on a Xevo TQ-S Q-TOF with an Aquity UPLC HILIC Column.

2.2.5 Indirect Calorimetry

Indirect calorimetry measurements were performed by the Nutrition and Obesity Research Center at UW South Lake Union. Body weight, energy intake (recording of food/water consumption) and expenditure (beam breaks) were measured in 5-6 month old WT and KO mice (n = 6 for each group). Total energy expenditure was measured by continuous recording of respiratory gaseous exchanges. For this recording, mice were placed at 10 am in individual cages with wire bottoms placed in a room with controlled temperature (22 °C) and maintained on a 12:12 light/dark cycle in an SPF facility. These cages ad libitum access to water and standard laboratory chow were ventilated with room air. After a three day acclimation period, measurements of O_2 consumption (VO_2) and CO_2 (VCO_2) production were started at 9am and continued during a three day period. Baseline measurements with standard chow were recorded for 24 hours, then fasting measurements with food removed were recorded for 24-hours, then refeeding with standard chow

replaced for 24 hours respiratory exchange ratio (RER) is the ratio of VCO_2/VO_2 and is an indicator of the relative amounts of lipid and carbohydrate oxidized. Body composition was evaluated in live, conscious animals in triplicate by quantitative nuclear magnetic resonance spectroscopy (EchoMRI 3-in-1 in an Animal Tissue Composition Analyzer, Echo Medical Systems, Houston TX).

2.2.6 Glucose Tolerance Test, In Vivo Tests for Gluconeogenesis

Mice (5-6 months old) were fasted for 24 hours before pyruvate, glycerol and glutamine tolerance tests. Mice (10 weeks old) were fasted for 16 hours for glucose tolerance test. Mice were injected intraperitoneally with sodium pyruvate (0.25-5kg/bw), glycerol (.5-2 g/kg body weight), glutamine (0.5-2 g/kg/bw) and glucose (1-2g/kg/bw), respectively for the above-mentioned tests. Blood glucose levels were monitored every 15-30 min for up to 120 min using a glucometer.

2.2.7 Statistical Analysis

All data are presented as mean ± SEM. An unpaired Student's t test was used to detect significant differences when two groups were compared. One-way or two-way ANOVA was used to compare the differences among three or more groups. ANOVA with repeated measures was used for multiple group comparisons over multiple time points. Bonferroni post hoc analysis was used for all ANOVAs as applicable (SPSS 16.0 software). The p values <0.05 were considered statistically significant.

2.3 Results

The PP2Cm-KO mouse has reduced endurance exercise capacity

We utilized two treadmill-based exercise tests to investigate the impact of defective BCAA catabolism on exercise capacity in the mouse. KO mice have a 19% decrease in high intensity exercise capacity (N = 6-10, P = NS [no significant difference]) and a 20% decrease in endurance exercise capacity (N = 12-14, P < .001) compared to WT controls. (Fig 2.2a-b) Systemic knock

out of PP2Cm inhibits the rate-limiting step of the catabolic pathway, BCKDH, causing a 2-4 fold increase in BCAA levels in serum and muscle tissues while remaining unchanged in the liver. (Fig 2.2c) BCKA levels are elevated 5-10 fold in liver and serum, while remaining exchanged in the skeletal muscle. (Fig 2.2d) We had previously shown no changes in mRNA levels governing pathways regulating glucose uptake, glycolysis, glycogenosis, and fatty acid oxidation[23]. At baseline, there was no change in glycogen or triglyceride pools in the liver and skeletal muscle (Fig 2.2e-f), indicating that decreased exercise capacity was not due to a decrease in endogenous substrate levels and could be caused by issues with supply of substrate (glucose or fatty acids) to the skeletal muscle.

Chronic accumulation of BCAAs has no effect on anaplerosis in skeletal muscle

During exercise, TCA intermediate pool size and flux through the TCA cycle[22] drastically increases, and BCAA catabolism is increased to keep up with increased substrate demand. It was hypothesized that that decreased BCAA catabolism would lead to decreased TCA cycle intermediate pool size. To test this, skeletal muscle and liver were harvested from sedentary mice (baseline), after 30 or 45 min of exercise (intermediate), and at the end of the Endurance Test (exhaustion). WT and KO animals had a 2-3 fold increase in TCA cycle intermediates (summed peak areas from citrate, isocitrate, a-KG, succinate, fumarate and malate) at the end of exhaustive exercise, but we found no significant difference between the two genotypes either at baseline, intermediate or exhaustion time points. (Fig 2.3a-b).

Chronic accumulation of BCAAs has no effect on substrate utilization in skeletal muscle

To determine if systemic accumulation of BCAAs suppressed glucose utilization in the skeletal muscle of KO mice, we performed indirect calorimetry to measure the relative ratio of lipid and carbohydrate used at baseline and in the fasted state. Six-month old KO mice had no change in their RER either at baseline, during 24 hours of fasting, or during refeeding. Additionally, KO mice had no significant changes in body weight, food and water intake, and

energy expenditure compared to CON mice (Fig 2.4 b-e), and there was no difference in body composition (% lean mass vs % fat mass) across any of the time points (Fig 2.4f,g).

Activation of PDH decreases exercise capacity in the PP2Cm knock out mouse

Given the finding that BCAAs directly inhibit PDH in the KO heart[23], we wanted to determine if increasing PDH activity in the skeletal muscle would rescue exercise capacity. Three-four month old mice completed an endurance test after receiving a dose of DCA, a PDH kinase inhibitor that increases PDH activity in vivo. DCA treatment had no effect on maximal exercise capacity tests in WT and KO mice. However, DCA treatment caused a 20% decrease in endurance exercise capacity in the KO mice while WT exercise capacity was unchanged (N = 6, P < .01) (Fig 2.5a) There were no changes in blood glucose levels between the two groups at the end of exhaustion (N = 6, P = NS) (Fig 2.5b). These data imply that, contrary to our previous hypothesis, increasing glucose utilization in skeletal muscle is detrimental to exercise capacity in KO mice.

PP2Cm knock out- mice have impaired glucose homeostasis

We next investigated the effects of knocking out PP2Cm on whole-body glucose homeostasis. 10-week old KO mice and WT littermates were fasted overnight and injected intraperitoneally with a bolus of glucose. The blood glucose levels reached similar peaks and then declined at similar rates in the two genotypes (Fig 2.6a). Blood glucose levels were normal in the KO mice at baseline and after fasting. We then carried out a series of tolerance tests using different glucogenic precursors to investigate the mechanisms underlying the 20% reduction in exercise capacity in the DCA treated KO mice. Six month old KO mice had significantly decreased ability to produce blood glucose from both pyruvate (N = 5-9, P < .001) and glutamine (N = 6, P < .001) (Fig 2.6b,c) indicating suppression of gluconeogenesis. WT and KO mice were similarly sensitive to glycerol (N = 5-6, P = NS) (Fig 2.6d), which enters the gluconeogenic pathway at a later step, indicating that suppression of gluconeogenesis may be occurred before or at the rate-limiting enzyme PEPCK.

Elevated BCAA and BCKA levels do not inhibit PEPCK activity

Gluconeogenesis occurs primarily in the liver[24]. We found no change in mRNA expression of genes controlling the rate limiting steps of gluconeogenesis. There was no difference in the activity of PEPCK isolated from fasted WT and KO livers (N = 3, P = NS) (Fig 2.6f). To determine whether BCAAs or BCKAs directly inhibit PEPCK activity, we incubated PEPCK with increasing concentrations of BCAAs 4- to 5-fold above and below the physiological blood level in mice (N = 3, P = NS) (Fig 2.6g). We also tested the effect of BCKAs, the second metabolites in the BCAA catabolism pathway, at high physiological concentrations (N = 3, P = NS) (Fig 2.6h). Increasing doses of the BCAAs or BCKAs does not exhibit any inhibitory effect on PEPCK activity. These findings suggest that inhibition of gluconeogenesis in KO occurs prior to the PEPCK reaction.

Blood glucose levels to not effect exercise capacity in the PP2Cm knock out mouse

We hypothesized that reduced gluconeogenesis in the liver was the cause of reduced exercise capacity in KO mice. To test this, blood glucose was collected from mice and different time points during an endurance exercise capacity test. However, there was no difference in blood glucose levels at any time point during exercise (N = 6, P = NS). (Fig 2.7a) Supplementation with glycerol, which elevated blood glucose in both WT and KO mice, caused a 2-fold increase in blood glucose levels at the end of exhaustive exercise (N = 6) (Fig 2.7c). However, increased blood glucose levels did not impact exercise capacity in either WT or KO mice (N = 6, P = N.S.). (Fig 2.7b)

2.4 Discussion

In the present study, we demonstrate that chronic accumulation of BCAAs due to systemic deletion of PP2Cm negatively impacts endurance exercise capacity and gluconeogenesis in adult male mice. KO mice have a 20% decrease in both high-intensity and prolonged exercise capacity. Despite this finding, there was no measurable change in endogenous substrate levels or

metabolites in the skeletal muscle. However, increasing glucose utilization in the skeletal muscle by activation of PDH, the rate limiting enzyme for pyruvate oxidation, caused a further decrease in exercise capacity. Even through the metabolic remodeling caused by defective BCAA catabolism is well tolerated under unstressed conditions[23], it decreased the KO's ability to upregulate gluconeogenesis during substrate scarcity. Our results, therefore, reveal a role of BCAA catabolism in the maintenance of full body glucose homeostasis under stress conditions.

The rate limiting step in the BCAA catabolic pathway is the decarboxylation of the BCKAs to the branched chain CoAs (BC-CoAs) by BCKDH[7]. PP2Cm activates BCKDH by dephosphorylating the complex, and deletion of PP2Cm renders BCKDH in its phosphorylated, inactive, form. BCKDH is heavily phosphorylated in non-contracting muscle, and is activated by Ca+ influx from contracting muscle[25]. Exercise inhibits protein synthesis and promotes skeletal muscle breakdown, freeing up additional BCAAs and other anaplerotic amino acids as substrates for oxidative metabolism[8].

During exercise, flux through the TCA cycle can intensify up to 100-fold[22], and ATP turnover rate within working skeletal muscle can be 70-100-fold greater compared to at rest[25]. Pathways regulating anaplerotic mechanisms, including BCAA catabolism, are increased to keep up with increased substrate demand[8]. This lead us to hypothesize that decreased exercise capacity in the KO mouse was due to an acute inability to upregulated BCAA catabolism in contracting muscle. It was hypothesized that the inability to upregulate BCAA catabolism during exercise would decrease the availability of anaplerotic substrates in the skeletal muscle, leading to a decrease in TCA cycle intermediate (TCAi) pool size. However, our results showed that there was no change in TCAi levels at any point during endurance exercise, thus refuting the hypothesis.

It was previously shown that in isolated perfused hearts, KO animals demonstrated reduced glucose oxidation at baseline, and addition of BCAAs to the perfused heart-shifted substrate preference to fatty acids in WT hearts[23]. It was hypothesized that elevated BCAA levels

in the KO would lead to a shift in substrate preference towards fatty acids in the skeletal muscle, and the inability to utilize glucose would lead to decreased ATP production in contracting muscle. However, we found that KO mice had no change in RER at baseline, fasting or refeeding compared to littermate controls.

Previous studies in the Tian Laboratory have shown that chronic accumulation of BCAAs due to PP2Cm deletion decreased glucose metabolism in the heart by inhibiting mitochondrial pyruvate utilization through inhibition of PDH [23]. This led us to hypothesize that elevated BCAA levels in the skeletal muscle was inhibiting PDH activity, leading to reduced glucose utilization in the muscle. We were unable to directly measure PDH activity in skeletal muscle via enzymatic assay, so we performed a gain-of-function experiment to determine the effect of increased PDH activity on exercise capacity. Mice were given DCA, a PDH kinase inhibitor that increases PDH activity in vivo, prior to performing either a MAX or Endurance Capacity test. Contrary to our hypothesis, addition of DCA caused a further inhibition of endurance exercise capacity in KO mice while leaving WT animals unaffected. This lead to a shift in thinking: perhaps this phenotype is not due to an inability to utilize substrate in the skeletal muscle but rather to an inability to produce substrate in the liver.

During exercise, glucose homeostasis is maintained by the liver via the Cori Cycle, which converts glucogenic precursors derived from the byproducts of glycolysis in contracting skeletal muscle (lactate and alanine) and lipolysis (glycerol) to glucose via gluconeogenesis[24]. Gluconeogenesis is essential for maintaining blood glucose levels during exercise and during fasting. To determine the liver's ability to maintain blood glucose homeostasis during times of low substrate availability, fasted mice underwent a series of tolerance tests to determine their ability to produce glucose from a variety of gluconeogenic precursors. There are three rate limiting steps in the gluconeogenic pathway; the conversion of oxaloacetate to phosphoenolpyruvate via (PEPCK), the conversion of fructose 1,6-bisphosphate to fructose-6-phosphate via fructose 1,6-bisphosphatase (F-1,6BPase), and the conversion of fructose-6-phosphate to glucose-6-

phosphate via glucose 6-phosphatase (G6Pase) [28]. (Fig 1.3) An additional site of regulation is pyruvate entry into the mitochondria via mitochondrial pyruvate transporter (MPT1) [29]. KO mice were able to increase their blood glucose from glycerol, but not pyruvate and glutamine. Glycerol enters the gluconeogenic pathway at glyceraldehyde-3-phosphate and bypasses PEPCK, indicating no change in the activity of F6Pase and G6Pase. Because glutamine and pyruvate are metabolized to OAA through independent pathways, our results suggest that the inhibition does not lie at PDH, PC or MPT1. Results from the tolerance tests indicate that inhibition of gluconeogenesis is caused by a defect in PEPCK. However, there was no difference in PEPCK activity in fasted WT and KO mice, and PEPCK was not inhibited by either BCAAs or BCKAs. These results imply that there is an external factor regulating gluconeogenesis in these mice.

As exercise progresses and glycogen stores are depleted, the liver is responsible for maintaining blood glucose homeostasis by producing glucose from gluconeogenic precursors generated from contracting muscle[12]. If liver gluconeogenesis is suppressed by the same mechanism at the end of exhaustive exercise as in fasting, exercise capacity would be decreased. This would result in blood glucose levels in the KO to decrease more rapidly than their WT controls. However, we found no difference between KO and WT blood glucose levels at any time during exercise. This result does not completely rule out our hypothesis, as the rate of glucose uptake in peripheral tissues may decrease in the KO to maintain blood glucose levels. If decreased exercise capacity were the result of suppressed gluconeogenesis, then increasing glucose availability should rescue the exercise phenotype. However, supplementation with glycerol prior to exercise increased post-exercise blood glucose in both WT and KO mice, without impacting exercise capacity. This indicates that while PP2Cm deletion has a significant impact on exercise capacity and glucose homeostasis in the mouse, decreased glucose production is not a cause of decreased exercise capacity. Rather, these two phenotypes are most likely two related symptoms of an unknown cause.

In conclusion, we demonstrate that systemic elevation of BCAAs and BCKAs by the whole-body deletion of PP2Cm leads to decreased exercise capacity and suppressed gluconeogenesis. Chronic accumulation of BCAAs and BCKAs in the liver suppresses glucose production from the gluconeogenic precursors pyruvate and glutamine, but not from glycerol. This affect is more pronounced in older (6 month) mice, and is not seen in younger mice. Much like elevated plasma BCAA levels are a positive biomarker for the risk of developing metabolic disease later on in life, the effects of elevated BCAAs on liver glucose homeostasis accumulate over time. This inability to regulate glucose homeostasis is inconsequential at baseline, but negatively impacts the KOs ability to regulate substrate balance when exposed to physiological stressors like fasting and exercise. This suppression in gluconeogenesis could explain the decrease in exercise capacity under fed conditions. Once glycogen stores are depleted, the KO would be unable to upregulate gluconeogenesis to keep up with energetic demand, leading to reduced skeletal muscle output. However, increasing glucose availability had no effect on exercise capacity in either WT or KO mice. It is likely that there are one or more compensatory changes resulting from PP2Cm deletion that are influencing exercise capacity in these mice, but further study is required to determine the mechanism governing these reactions. Our results, therefore, reveal a role of BCAA catabolism in regulating liver control of glucose homeostasis during times of physiological stress.

Figures and Tables

Figure 2.1

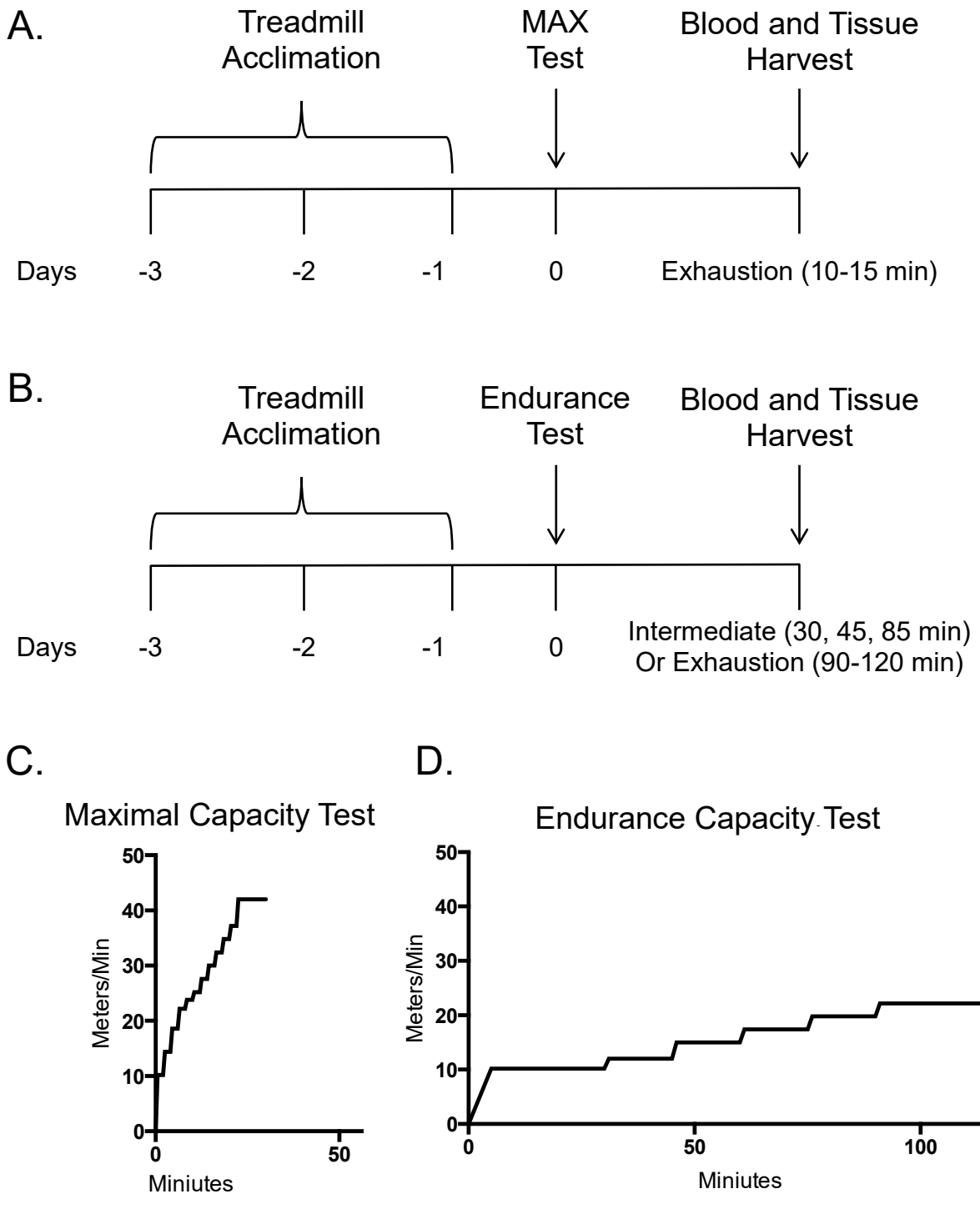

Treadmill testing scheme.

Figure 2.2

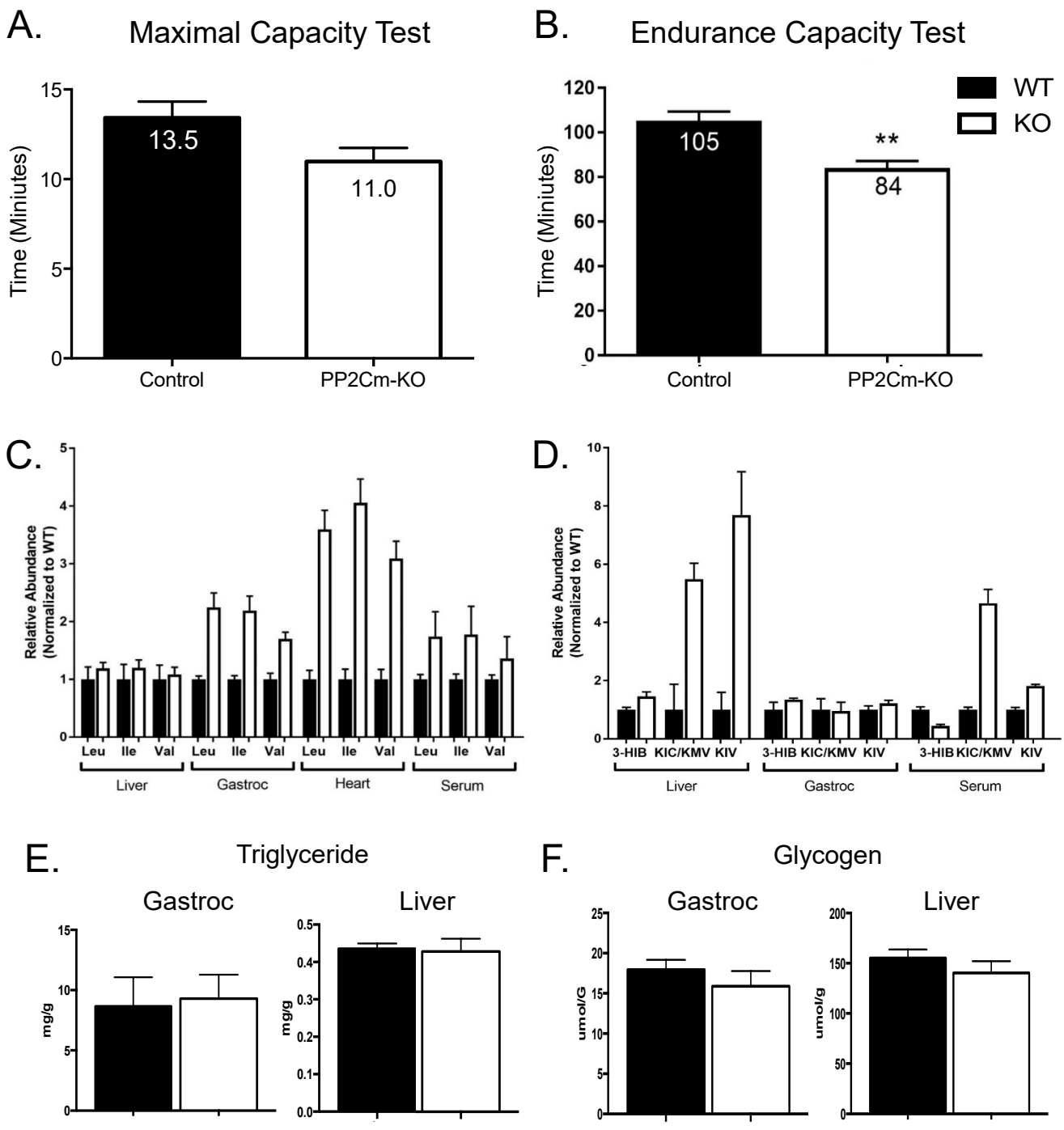

The PP2Cm-KO mouse has reduced endurance exercise capacity. A and B show the results for the MAX Capacity Test (N = 6-10, P = .06) and the Endurance Capacity Test (N = 12-14, P < .001), respectively. C and D show BCAA levels (N = 6) and BCKA levels (N = 6), respectively. E and F show triglyceride (N = 6, P = NS) and glycogen (N = 6, P = NS), for gastrocnemius muscle and liver.

Figure 2.3

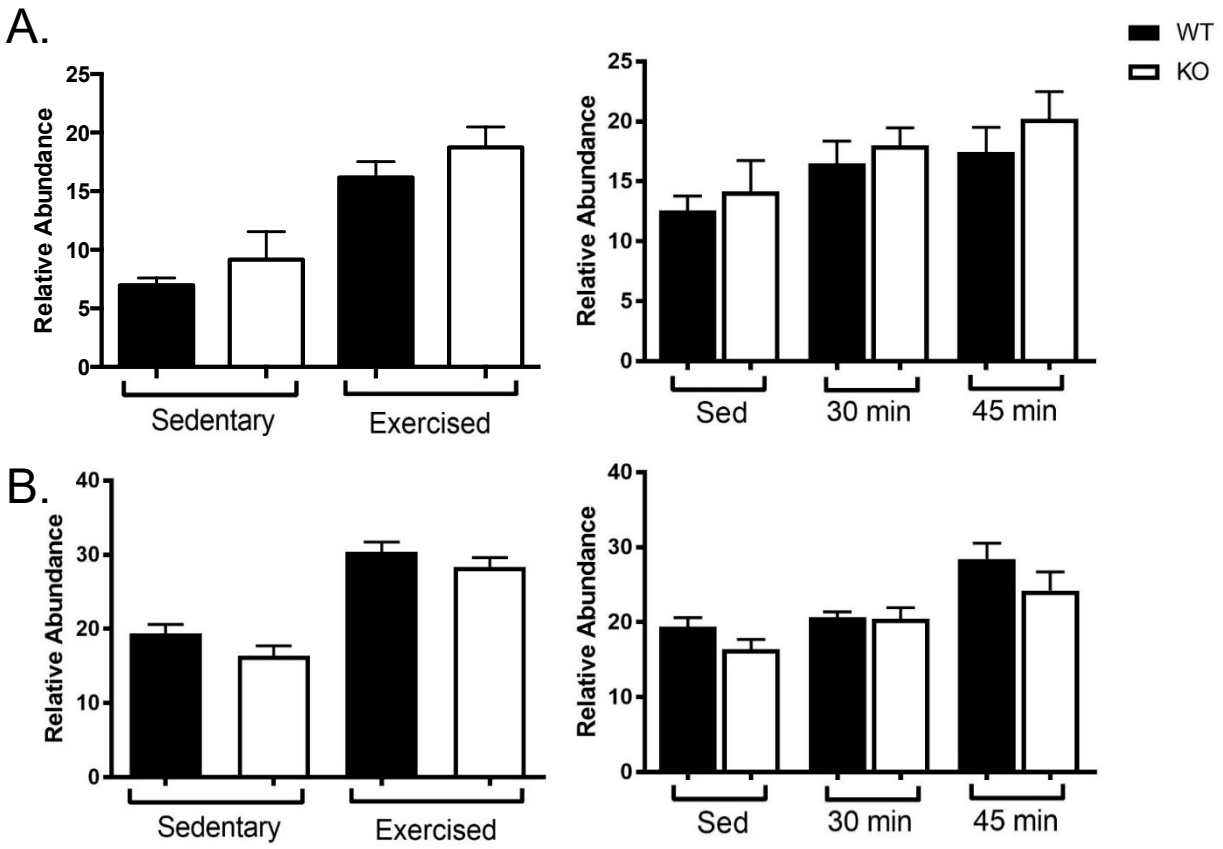

Chronic accumulation of BCAAs has no effect on anaplerosis in skeletal muscle. TCA intermediate pool size (a-ketoglutarate, citrate, isocitrate, succinate, fumerate, malate) in A) skeletal muscle and B) liver of sedentary and exercising animals at baseline (sedentary), intermediate timepoints and at exhaustion. (N = 6, P = NS)

Figure 2.4

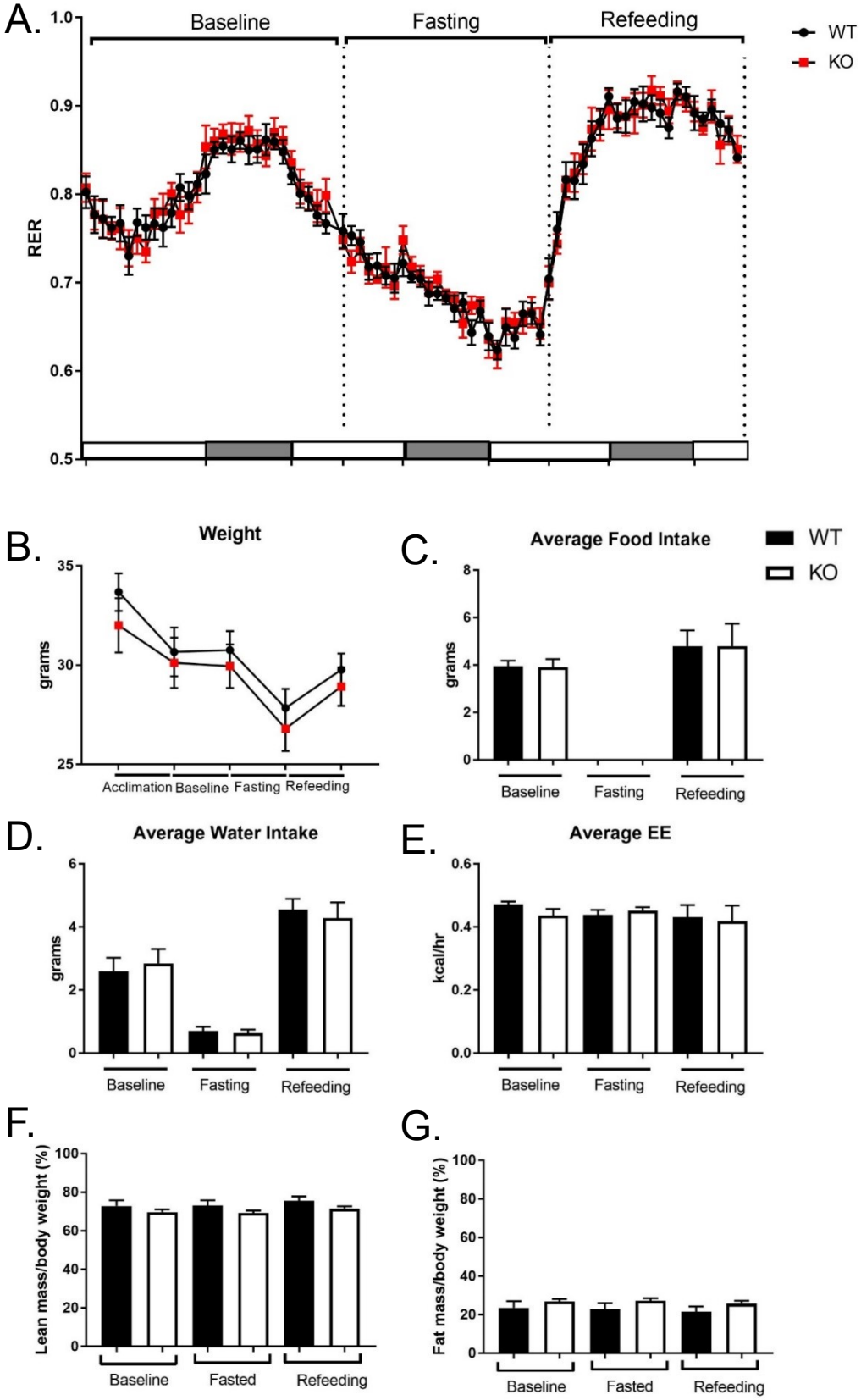
A.
Baseline
Fasting
Refeeding
WT
KO
RER
1.0
0.9
0.8
0.7
0.6
0.5
B.
Weight
grams
35
30
25
Acclimation Baseline Fasting Refeeding
C.
Average Food Intake
WT
KO
grams
8
6
4
2
0
Baseline
Fasting
Refeeding
D.
Average Water Intake
grams
6
4
2
0
Baseline
Fasting
Refeeding
E.
Average EE
kcal/hr
0.6
0.4
0.2
0.0
Baseline
Fasting
Refeeding
F.
Lean mass/body weight (%)
100
80
60
40
20
0
Baseline
Fasted
Refeeding
G.
Fat mass/body weight (%)
100
80
60
40
20
0
Baseline
Fasted
Refeeding

Chronic accumulation of BCAAs has no effect on substrate utilization in skeletal muscle. A) Indirect calorimetry measurements in mice at baseline, fasting and refeeding. B) Weight measurements, C) food and D) water intake, E) energy expenditure and F) % lean mass and G) % fat mass at baseline, fasting and refeeding. (N = 6, P = NS)

Figure 2.5

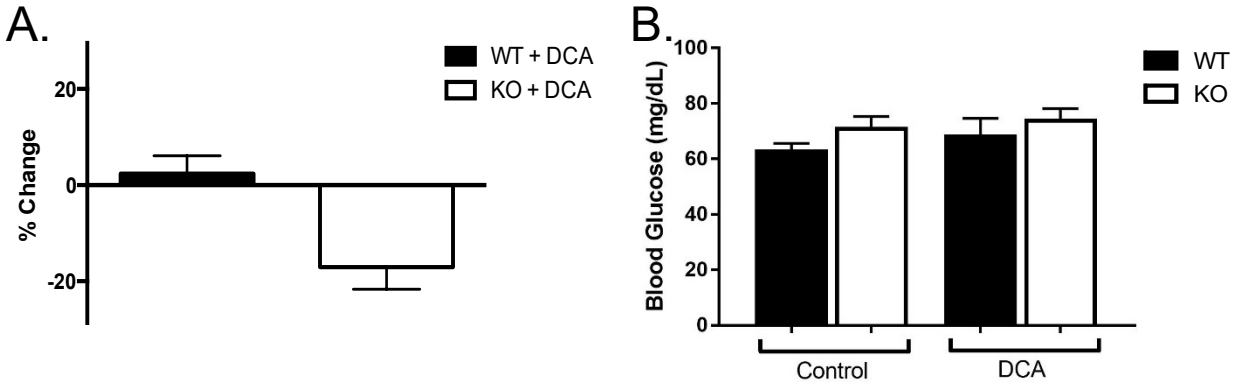

Activation of PDH decreases exercise capacity in the PP2Cm$^{-/-}$. A) Change in endurance capacity in mice given DCA prior to exercise compared to untreated controls (N = 6, P < .01) B) Blood glucose levels post exercise (exhaustion) in control and DCA treated groups (N = 6, P = N.S).

Figure 2.6

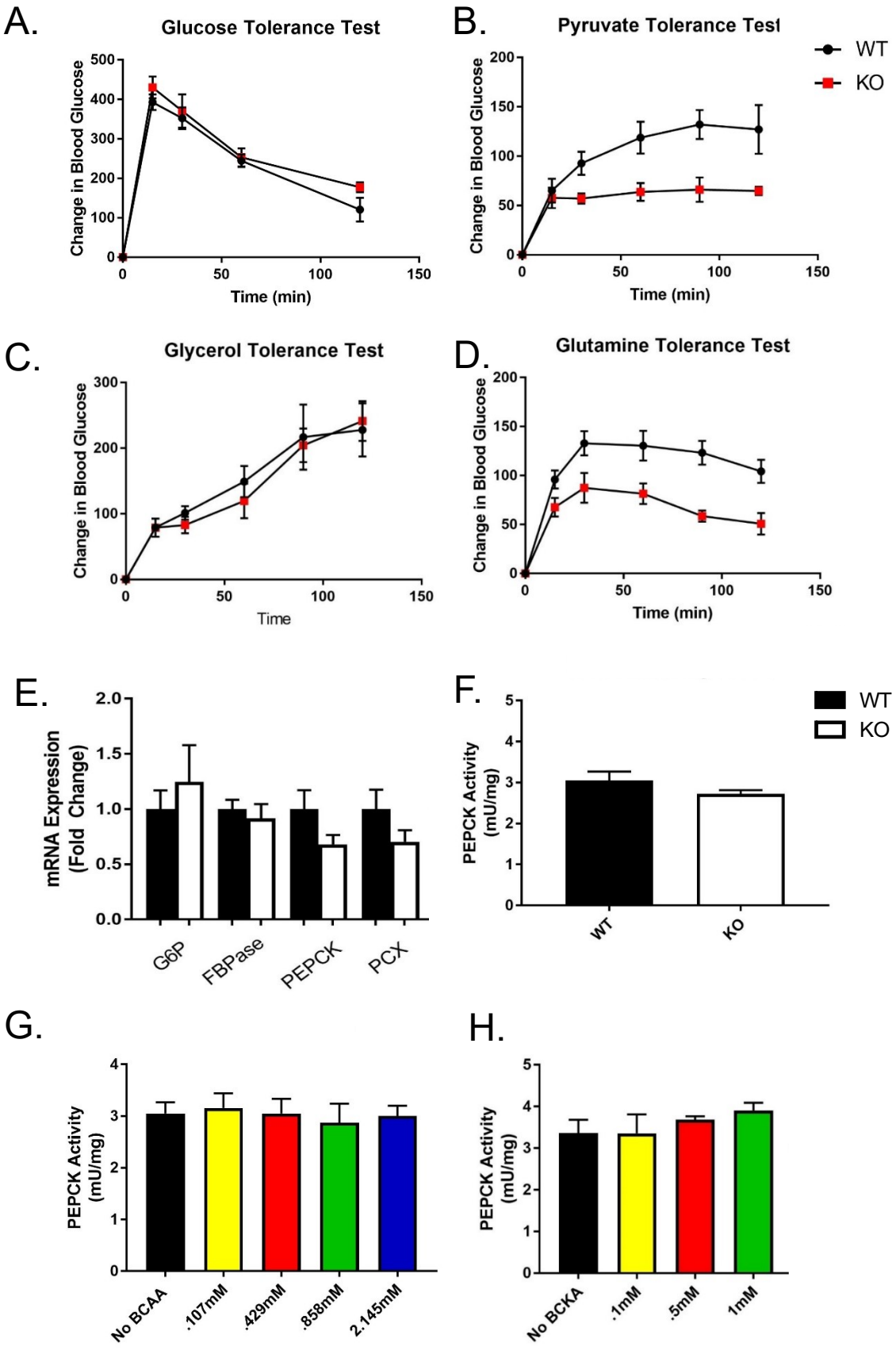
A.
Glucose Tolerance Test
Change in Blood Glucose
Time (min)
B.
Pyruvate Tolerance Test
WT
KO
Change in Blood Glucose
Time (min)
C.
Glycerol Tolerance Test
Change in Blood Glucose
Time
D.
Glutamine Tolerance Test
Change in Blood Glucose
Time (min)
E.
mRNA Expression (Fold Change)
G6P
FBPase
PEPCK
PCX
F.
WT
KO
PEPCK Activity (mU/mg)
WT
KO
G.
PEPCK Activity (mU/mg)
No BCAA
.107mM
.429mM
.858mM
2.145mM
H.
PEPCK Activity (mU/mg)
No BCKA
.1mM
.5mM
1mM

PP2Cm$^{-/-}$ mice have impaired liver glucose homeostasis. A) Glucose tolerance test (P = N.S, N = 5 per group), B) pyruvate tolerance test (P < .01, N = 6 per group), C) glycerol tolerance test (P = N.S, N = 5-6 per group) and D) glutamine tolerance test (P < .01, N = 5-9 per group). E) mRNA expression for regulators of gluconeogenesis. F) The PEPCK activity in WT and KO livers (N = 6) G) The average PEPCK activity at each [BCAA] measured as nanomole of NADH generated per min at pH 7.5 at 37C (mU, n = 3). H) The average PEPCK activity at each [BCKA] measured as nanomole of NADH generated per min at pH 7.5 at 37C (mU, n = 3).

Figure 2.7

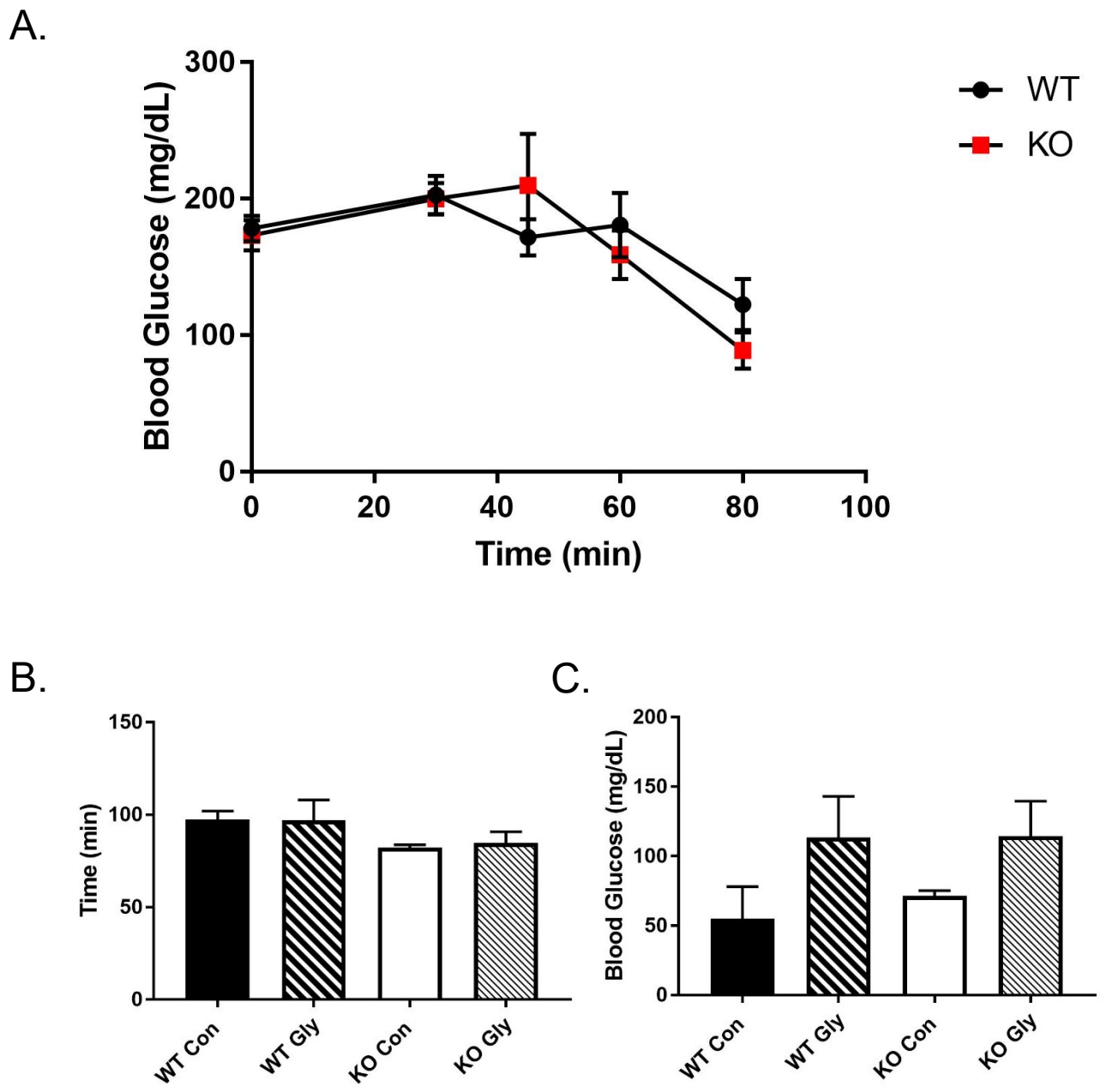

Blood glucose levels are not altered in the PP2Cm$^{-/-}$ mouse during exercise. A) Blood glucose measured at sedentary (baseline), intermediate and exhaustion time points during an exercise capacity test (N = 6, P = NS). B) Run time and C) blood glucose levels in mice after receiving a dose of saline (con) or glycerol (gly).

Table 1: RT-PCR Primers

G6Pase	Fw	CGACTCGCTATCTCCAAGTGA
	Rv	GTTGAACCAGTCTCCGACCA
FBPase	Fw	CAGGGACGTGAAGATGAAGAAGAA
	Rv	TTGTTGGCGGGGTATAAAAAGA
PEPCK	Fw	GGTGCATGAAAGGCCGCACCATGTA
	Rv	GGTTGCAGGCCCAGTTGTTGACCA
Pcx	Fw	GATGACCTCACAGCCAAGCA
	Rv	GGGTACCTCTGTGTCCAAAGGA
PGC-1a	Fw	AGCCGTGACCACTGACAACGAG
	Rv	GCTGCATGGTTCTGAGTGCTAAG

2.6 References

1) Mero, A., *Leucine supplementation and intensive training.* Sports Med, 1999. 27(6): p. 347-58.
2) Glynn, E.L., et al., *Impact of combined resistance and aerobic exercise training on branched-chain amino acid turnover, glycine metabolism and insulin sensitivity in overweight humans.* Diabetologia, 2015. 58(10): p. 2324-35.
3) Greer, B.K., et al., *Branched-Chain amino acid Supplementation and Indicators of Muscle damage after endurance excercise.* International Journal of Sport Nutrition and Exercise Metabolism, 2007.
4) Coombes, J.S. and L.R. McNaughton, *Effects of branched-chain amino acid supplementation on serum creatine kinase and lactate dehydrogenase after prolonged exercise.* J Sports Med Phys Fitness, 2000. 40(3): p. 240-6.
5) Shimomura, Y., Murakami T, Nakai N, Obayyashi M, Li Z, Xu M, Sato Y, Kato T, Shimomura N, Fujitsuka N, Tanaka K, Sato M, *Suppression of glycogen consumption during acute exercise by dietary branched-chain amino acids in rats.* J Nutr Sci Vitaminol (Tokyo), 2000. 46(2): p. 71-7
6) Kainulainen, H., J. Hulmi, and U. Kujala, *Potential Role of Branched-Chain Amino Acid Catabolism in Regulating Fat Oxidation.* 2013.
7) Harper, A.E., R.H. Miller, and K.P. Block, *Branched-chain amino acid metabolism.* Annu Rev Nutr, 1984. 4: p. 409-54.
8) Crowe, M.J., J.N. Weatherson, and B.F. Bowden, *Effects of dietary leucine supplementation on exercise performance.* Eur J Appl Physiol, 2006. 97(6): p. 664-72.
9) Shimomura, Y, Honda T, Shiraki M, Murakami T, Sato J, Kobayashi H, Mawatari K, Obayashi M, Harris RA. *Branched-Chain Amino Acid catabolism in excercise and liver disease.* The Journal of Nutrition, 2006.

10) Lu, G., Sun H, She P, Youn JY, Warburton S, Ping P, Vondriska TM, Cai H, Lynch CJ, Wang Y. l., *Protein phosphatase 2Cm is a critical regulator of branched-chain amino acid catabolism in mice and cultured cells.* J Clin Invest, 2009. 119(6): p. 1678-87.
11) Neinast MD, Jang C, Hui S, Murashige DS, Chu Q, Morscher RJ, Li X, Zhan L, White E, Anthony TG, Rabinowitz JD, Arany Z. *Quantitative Analysis of the Whole-Body Metabolic Fate of Branched-Chain Amino Acids*, Cell Metabolism. 2019 Feb 5;29(2):417-429.e4
12) Trefts E, Williams A, Wasserman D. *Exercise and the Regulation of Hepatic Metabolism*, Prog Mol Biol Transl Sci. 2015 ; 135: 203–225.
13) Brooks G, Mercier J. *Balance of carbohydrate and lipid utilization during exercise: the crossover concept*. Americal Physiological Society, 1994 Jun;76(6):2253-61.
14) Brooks GA, *The lactate shuttle during exercise and recovery*. Med Sci Sports Exerc. 1986 Jun 18(3):360-8.
15) Brooks GA, *Amino acid and protein metabolism during exercise and recovery*. Med Sci Sports Exerc. 1987 Oct;19(5 Suppl):S150-6.
16) Newgard, C.B., et al., *A branched-chain amino acid-related metabolic signature that differentiates obese and lean humans and contributes to insulin resistance.* Cell Metab, 2009. 9(4): p. 311-26.
17) Shah, S.H., et al., *Branched-chain amino acid levels are associated with improvement in insulin resistance with weight loss.* Diabetologia, 2012. 55(2): p. 321-30.
18) Shah, S.H., et al., *Association of a peripheral blood metabolic profile with coronary artery disease and risk of subsequent cardiovascular events.* Circ Cardiovasc Genet, 2010. 3(2): p. 207-14.
19) Tai, E.S., et al., *Insulin resistance is associated with a metabolic profile of altered protein metabolism in Chinese and Asian-Indian men.* Diabetologia, 2010. 53(4): p. 757-67.

20) Huffman, K.M., et al., *Relationships between circulating metabolic intermediates and insulin action in overweight to obese, inactive men and women.* Diabetes Care, 2009. 32(9): p. 1678-83.

21) Beylot, M., et al., *Perilipin 1 ablation in mice enhances lipid oxidation during exercise and does not impair exercise performance.* Metabolism, 2012. 61(3): p. 415-23.

22) Gibala MJ, MacLean DA, Graham TE, Saltin B. *Tricarboxylic acid cycle intermediate pool size and estimated cycle flux in human muscle during exercise*. Am J Physiol. 1998 Aug; 275(2): E235-42.

23) Li, T., et al., *Defective Branched-Chain Amino Acid Catabolism Disrupts Glucose Metabolism and Sensitizes the Heart to Ischemia-Reperfusion Injury.* Cell Metab, 2017. 25(2): p. 374-385.

24) Rui L. *Energy metabolism in the liver*. Compr Physiol. 2014 January ; 4(1): 177–197.

25) Shimomura, Y., Murakami T, Makai N, Magasaki M, Harris R, *Exercise promotes BCAA catabolism: effects of BCAA supplimentation on skeletal muscle during exercise*. The Journal of Nutrition, 2004

26) Egan B, Zierath JR. *Exercise metabolism and the molecular regulation of skeletal muscle adaptation*. Cell Metabolism. 2013 Feb 5;17(2):162-84.

27) Shimomura, Y, Honda T, Shiraki M, Murakami T, Sato J, Kobayashi H, Mawatari K, Obayashi M, Harris RA. *Branched-Chain Amino Acid catabolism in excercise and liver disease.* The Journal of Nutrition, 2006.

28) Chung ST, Chacko SK, Sunehag AL, Haymond MW. *Measurements of Gluconeogenesis and Glycogenolysis: A Methodological Review*. Diabetes. 2015 Dec;64(12):3996-4010.

29) Gray L, Sultana R, Rauckhorst A, Oonthonpan L, Tompkins S, Sharma A, Fu X, Miao R, Pewa A, Brown K, Lane E, Ashley Dohlman A, Zepeda-Orozco D, Xie J, Rutter J, Norris A, Cox J, Burgess S, Potthoff M, Taylor E. *Hepatic Mitochondrial Pyruvate Carrier 1 is*

Required for Efficient Regulation of Gluconeogenesis and Whole-body Glucose Homeostasis Cell Metabolism. 2015 October 6; 22(4): 669–681.

Chapter 3

Determining the role of branched chain amino acid metabolism in the perfused heart using stable isotope tracing and gas chromatography mass spectrometry

3.1 Introduction

A common feature of cardiac dysfunction and susceptibility to injury is dysregulation of cardiac energy metabolism[1]. Recent studies have highlighted the importance of regulating the metabolism of the three essential branched-chain amino acids (BCAAs) leucine, isoleucine and valine, which are significantly altered during the development of cardiovascular and metabolic disease[2-6]. Application of metabolomics technology has shown that blood levels of BCAAs and associated catabolites are strongly and positively correlated with the development of coronary heart disease and insulin resistance[4-6] and that this BCAA-related metabolite signature is predictive of responsiveness to therapeutic interventions[7-8].

The rate-limiting step in BCAA catabolism is branched-chain ketoacid (BCKA) decarboxylation in the mitochondria catalyzed by branched-chain ketoacid dehydrogenase (BCKDH). Phosphorylation of BCKDH by BCKD kinase (BDK) inactivates the enzyme[9] ,and dephosphorylation by a mitochondria localized phosphatase 2C (PP2Cm) is responsible for the activation of the complex[10]. Deletion of PP2Cm in mice resulted in higher levels of plasma BCAA and BCKA, sensitized the heart to ischemia reperfusion injury, and reduced glucose utilization in a perfused heart model[11]. These findings highlight the importance of understanding the cellular metabolism of BCAAs and their impact on cardiovascular substrate utilization.

Metabolic homeostasis in the heart requires a balance between carbohydrate and fatty acid utilization, as well as anaplerotic and cataplerotic reactions to balance the TCA cycle[12]. Anaplerosis refers to metabolic pathways that replenish citric acid cycle intermediates, while cataplerosis refers to the removal of intermediates to prevent accumulation in the mitochondrial matrix. Anaplerosis is essential for normal function of the heart, and increasing anaplerotic flux, particularly in the setting of cardiac disease, has typically been considered beneficial[13].

Balancing the levels of TCA cycle intermediates (TCAi) are crucial for the normal functioning and regulation of the cycle. Metabolic pathways that are potential sites for anaplerosis and cataplerosis include; (i)pyruvate carboxylation (PC) to oxaloacetate (OAA), (ii) malate decarboxylation to pyruvate, (iii) transamination of a-KG to glutamate, (iv) transamination of OAA to aspartate, and (v) formation of succinyl-CoA from propionyl-CoA precursors such as the branched chain amino acids[14]. In order to determine the effect of dysregulated BCAA catabolism on metabolic homeostasis in the heart, we used a ^{13}C mass spectrometry approach to measure substrate fluxes in the perfused hearts of WT and PP2Cm KO mice.

Mass spectrometry (MS) is a sensitive, reliable, and highly accurate method for the measurement of isotopic labeling, making it particularly useful for the detection of mass isotopomers of low concentration metabolites[15]. Gas-chromatography mass spectrometry (GC/MS) is particularly effective in the analysis of primary metabolites, specifically those involved in central carbon metabolism. TCA cycle intermediates are present in very low concentrations, usual <2 µmol of total intermediates per gram tissue, with OAA being present in miniscule concentrations (5-10 nmol/g) [12]. While the measurement of metabolite concentrations can be very informative regarding metabolism and metabolic changes in cells, this information is incomplete. Steady-state concentrations of metabolite levels provide relatively little insight into the dynamics of cellular metabolism. Many metabolites can be found in a number of different metabolic pathways, with different metabolic precursors and products. Quantitative analysis of such metabolites does not distinguish the same metabolites derived from multiple pathways[16].

To circumvent this issue, stable isotope tracer (SIT) based metabolite profiling provides insights into the functions and dynamics of specific anaplerotic and cataplerotic pathways[17]. In SIT studies, cells or tissues are supplied with single or multiple isotope tracers such as uniformly or site specific ^{13}C-labeled glucose, which enable measurements of its consumption as well as concentrations of the fractions of the downstream metabolites of the isotope tracer. Tracing the number and distribution of ^{13}C carbons in downstream intermediates can be crucial for

unambiguously distinguishing different pathways involving the same metabolite (for example pyruvate entering TCA cycle through pyruvate carboxylase or pyruvate dehydrogenase) [12]. In the present study, we utilized stable isotope labeling in the perfused heart to determine the effects of elevated BCAA levels on glucose utilization in the heart.

2.2 Materials and Methods

2.2.1 Animal Models

All animal experiments were performed with the approval of the Institutional Animal Care and Use Committee of the University of Washington. Mice were weaned at 21 days of age (P-21). KO mice were housed with littermate controls. Homozygous PP2Cm-knock out mice were developed by Dr. Wang as previously described[10]. In brief, a LacZ-expression cassette was inserted into the translational initiation site of the PP2Cm allele, while replacing the major portion of exon 2 of the mouse PP2Cm gene on a C57BL6 background. Loss of PP2Cm in genetic models impaired BCAA catabolism, increased oxidative stress, and decreased cardiovascular glucose oxidation and utilization[10-11].

2.2.2 Heart Perfusions

Isolated mouse hearts were perfused in Langendorff mode as previously described[18]. Fed male KO and WT mice (age 10-12 weeks) weighing 23-26g were heparinized (100 U intraperitoneally) and anesthetized by intraperitoneal injection of sodium pentobarbatol (150mg/kg). The hearts were quickly isolated and mounted on a Langendorff apparatus and perfused at a constant perfusion pressure of 80 mmHg with phosphate-free Krebs-Henseleit (KH) buffer containing (mM): 118 NaCl, 25 $NaHCO_3$, 5.3 KCl, 2 $CaCl_2$, 1.2 $MgSO_4$, 0.5 EDTA and one of the following two different combinations of substrates: “glucose/pyruvate buffer” (containing 10 mM glucose and 0.5 mM pyruvate) or “mixed-substrate buffer” (containing 5.5 mM glucose, 0.4 mM mixed long-chain fatty acids bound to 1% albumin, 1 mM lactate, and 50 μU/mL insulin). A

subset of hearts were perfused with physiological levels of BCAAs (.429mM), containing 145.9 μM leucine, 85.8 μM isoleucine, and 197.3 μM valine. The perfusate was equilibrated with 95% O_2 and 5% CO_2 (pH 7.4) and maintained at 37 °C throughout the experimental protocol[11].

The following parameters were continuously monitored through instruments linked to a computer; (i) buffer temperature using a thermocouple, (ii) perfusion pressure using a pressure sensor, and (iii) contractile function using a plastic balloon filled with water inserted into the left ventricular cavity and connected to a pressure sensor, which allowed for measurement of heart rate, systolic and diastolic function. Balloon volume was set to keep end diastolic pressure (EDP) between 5-10 mmHg. Coronary flow was monitored by measuring flow-through volume every several min. For perfusion with ^{13}C glucose, hearts underwent 5 min of stabilization with unlabeled glucose/pyruvate buffer, then 15-20 min of equilibration with unlabeled mixed substrate buffer before labeling with mixed-substrate buffer containing 99% [U-$^{13}C_6$]glucose for 40 min (Figure 3.1). At the end of the experiment hearts were freeze clamped and stored in liquid nitrogen.

3.2.3 Metabolite Extraction GCMS

For metabolomics analysis, frozen mouse cardiac tissue (20-25 mg) specimens were mixed with a 1.2 mL mixture of cold methanol/chloroform (1:2 v/v; 4 ^oC) and homogenized using a *Tissue Tearor* homogenizer (Biospec) and sonicated for 20 seconds. A further 800 μL cold chloroform/distilled water solution (1:1 v/v) was added, the sample was then vortexed and set aside for 30 min on ice to separate the solvent layers. After centrifugation at 2000 rpm for 20 min, the aqueous (top) layer was separated and filtered using a 1.5 mL 0.2 μm syringe filter and 150 μL was dried using Vacufuge Plus (Eppendorf) and used for each analysis.

To prepare the samples for GC/MS analysis, 30 μL of 20 mg/mL methoxyamine hydrochloride dissolved in pyridine was added to the dried aqueous layer and incubated at 37 ^oC for 90 min. After that, samples were derivatized with 70 μL of N-methyl-N-tert-butyldimethylsilyl trifluoroacetamide (MTBSTFA) was added and incubated at 37^oC for 30 min.

2.2.4 GCMS Conditions

All metabolites were analyzed using an Agilent 7890B GC coupled to a 5977A MS. Samples were reported chromatographically using a HP-5MS UI capillary column (30 m, .2-mm inner diameter, .33 um film thickness). The injector was heated at 250 ^{o}C and operated in pulsed splitless mode with helium maintained at 1mL/min for the duration of the separation. The sample was introduced at an initial oven temperature of 60 °C, held for 1 min, then ramped 10°C/min to a final temperature of 320 °C, and held for 5 min. The total run time was 32 min. The mass spectrometer was operated in the electron impact mode. For each metabolite, we monitored the signals at the nominal *m/z* (M0) and at all detectable naturally labeled mass isotopomers (M1, M2, and M3…etc) (Fig 3.2a). Interpretation of the ^{13}C-mass isotopomer distribution (MID) of TCA metabolites (citrate, isocitrate, aKG, succinate, malate, fumarate and pyruvate) and associated metabolites (aspartate, glutamate/glutamine, lactate, alanine, pyruvate) in perfused hearts was determined according to published GCMS methods (Fig 3.2b)[12,15].

3.2.5 Statistical Analysis

All data are presented as mean ± SEM. An unpaired Student's t test was used to detect significant differences when two groups were compared. One-way or two-way ANOVA was used to compare the differences among three or more groups. ANOVA with repeated measures was used for multiple group comparisons over multiple time points. Bonferroni post hoc analysis was used for all ANOVAs as applicable (SPSS 16.0 software). The p values <0.05 were considered statistically significant.

3.2 Results

BCAA concentrations in the perfusate directly alters BCAA concentrations in the perfused heart

We used GCMS to measure metabolite levels in KO mice and littermate controls (WT). As expected, systemically impaired BCAA catabolism in the KO elevates cardiac BCAA levels between 3-4 fold higher than baseline (Fig 3.3a). Isolated heart perfusion with Krebs buffer normalizes BCAA levels between WT and KO hearts (Fig 3.3b). BCAA levels in the perfusate linearly alters BCAA levels in cardiac tissue after an hour of perfusion (which included 5 min stabilization with glucose/pyruvate buffer and 40 min perfusion with mixed substrate buffer) (Fig 3.1). BCAA levels in hearts post perfusion are directly reflected by the level of BCAA added to the perfusion buffer. Perfusion with 0 mM BCAAs decreased endogenous BCAA levels in WT heart. Perfusion with .2 mM BCAAs raised BCAA levels to that comparative to the WT, and perfusion with physiological levels of BCAAs (.429 mM) most closely corresponds to BCAA levels in the KO heart (Fig 3.3c).

Because perfusion without BCAAs normalized the increased BCAA levels in KO tissue, we chose to focus on the effect of elevated BCAA levels on glucose utilization in WT hearts with and without BCAAs in the perfusion buffer. The concentration of substrates in the perfusate were chosen to be close to physiological values. Hearts were perfused with unlabeled mixed-substrate buffer for 20 min, then switched over to mixed substrate buffer containing a mixture of fatty acids plus uniformly labeled ^{13}C-glucose. TCA cycle intermediates and their associated amino acids were measured by GCMS.

BCAAs deplete TCA cycle intermediate pool size

The incorporation of ^{13}C-labeled glucose into downstream intermediates can be determined by measuring the relative abundance of ^{13}C carbons within each metabolite pool. Perfusion with physiological or elevated levels of BCAAs did not affect overall ^{13}C pool size in pyruvate and TCAi (Fig 3.4a). However, increasing BCAA levels to physiological concentrations (.429 mM) decreased total pyruvate pool size by 50%, citrate pool size by 35% in the presence

of .429 mM BCAA and ~75% in the presence of 1.2 mM BCAA, α-KG pool size by ~70-80%, fumarate pool size by ~60%, and malate pool size by ~65% in the presence of .429 mM BCAA and ~75% in the presence of 1.2 mM BCAA. This reduction in intermediate pool size increased the ratio of $^{13}C/^{12}C$ for TCA cycle intermediates (Fig 3.4b). BCAAs also altered the labeling and quantity of cataplerotic amino acids. Addition of BCAAs increases aspartate pool size by approximately 3-fold and the $^{13}C/^{12}C$ ratio from ~30% to 50%. High BCAAs increase the $^{13}C/^{12}C$ ratio of glutamate from ~30% to ~50% without significantly changing the metabolite pool size (Fig 3.4c). These data indicate that elevated BCAA levels impact carbon flux into and out of the TCA cycle.

BCAAs alter the labeling pattern of TCA cycle intermediates

This data can also be illustrated by the ^{13}C labeling pattern of each metabolite (Fig 3.2b and Fig 3.5). MS identifies metabolites based on their mass to charge ratio (m/z), and each ^{13}C carbon increases the mass of its metabolite by +1 without altering the charge, so unlabeled metabolites are designated my M, while metabolites containing 1-^{13}C carbon are designated M+1, 2-^{13}C carbon designated by M+2, etc. (Fig 3.2a). Labeled citrate in WT hearts perfused without BCAA has a high M+2 peak (~20% labeling) with low M+5 and M+6 peaks (7% and 2% labeling, respectively) (Fig 3.5a). This labeling pattern is caused by the combination of unlabeled oxaloacetate (OAA) with [1,2-^{13}C]acetyl-CoA to form citrate containing two labeled carbons (Fig 3.2b). Addition of BCAAs to the perfusion buffer shifts this pattern, resulting in a citrate pool with relatively low M+2 levels (~12% labeled) and high M+5 levels (~25% labeled) (Fig 3.5a). This labeling pattern is due to increased conversion of [U-^{13}C]pyruvate to [1,2,3-^{13}C]OAA by pyruvate carboxylase (PC), which combines with [1,2-^{13}C]acetyl-CoA to form citrate with 5 labeled carbons (Fig 3.2b). A similar pattern is seen in the labeling pattern of aspartate. The addition of BCAAs in the perfusate shifts the labeling pattern of aspartate from mainly unlabeled (M+0) to having high M+3 and M+4 peaks (Fig 3.5b). Addition of BCAAs also increases the conversion of [U-^{13}C]pyruvate to [U-^{13}C]alanine, as seen by the higher M+3 alanine pool, and decreases the

labeled M+2 pool (Fig 3.5c). Addition of BCAAs has no effect on the labeling pattern of lactate (Fig 3.5d). These data indicate that elevated BCAAs impact the carbon flux through pathways regulating glucose entry into the TCA cycle.

3.4 Discussion

In the present study, we demonstrate that the level of BCAAs plays an important role in regulating glucose and TCA cycle metabolism in the perfused heart. WT hearts perfused with [U-^{13}C] glucose in the presence of physiological levels of BCAAs show a depletion of total pyruvate and TCAi pool size, increased labeling in anaplerotic substrates, and a shift in ^{13}C labeling pattern towards M+3, M+4, and M+5 isotopomer distributions. Our findings in the perfused heart demonstrate that this effect of central carbon metabolism is directly caused by increased BCAA levels, rather than by the suppression of decreased BCAA catabolism. This study also presents our labeling data in three different formats; by pool size, percent enrichment, and by labeling pattern. These three formats can lead to different interpretations when taken independently, thereby emphasizing the importance of developing multiple views of the data.

Metabolic comparison of WT hearts at baseline or perfused with different concentrations of BCAAs demonstrates that metabolite levels vary dramatically based on the substrate composition of the perfusion buffer. The concentration of BCAAs in the perfusion buffer directly impacted the final concentrations of BCAAs in cardiac tissue, regardless of genotype. This illustrates the importance of carefully considering what should be included in the perfusate, as the addition of different substrates will directly influence metabolite levels in the beating heart. Because perfusion without BCAAs normalized the increased BCAA levels in KO tissue, and the concentration of BCAAs in the perfusate dictated the BCAA levels in the WT heart, it was decided to study glucose metabolism in a WT cohort perfused with +/- BCAAs rather than comparing the WT and the KO. There is still debate as to whether the correlation between elevated BCAAs and metabolic disorder is due to increased systemic BCAA levels or suppressed catabolism, so this

approach focused solely on the effect of elevated BCAAs on substrate utilization and energetics in the perfused WT heart.

To determine if elevated BCAA levels negatively impact glucose metabolism. WT hearts were perfused with uniformly labeled glucose and varying concentrations of the three BCAAs and then assayed for ^{13}C incorporation into downstream intermediates. Although the pool of ^{13}C labeled metabolites was not affected by increasing BCAA levels, addition of BCAAs in the buffer decreases TCA intermediate pool size. This change resulted in increased $^{13}C/^{12}C$ ratios for the TCA cycle intermediates. There are two ways of presenting these data (Fig 3.4a and 3.4b) that provide very different insights. At first glance the Fig 3.4b shows that increasing levels of BCAAs increases $\%^{13}C$ enrichment for each metabolite, and this could be interpreted as increasing BCAA concentration increases glucose utilization and incorporation into the TCA cycle. However, when the data are presented as in Figure 3.4a, it is clear that although the relative levels of ^{13}C enrichment in each metabolite pool remains constant, addition of BCAAs in the buffer depletes pyruvate and TCAi pool size. Changing the data presentation parameters thus changes the overall conclusion.

The reason high BCAA levels deplete TCA cycle intermediates is shown by the $^{13}C/^{12}C$ ratios and the pool size of two anaplerotic metabolites, aspartate and glutamate. (Fig 3.4c) Addition of BCAAs increases both the aspartate pool size and the $\%^{13}C$ enrichment. One possible explanation for this phenotype is related to a previous study demonstrating that elevated BCAA levels has an inhibitory effect on PDH activity in the heart[11]. In the presence of high BCAAs, labeled pyruvate derived from [U-^{13}C]glucose enters the TCA cycle through PC as OAA rather than through PDH as acetyl-CoA, increasing the OAA pool. Excess OAA can exit the TCA cycle through aspartate. This results in more ^{13}C carbons from glucose entering the aspartate pool, and increased aspartate pool size.

Addition of BCAAs increases the $\%^{13}C$ enrichment in the glutamate pool without significantly increasing its pool size. The conversion of BCAAs to the branched chain keto-acids

(BCKAs) is a transamination reaction paired with the conversion of α-KG to glutamate. This reaction draws carbons out of the TCA cycle (cataplerosis), and could partially explain the depletion of TCA cycle intermediates seen post-perfusion. In order to maintain metabolic homeostasis in the perfused heart, it may also be necessary to add anaplerotic amino acids into the perfusate to counteract the cataplerotic effect of the BCAAs.

The ^{13}C labeling pattern of TCA cycle intermediates and related metabolites also provides supporting evidence for PDH as a key regulatory point through which BCAAs modulate cardiac metabolism[11]. In hearts perfused without BCAAs, [U-^{13}C]glucose is converted to [U-^{13}C]pyruvate through glycolysis and unlabeled lactate is metabolized to unlabeled pyruvate through lactate dehydrogenase (LDH). These two isotopomers of pyruvate will be decarboxylated via PDH leading to the formation of either uniformly labeled acetyl-CoA or unlabeled acetyl-CoA. The oxidation of unlabeled fatty acids will also contribute to the unlabeled acetyl-CoA pool. Citrate synthase catalyzes the condensation of these two isotopomers of acetyl-CoA with unlabeled oxaloacetate (OAA) resulting in the formation of either M+0 (unlabeled) or M+2 citrate (Fig 3.2b).

[U-^{13}C]pyruvate can also enter the TCA cycle through carboxylation by PC to form [1,2,3-^{13}C]OAA. Thus, [1,2-^{13}C]acetyl-CoA can condense with either unlabeled OAA or with [1,2,3-^{13}C]OAA, resulting in either M+2 or M+5 citrate. Therefore, based on the labeling pattern of citrate one can determine the relative contributions of PDH and PC in supplying pyruvate to the TCA cycle (Fig 3.2b). WT hearts perfused without BCAA show a high M+2 peak with low M+5 and M+6 peaks in citrate. Addition of BCAAs to the perfusion buffer shifts this pattern, resulting in a citrate pool with relatively low M+2 levels and high M+5 levels. This data agrees with previous studies from the Tian lab that demonstrate elevated levels of BCAAs directly inhibit the activity of purified PDH[11].

The shift from PDH to PC can also be seen in the labeling pattern of aspartic acid. The addition of BCAAs increases the conversion of OAA to aspartate, increasing the pool size and $^{13}C/^{12}C$ ratio. Despite our inability to measure OAA via GCMS, we can interpret its labeling pattern

based on the labeling of aspartate. The addition of BCAAs in the perfusate shifts the labeling pattern of aspartate from mainly unlabeled (high M+0) to high M+3 and M+4. This indicates that the OAA pool also has high levels of M+3 and M+4.

Addition of BCAAs also increases the conversion of [U-^{13}C]pyruvate to [U-^{13}C]alanine, as seen by the higher M+3 alanine pool. Inhibition of PDH would decrease the flow of pyruvate into the TCA cycle, shunting it into other pathways. When [U-^{13}C]pyruvate enters the TCA cycle through PDH it forms [1,2-^{13}C]citrate from unlabeled OAA and [1,2-^{13}C]acetyl-CoA. This M+2 labeled metabolite passes through the TCA cycle to form [1,2-^{13}C]malate, which converted to pyruvate through malic enzyme, forming [1,2-^{13}C]pyruvate. The disappearance of the 20% M+2 alanine peak in hearts perfused with BCAA supports the inhibition of this cycle by BCAAs.

Unlike most of the amino acids, which are degraded by the liver, BCAAs are oxidized extensively in extra hepatic tissue, allowing dietary BCAAs to appear in the bloodstream after a protein containing meal[7]. Plasma BCAA levels have been shown to act as a satiation signal in the brain to dictate whether the animal is in the fasted or the fed state, and whether the body should focus on breaking down dietary carbohydrates, proteins or fats[19]. There is no amino acid storage system, so dietary amino acids are either incorporated into skeletal muscle or broken down to make metabolic intermediates. This could be the cause of reduced glucose utilization, as high BCAA levels indicate to the heart that high levels of dietary protein are being consumed.

As the rate limiting enzyme for pyruvate oxidation, the activity of PDH serves as a set point for the relative contributions of carbohydrates versus fatty acids for the oxidative metabolism in the mitochondria[20]. Thus, by competing against glucose for oxidative degradation through modulating PDH activity, BCAAs and their catabolism play a pivotal role in the regulation of cardiac substrate metabolism. Supplementation with BCAAs preserves lean muscle mass and promotes oxidation of fatty acids[21]. This could be due to BCAAs competing against glucose for oxidative degradation, suppressing glucose utilization and promoting fatty acid utilization.

In conclusion, we demonstrate the effect of elevated BCAAs on regulating glucose catabolism and TCA cycle anaplerosis in the perfused heart. This study presents our labeling data in three different formats; by pool size, percent enrichment, and by labeling pattern, and demonstrates how multiple views of the data can shift interpretation. We show that increasing the concentration of BCAAs in the perfusion buffer depletes TCA cycle intermediates after an hour of perfusion, highlighting the importance of carefully considering the balance of amino acids and other substrates within the perfusate. BCAAs caused a shift in the labeling pattern in TCA cycle intermediates, highlighting their role of regulating the incorporation of pyruvate into the TCA cycle.

Figure 3.1

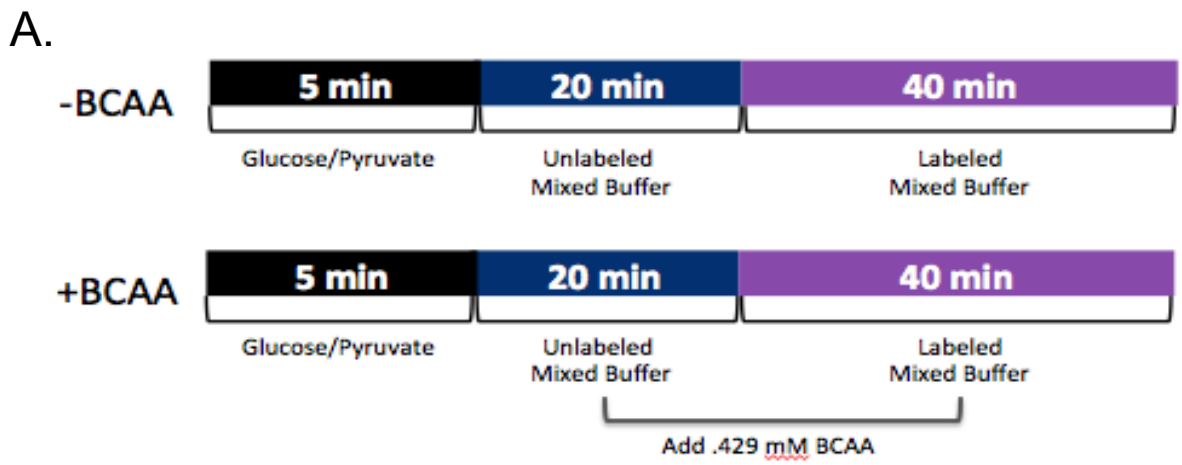

Isolated heart perfusion protocol. Hearts were perfused with buffer containing either unlabeled or [U-^{13}C]glucose, in the presence or absence of BCAAs (leucine, isoleucine, and valine).

Figure 3.2

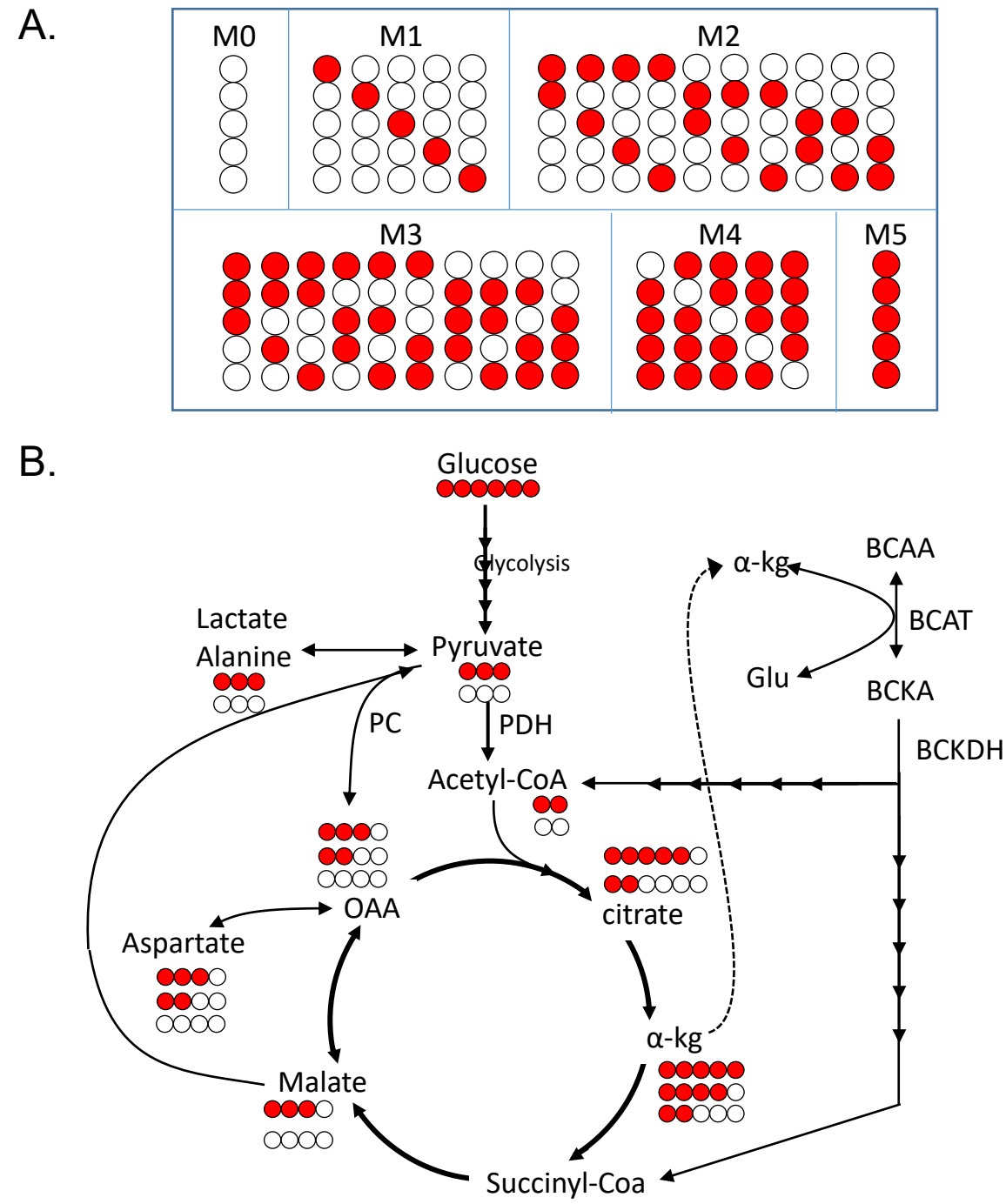

Mass isotopomer positons. A) Mass and positional isotopomers of all possible versions of a 5-carbon molecule containing either ^{12}C (open circles) or ^{13}C (closed circles). B) Schematic demonstrating the ^{13}C labeling of citrate and other citric acid cycle intermediates with [U-^{13}C]glucose as substrate. Unlabeled and ^{13}C-labeled pyruvate enters the TCA cycle via (1) decarboxylation through PDH to form M or M+0 to acetyl-CoA or (2) carboxylation via the anaplerotic pathway to M0 or M+3 OAA. The condensation of acetyl-CoA (M0 or M+2) with OAA (M0 or M+3) leads to the formation of various isotopomers of citrate.

Filled circle, ^{13}C; open circles, ^{12}C; PDH, pyruvate dehydrogenase; PC, pyruvate carboxylase; BCAT, branched chain amino transferase; BCKDH, branched-chain ketoacid dehydrogenase

Figure 3.3

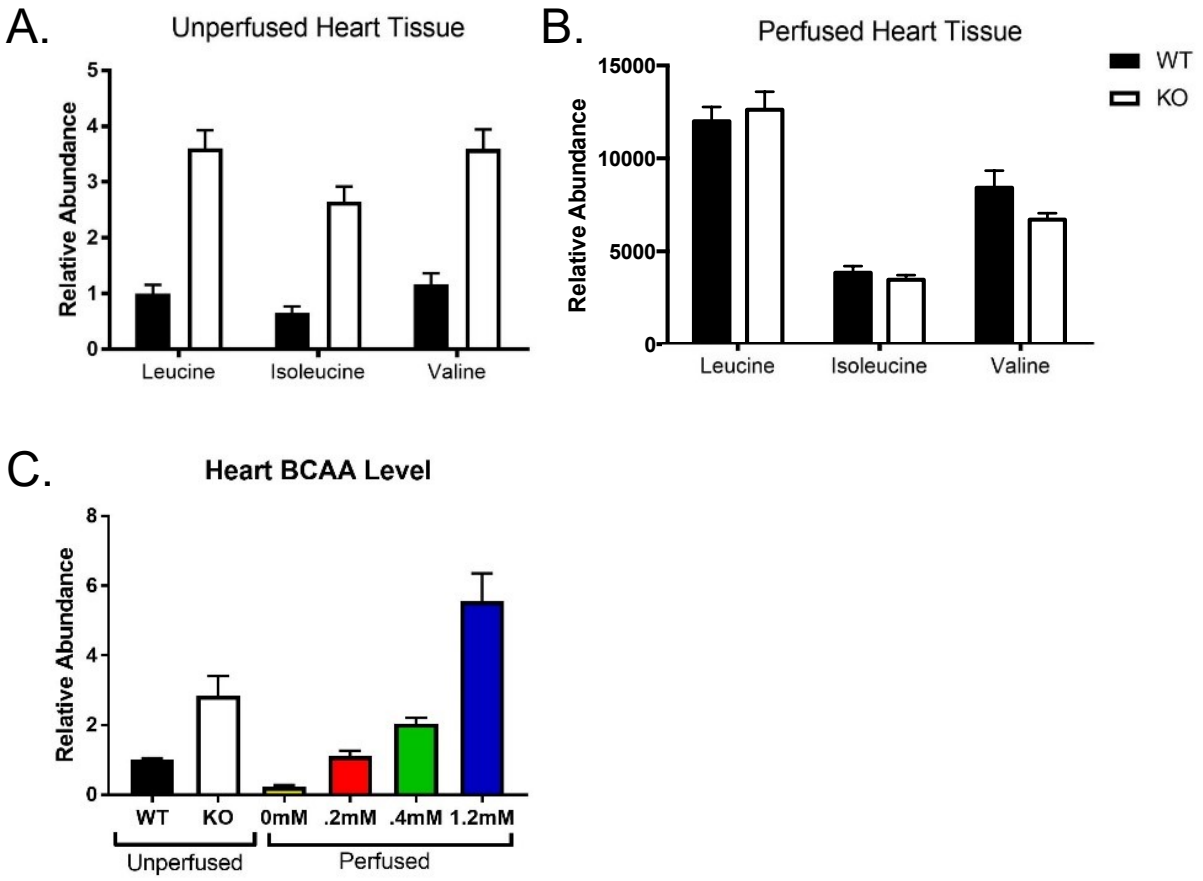

BCAA concentration in the perfusate directly alters BCAA concentration in the perfused heart. BCAA metabolite pool size in A) unperfused cardiac tissue (N = 4-5, P < .001) and B) perfused cardiac tissue (N = 4-5, P = NS). C) Relative abundance of BCAAs in either unperfused hearts or hearts perfused with varying concentrations of BCAAs (N = 2-4).

Figure 3.4

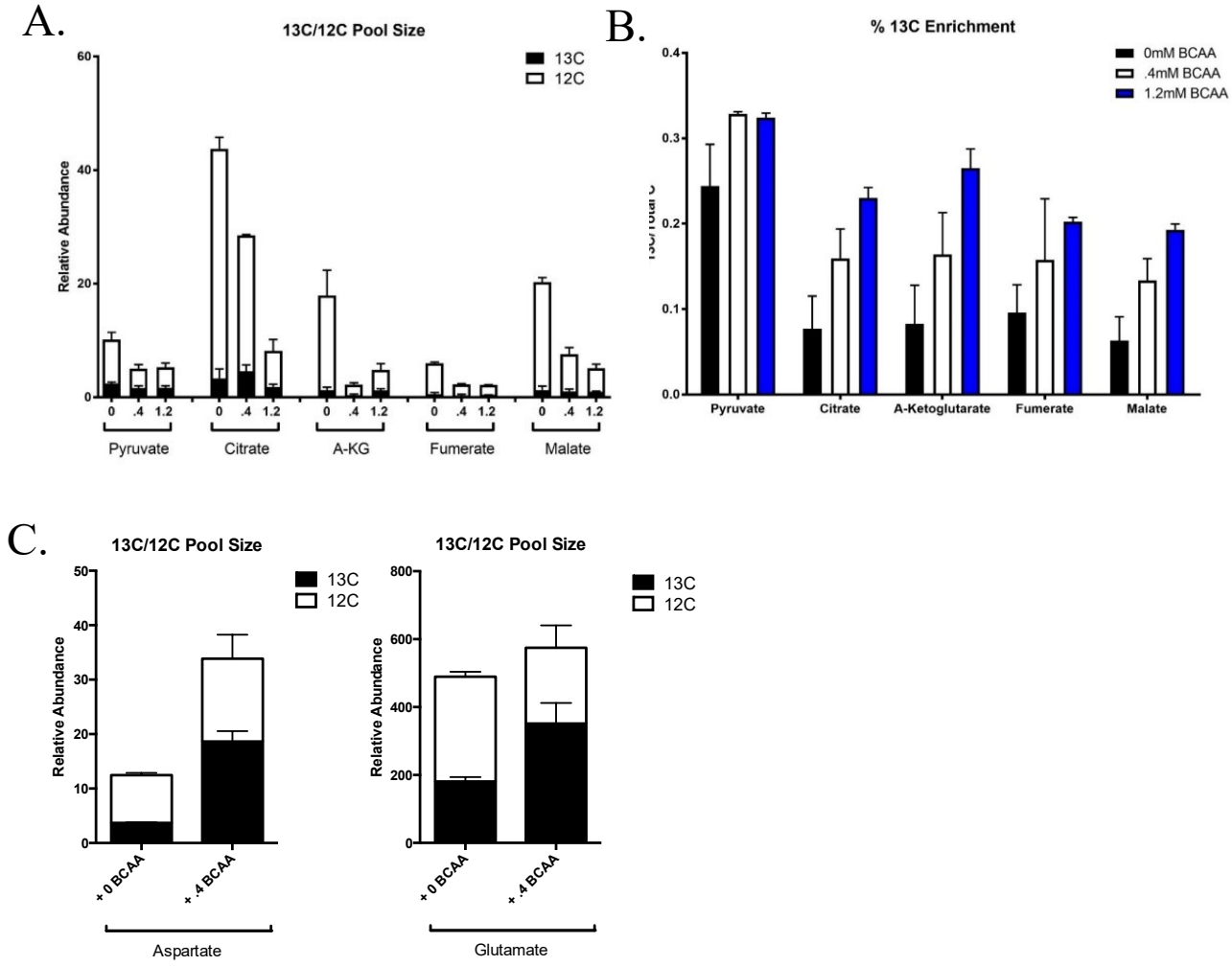

BCAAs deplete TCA cycle intermediate pool size. Pyruvate and TCA cycle intermediate levels in WT hearts after perfusion with either 0 mM, .429 mM or 1.2 mM BCAAs represented by A) relative abundance of ^{13}C labeled (black) and unlabeled (white) pool size (N = 2-3) and B) percent of ^{13}C/total pool size (N = 2-3). C) WT heart aspartate and glutamate levels after perfusion with 0 mM or .429 mM BCAAs represented by relative abundance of ^{13}C labeled (black) and unlabeled (white) pool size (N = 4-5).

Figure 3.5

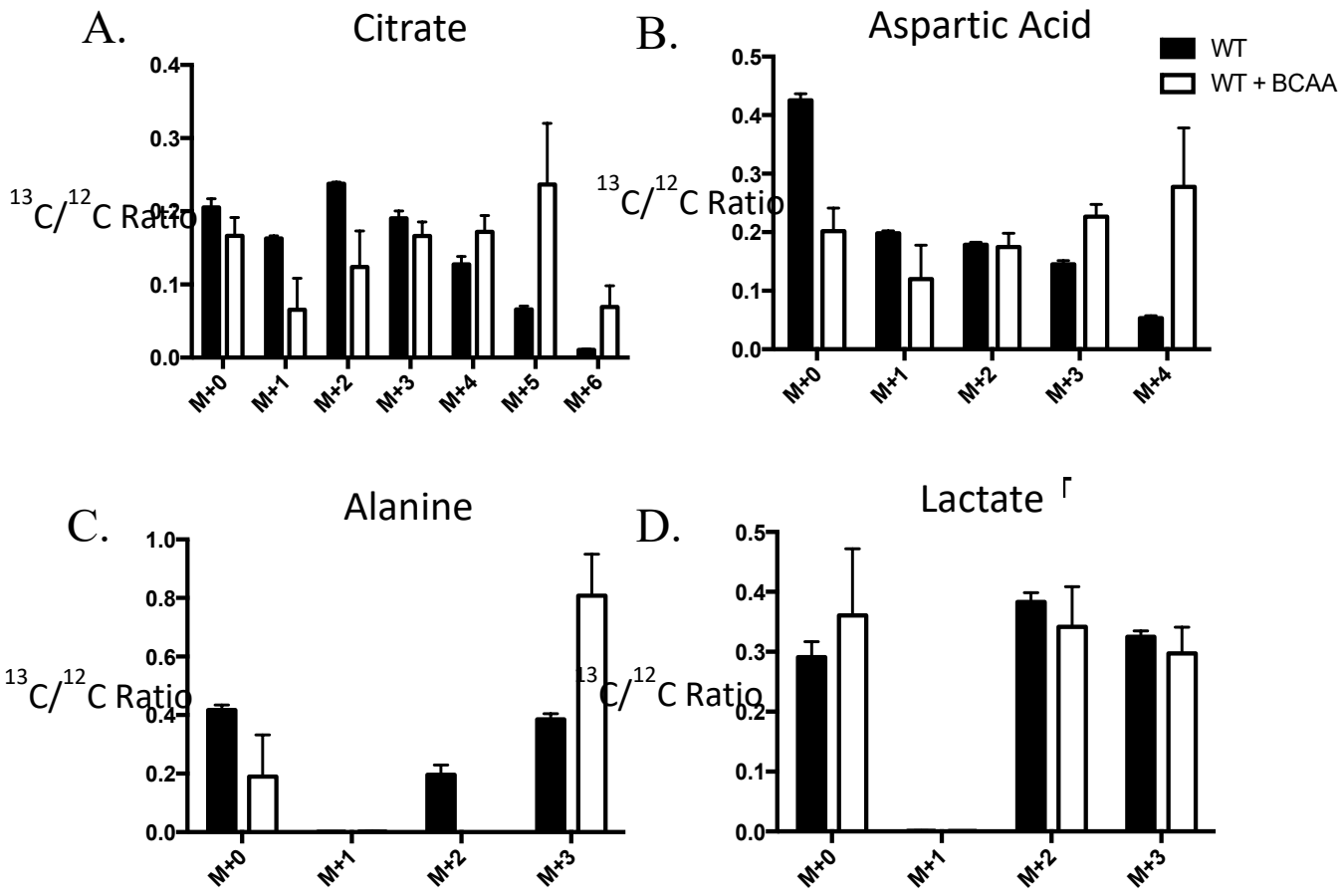

BCAAs alter the labeling pattern of TCA cycle intermediates from glucose. Mass isotopomer distribution of a) citrate, b) aspartic acid, c) alanine and d) lactate isolated from WT hearts perfused with [U-^{13}C]glucose in the presence or absence of .429 mM BCAAs. (N = 4-6)

4.6 References

1) Lopaschuk GD, Ussher JR, Folmes CD, Jaswal JS, Stanley WC. *Myocardial fatty acid metabolism in health and disease*. Physiol Rev 2010;90:207–258
2) Newgard, C.B., et al., *A branched-chain amino acid-related metabolic signature that differentiates obese and lean humans and contributes to insulin resistance.* Cell Metab, 2009. 9(4): p. 311-26.
3) Shah, S.H., et al., *Branched-chain amino acid levels are associated with improvement in insulin resistance with weight loss.* Diabetologia, 2012. 55(2): p. 321-30.
4) Shah, S.H., et al., *Association of a peripheral blood metabolic profile with coronary artery disease and risk of subsequent cardiovascular events.* Circ Cardiovasc Genet, 2010. 3(2): p. 207-14.
5) Tai, E.S., et al., *Insulin resistance is associated with a metabolic profile of altered protein metabolism in Chinese and Asian-Indian men.* Diabetologia, 2010. 53(4): p. 757-67.
6) Huffman, K.M., et al., *Relationships between circulating metabolic intermediates and insulin action in overweight to obese, inactive men and women.* Diabetes Care, 2009. 32(9): p. 1678-83
7) Laferrère B, Reilly D, Arias S, Swerdlow N, Gorroochurn P, Bawa B, Bose M, Teixeira J, Stevens RD, Wenner BR, Bain JR, Muehlbauer MJ, Haqq A, Lien L, Shah SH, Svetkey LP, Newgard CB. *Differential metabolic impact of gastric bypass surgery versus dietary intervention in obese diabetic subjects despite identical weight loss*. Sci Transl Med. 2011 Apr 27;3(80):80re2.
8) Wang, T.J., et al., *Metabolite profiles and the risk of developing diabetes.* Nat Med, 2011. 17(4): p. 448-53.
9) Harper, A.E., R.H. Miller, and K.P. Block, *Branched-chain amino acid metabolism.* Annu Rev Nutr, 1984. 4: p. 409-54.

10) Lu, G., Sun H, She P, Youn JY, Warburton S, Ping P, Vondriska TM, Cai H, Lynch CJ, Wang Y. l., *Protein phosphatase 2Cm is a critical regulator of branched-chain amino acid catabolism in mice and cultured cells.* J Clin Invest, 2009. 119(6): p. 1678-87.

11) Li, T., et al., *Defective Branched-Chain Amino Acid Catabolism Disrupts Glucose Metabolism and Sensitizes the Heart to Ischemia-Reperfusion Injury.* Cell Metab, 2017. 25(2): p. 374-385.

12) Des Rosiers, Labarthe F, Lloyd S, Chatham C, *Cardiac anaplerosis in health and disease: food for thought*, Cardiovascular Research (2011) 90, 210–219

13) Beadle RM, Frenneaux M. *Modification of myocardial substrate utilisation: a new therapeutic paradigm in cardiovascular disease*. Heart. 2010;96:824–830.

14) Lehninger D, Cox M. *Lehninger Principles of Biochemistry, 5th Edition*

15) Ruiz M, Gelinast R, Vaillant F, Lauzier B, Des Rosiers C. *Metabolic tracing using stable isotope-labeled substrates and mass spectrometry in the perfused mouse heart*. Methods in Enzymology, 2015, Volume 561

16) Des Rosairs C, Lloyd S, Comte B, Chatham J. *A critical perspective of the use of 13C-isotopomer analysis of GCMS and NMR as applied to cardiac metabolism*, Metabolic Engineering, 2004, 44-58

17) Zamboni N, Fendt SM, Rühl M, Sauer U. *(13)C-based metabolic flux analysis*. Nat Protoc. 2009;4(6):878-92.

18) Kolwicz Jr., S. C., Tian, R. *Assessment of Cardiac Function and Energetics in Isolated Mouse Hearts Using ^{31}P NMR Spectroscopy*. *J. Vis. Exp.* (42), e2069, doi:10.3791/2069 (2010).

19) Su Y, Lam TK, He W, et al. *Hypothalamic leucine metabolism regulates liver glucose production*. *Diabetes*. 2011;61(1):85–93. doi:10.2337/db11-0857

20) Stanley WC, Recchia FA, Lopaschuk GD. *Myocardial substrate metabolism in the normal and failing heart*. Physiol Rev. 2005 Jul;85(3):1093-129.

21) Glynn, E.L., et al., *Impact of combined resistance and aerobic exercise training on branched-chain amino acid turnover, glycine metabolism and insulin sensitivity in overweight humans.* Diabetologia, 2015. 58(10): p. 2324-35.

Chapter 4

Simultaneous Analysis of Major Coenzymes of Cellular Redox Reactions and Energy Using *Ex vivo* ^{1}H NMR Spectroscopy

4.1 Abstract

Coenzymes of cellular redox reactions and cellular energy mediate biochemical reactions fundamental to the functioning of all living cells. Despite their immense interest, no easy method exists to gain insights into their cellular concentrations in a single step. We show that a simple ^{1}H NMR experiment can simultaneously measure oxidized and reduced forms of nicotinamide adenine dinucleotide (NAD^+ and NADH), oxidized and reduced forms of nicotinamide adenine dinucleotide phosphate ($NADP^+$ and NADPH), adenosine triphosphate (ATP) and its precursors, adenosine diphosphate (ADP) and adenosine monophosphate (AMP), using mouse heart, kidney, brain, liver and skeletal muscle tissue extracts as examples. Combining 1D/2D NMR experiments, chemical shift libraries, and authentic compound data, reliable peak identities for these coenzymes have been established. To assess this methodology, cardiac NADH and NAD^+ ratios/pool sizes were measured using mouse models with a cardiac specific knockout of the mitochondrial Complex I *Ndufs4* gene (cKO) and cardiac-specific overexpression of nicotinamide phosphoribosyltransferase (cNAMPT) as examples. Sensitivity of NAD^+ and NADH to cKO or cNAMPT was observed, as anticipated. Time dependent investigations showed that the levels of NADH and NADPH diminish by up to ~50% within 24 h; concomitantly, NAD^+ and $NADP^+$ increase proportionately; however, degassing the sample and flushing the sample tubes with helium gas halted such changes. The analysis protocol along with the annotated characteristic fingerprints for each coenzyme is provided for easy identification and absolute quantification using a single internal reference for routine use. The ability to visualize the ubiquitous coenzymes fundamental to cellular functions, simultaneously and reliably, offers a new avenue to interrogate the mechanistic details of cellular function in health and disease.

4.2 Introduction

Important coenzymes NAD^+ (nicotinamide adenine dinucleotide, oxidized), NADH (nicotinamide adenine dinucleotide, reduced), $NADP^+$ (nicotinamide adenine dinucleotide phosphate, oxidized) and NADPH (nicotinamide adenine dinucleotide phosphate, reduced) mediate biochemical reactions fundamental to cellular functions in health and disease. These coenzymes undergo reversible oxidation and reduction in numerous electron-transfer reactions, while the concentration ratios of the reduced and oxidized forms reflect important cellular functions including the overall redox status and regulation of ion channels, cell signaling, cell survival and death.[1-4] This balance is also an important indicator of normal and pathological conditions including heart disease, diabetes and cancer. Investigations into the metabolism and function of these coenzymes are therefore of immense interest for uncovering fundamental cellular properties, including the slowing of aging processes and treatment of diseases.[3,5,6] The coenzyme adenosine triphosphate (ATP) is considered to be the energy currency of living cells as it fuels a large number of energy dependent biochemical processes. Adenosine diphosphate (ADP) and adenosine monophosphate (ADP) are closely associated with ATP as its precursors/products; hence the levels of ATP, ADP and AMP represent a measure of the energetics of the functioning cells and their mitochondria.[7] Reliable and high throughput measurement of the coenzymes of redox reactions and energy, therefore, is important for investigations focused on the mechanistic understanding of normal and impaired cellular functions.[8]

A limited number of analytical methods exist to reliably and simultaneously measure the levels of these coenzymes. Currently, the most often-used methods involve enzymatic assays, which are suboptimal as they necessitate separate protocols for analysis of each coenzyme or their ratios.[9.12] In addition, these assays are often met with challenges due to confounding factors such as interference from other substances in the sample matrix and the finite linear range of the assays. Separately, efforts have been made to simultaneously analyze the coenzymes based on

chromatographic separation and UV-vis absorption[13] or detection using targeted mass spectrometry (MS).[14, 15] While targeted MS typically provides highly sensitive and robust detection, ion suppression and peak interference make reliable quantification of these coenzymes challenging. For example, NAD^+ and $NADP^+$ can overlap with NADH and NADPH, respectively, due to their unit mass differences. In addition, in-source fragmentation of ATP and ADP to AMP poses a major challenge for reliable analysis of these compounds using MS.[15]

Nuclear magnetic resonance (NMR) spectroscopy offers numerous benefits including the ability to reliably identify and simultaneously quantify many compounds in complex biological mixtures with high reproducibility and quantification accuracy.[16-21] To date, owing to NMR's ability to detect and quantify metabolites *in vivo,* the coenzymes, NAD^+, NADH and ATP, along with ADP and AMP have been measured directly or indirectly utilizing *in vivo* ^{31}P NMR.[22-24] More recently, a method to measure NAD^+ in the rat brain has been achieved using *in vivo* ^{1}H NMR.[25] The ability to analyze coenzymes *in vivo* by this approach is attractive as it promises better insights. However, the limited resolution and sensitivity due to many factors such as chemical shift anisotropy, dipolar and quadrupolar interactions, and changes in magnetic susceptibility, deleteriously affect reliable and simultaneous analysis of the coenzymes. In the case of ^{1}H detection *in vivo*, the need to suppress the abundant water signal adds to the challenges.

Ex vivo NMR, on the other hand, alleviates many challenges associated with *in vivo* NMR, and provides highly resolved spectra to enable routine quantification of metabolites down to sub-micromolar concentrations using a single internal reference.[26] To detect the coenzymes, it is necessary to establish their characteristic fingerprints and, in particular, isolated peaks that can be used for quantification on a routine basis. The complexity of biological mixtures combined with the instability of coenzymes, their virtually identical structures and low concentrations has so far prevented their reliable measurement by NMR. In the current study, we have overcome this bottleneck and provide a simple NMR method to quantify the coenzymes simultaneously. The outcome is based on comprehensive investigations of a variety of mouse tissues using both 1D

and 2D NMR spectroscopy methods, the development and use of a NMR chemical shift library and tissue harvesting and extraction method, and spiking with authentic compounds. As a result, the simultaneous and facile quantification of seven major coenzymes along with many other metabolites is demonstrated, using knock-out and transgenic mouse models as examples.

4.2 Materials and Methods

Methanol, chloroform, monosodium phosphate (NaH_2PO_4), disodium phosphate (Na_2HPO_4), sodium salt of 3-(trimethylsilyl)propionic acid-2,2,3,3-d_4 (TSP), potassium hydroxide and perchloric acid were obtained from Sigma-Aldrich (St. Louis, MO). Standard compounds used for chemical shift data and/or spiking experiments were all obtained from Sigma-Aldrich or Fisher (Waltham, MA), except for the coenzymes, NAD^+, NADH, $NADP^+$ and NADPH, which were generously provided by Dr. Jianhai Du, University of Washington (Supplementary Table S1). Deuterium oxide (D_2O) was obtained from Cambridge Isotope laboratories, Inc. (Andover, MA). Deionized (DI) water was purified using an in-house Synergy Ultrapure Water System from Millipore (Billerica, MA). All chemicals were used without further purification.

Solutions of authentic compounds for spiking experiments/chemical shift database

One-mL stock solutions (1 mM) for standard compounds (Supplementary Table S1) were prepared in D_2O by diluting their 50 mM solutions, which were first prepared by weighing each compound and dissolving it in D_2O. A 60 µL solution of each compound was mixed with 540 µL phosphate buffer (0.1 M; pH = 7.45) in D_2O containing 50 µM TSP to obtain solutions of 100 µM concentration, which were then transferred to 5 mm NMR tubes.

Mouse tissue separation and extraction

The investigations using mouse tissue were performed with the approval of the Institutional Animal Care and Use Committee of the University of Washington. After each mouse was anesthetized, heart, kidney, brain, liver and skeletal muscle tissues were separated, rinsed in cold phosphate-buffered saline (PBS), and snap frozen in liquid nitrogen (Supplementary Table S2). Different tissue harvesting and extraction methods were tested for the mouse heart tissue to determine the optimal method for the targeted coenzymes. The tissue harvesting procedures employed included: freeze clamping after 20 min of Langendorff isolated heart perfusion,[27] and freeze clamping separated hearts after washing with a solution in which glucose (10 mM) and pyruvate (0.5 mM) were present or in cold PBS.

The extraction procedures included the use of a mixture of methanol and water, perchloric acid (0.6 N) or methanol and chloroform. For methanol and water extraction, weighed tissue specimens were mixed with 200 µL cold water and methanol (1:5 v/v; 4 °C) in 2 mL Eppendorf vials and homogenized using a Tissue-Tearor (BioSpec) handheld homogenizer. A further 800 µL cold water/methanol solution (1:5 v/v) was added, each mixture was then vortexed and incubated on dry ice (-75 °C) for 30 min. Subsequently, the mixtures were sonicated in an ice bath for 10 min and centrifuged for 5 min at 2039 rcf and low temperature (4 °C). The soluble extracts were separated, frozen using dry ice, and then lyophilized to dryness.

For perchloric acid extraction, weighed tissue specimens were mixed with 400 µL cold 0.6 N perchloric acid (4 °C) in 2 mL Eppendorf vials and homogenized using a Tissue-Tearor homogenizer. Cold distilled water (400 µL) was added, each mixture was then vortexed and incubated on dry ice (-75 °C) for 30 min. Subsequently, the mixtures were sonicated in an ice bath for 10 min and centrifuged for 5 min at 2039 rcf and low temperature (4 °C). The soluble extracts were separated, neutralized using potassium hydroxide and the insoluble residue was pelleted by centrifugation for 5 min at 2039 rcf (4 °C). The soluble extracts were frozen using dry ice and lyophilized to dryness.

For methanol and chloroform extractions, weighed tissue specimens (~5 to 80 mg) were mixed with a 1 mL mixture of cold methanol and chloroform (1:2 v/v; 4 °C) in 2 mL Eppendorf vials and homogenized using aTissue-Tearor homogenizer and sonicated for 20 s. A further 800 µL cold chloroform/distilled water mixture (1:1 v/v) was added, the sample was then vortexed and set aside for 30 min on ice to separate the solvent layers. Next, after centrifugation at 2039 rcf, the aqueous (top) layer was separated and filtered using 1.5 mL 0.2 µm syringe filters and freeze dried. To test the extraction method using recovery experiments, a small set of heart tissue samples (n=6) were extracted with or without spiking with a standard mixture of the coenzymes. The dried extracts were mixed with 210 µL or 600 µL of a cold phosphate buffer (0.1 M; pH = 7.45; 4 °C) in D_2O containing 25 or 50 µM TSP and the solutions were transferred to sample tubes

for measurements; 3 mm sample tubes were used for 210 µL solutions and 5 mm sample tubes were used for 600 µL solutions.

NMR Spectroscopy

Experiments for a few tissue samples were performed at different temperatures (280, 290, and 298 K) to ensure that stability of the coenzymes was not affected by their analysis at room temperature. Subsequently, all NMR experiments were performed at 298 K. A Bruker Avance III 800 MHz spectrometer equipped with a cryogenically cooled probe and *z*-gradients suitable for inverse detection was used. A few experiments were performed on a Bruker Avance III 700 MHz spectrometer equipped with a room temperature probe and *z*-gradients suitable for inverse detection. The one-pulse or one dimensional NOESY pulse sequence with residual water suppression using presaturation, 10204 Hz (for 800 MHz) or 11160 Hz (for 700 MHz) spectral width, 6.6 s recycle delay, 128 transients and 32 K time domain points were used for ^{1}H 1D NMR experiments. For tissue extracts, NMR experiments were performed immediately after preparing the solutions and a second time 24 h after preparing the solutions to also assess the stability of the redox coenzymes. Separately, NMR experiments were also performed using degassed NMR solvent (D_2O buffer) and sample tubes flushed with helium gas to test whether oxidation of NADH/NADPH to NAD^+/$NADP^+$ could be prevented. After degassing, the sample tubes were sealed using parafilm and experiments were performed immediately after preparing the solutions and a second time 24 h after preparing the solutions. To aid identification, homonuclear two-dimensional (2D) experiments, such as ^{1}H-^{1}H double quantum filtered correlation spectroscopy (DQF-COSY) and ^{1}H-^{1}H total correlation spectroscopy (TOCSY) experiments, were performed at 800 MHz for all types of tissue specimens, in addition to the 1D NMR experiments. The 2D experiments were performed with suppression of the residual water signal by presaturation during the relaxation delay. A sweep width of 9600 Hz was used in both dimensions; 512 or 400 FIDs were obtained with t_1 increments for DQF-COSY or TOCSY, respectively, each with 2048 complex data points. The number of transients used was 8 or 16 for DQF-COSY and 8, 16 or 24 for

TOCSY. The relaxation delay was 2.0, 2.2 or 2.5 s for DQF-COSY and 1.0, 1.3 or 1.5 s for TOCSY. The resulting 2D data were zero-filled to 1024 points in the t_1 dimension. A 90^o shifted squared sine-bell window function was applied to both dimensions before Fourier transformation. To confirm the assigned peaks, spectra were also obtained before and after addition of 10-20 µL stock solutions (1 mM) of authentic coenzymes to the tissue extract solutions. Chemical shifts were referenced to the internal TSP signal for both the ^{1}H 1D and 2D spectra. Bruker Topspin versions 3.0 or 3.1 software packages were used for NMR data acquisition, processing, and analyses.

Peak assignments, coenzyme identification and quantification

Initial peak assignments relied on database searches[28-30] including the human metabolome database (HMDB)[28] and the biological magnetic resonance data bank (BMRB).[29] However unambiguous identification of the coenzymes necessitated the development of a new chemical shift database consisting of the coenzymes and other compounds in solutions at concentrations similar to their levels in tissue (Table 1). Spectral peaks for all the coenzymes were identified using this database along with peak multiplicity, *J* coupling measurements, and the comprehensive analyses of 2D DQF-COSY and TOCSY spectra. The coenzymes thus identified were further confirmed by spiking experiments using authentic compounds. The Chenomx NMR Suite Professional Software package (version 5.1; Chenomx Inc., Edmonton, Alberta, Canada) was used to quantify the coenzyme peaks. Chenomx allows fitting spectral lines using the standard metabolite library for 800 MHz ^{1}H NMR spectra, and in particular the determination of concentrations. Since the proximity of chemical shift values for signals from multiple compounds resulted in the software providing multiple library hits for the same peak, the correct identification of coenzymes' peaks relied on the newly established peak assignments. Peak fitting with reference to the internal TSP signal enabled the determination of absolute concentrations of the coenzymes.

4.3 Results and Discussion

The ^{1}H NMR spectra from mouse tissues are complex, with a large number of highly resolved peaks (Figure 1(a)), and the spectrum for each tissue type, namely liver, heart, kidney, brain, and skeletal muscle, is distinct (Supplementary Figure S1). Specifically, the region from ~0.5 to 6.3 ppm is more complex due to contributions from many small molecule metabolites when compared to the relatively sparse region from ~6.5 to 9.5 ppm. Based on their structures and the available chemical shift databases of authentic compounds,[28-30] the coenzymes were anticipated to have peaks in both regions of the spectra (Table 1). Using the chemical shift database that we have newly developed and comprehensive analyses of 1D and 2D NMR data, unambiguous identification of the coenzymes, NAD^{+}, NADH, $NADP^{+}$, NADPH and ATP, along with ADP and AMP, in all the types of tissue samples were made. NMR peaks from the coenzymes that appear below 6.3 ppm were largely overlapped with each other and with peaks from other compounds. The region between 6.5 to 9.5 ppm, on the other hand, was dominated by peaks from the coenzymes and each coenzyme showed one or more well resolved peaks (Figure 1(b) and Supplementary Figure S2; Table S1). Of particular interest is the narrow spectral region between 8.4 to 8.64 ppm; it showed a characteristic, well-resolved peak for each coenzyme for all the types of tissue studied (Figures 1(c) and 2). Each of these characteristic signals arises from the same lone proton of the five membered ring of the adenine moiety (Figure 1(d); Supplementary Figure S3).

Considering the challenges associated with the analysis of the coenzymes using current methods, the benefits offered by NMR spectroscopy as an alternative and simple approach are striking. A major limiting factor for NMR to date, however, has been the inability to obtain reproducible NMR spectra due the unstable nature of many coenzymes and challenges related to sample preparation (Figure 3), as well as a lack of knowledge regarding their unambiguous identification. The high spectral complexity of the coenzymes, their similarity in structure, the sensitivity of chemical shifts to parameters such as concentration, pH and ionic strength, and the

low concentration, specifically, for some of the coenzymes have made their unambiguous identification in NMR spectra difficult. For example, due to the structural similarity, NMR peaks for some of the coenzymes are virtually indistinguishable. In particular, the separation between the characteristic C_8-proton peaks for NADH and NADPH is only 0.004 ppm (3.2 Hz) due to their virtually identical structures (Supplementary Figure S3). ATP and ADP also exhibit similar peak characteristics (Figure 1(c); Table 1). The sensitivity of the chemical shift to numerous parameters such as concentration, pH, ionic strength and temperature can cause the closely spaced peaks for several coenzymes to interchange their peak positions in the chemical shift databases of authentic compounds.[28, 29] To circumvent this problem, we developed a unique NMR chemical shift library for the coenzymes by maintaining their concentrations similar to their physiological levels in the tissue extracts, and using solvent, pH and temperature conditions identical to those used for the tissue samples (Table 1). Combining this coenzyme chemical shift database with peak multiplicity and J-couplings, as well as comprehensive analysis using a series of 1D and 2D DQF-COSY and TOCSY spectra, characteristic peaks for the coenzymes were unambiguously identified. Finally, the identified coenzymes were further confirmed by spiking using authentic compounds.

For absolute quantification using NMR, the establishment of the identity of at least one isolated peak for each coenzyme is critical, and the 8.4 to 8.64 ppm region fulfills this requirement (Figure 1(c)). Fortuitously, within this fingerprint, none of the tissue types exhibited any interference from other compounds. Furthermore, and importantly, the peaks for the coenzymes in the fingerprint region are all singlets, as they all arise from the lone hydrogen atom on the five membered ring of the adenine moiety, which is very useful because it provides the best resolution and sensitivity compared to peak multiplets. This is particularly critical for identifying the coenzymes that are very closely spaced and exhibit concentrations of a few ng/mg tissue. Another useful characteristic of the fingerprint region shown in Figures 1(c) and 2 is that ratios between various coenzymes can be visualized directly and simultaneously from their peak heights without

resorting to any calculations, owing to the fact that each coenzyme's peak is represented by a single hydrogen atom (Supplementary Figure S3).

In general, numerous peaks observed for each coenzyme in different regions of the same spectra (Table 1; Supplementary Figures S2 and S4) serve to verify their identities, unambiguously, and determine their concentrations, reliably. In particular, it may be noted that ambiguity may arise for distinguishing between ATP and ADP when their peaks overlap or the ATP peak drifts to low frequency towards the ADP peak as for the heart and skeletal muscle tissues shown in Figures 2 and 3. Such a situation arises especially when the peak intensity for one of the compounds is overwhelmingly high compared to the other. In such a case, unambiguous identification and reliable quantification of ATP and ADP is achieved in combination with other peaks that appear in different parts of the same spectra that do not overlap with each other. For example, the spectral region that satisfies this condition is between ~4.1 to 4.5 ppm, in which peaks for ATP are well isolated from ADP as illustrated in the Supplementary Figure S4.

It is important to note that the coenzymes such as NADH, NADPH and ATP are extremely labile and they can evade detection wholly or partly depending on the procedure used for tissue harvesting/extraction. Using mouse hearts, we evaluated numerous different tissue harvesting/extraction protocols to assess their effects on the detection of the coenzymes. As seen in Figure 3, widely varying results were obtained for different harvesting/extraction conditions. Quickly washing the harvested tissue with a solution containing glucose and pyruvate and freeze clamping, followed by extraction using a mixture of methanol and chloroform provided the best results in terms of peak areas/concentrations of the detected coenzymes (Figure 3(a)). Notably, the other protocols resulted in a significant or complete loss of NADH and NADPH (Figure 3(b)) or ATP (Figures 3(c) and 3(d)). Subsequent investigations for heart tissue, in this study, utilized the optimized protocol as shown for Figure 3(a). The robustness of the extraction method can be visualized from results of a recovery test made by adding a mixture of standard compounds (Supplementary Table S3). It may be noted that, as shown in Figure 2, kidney, brain and liver

tissue exhibited a significant loss of ATP signals and gain of ADP and AMP signals. These changes are likely to be due to the fact that tissue from kidney, brain and liver were obtained from the same mouse after the heart was separated. Interestingly, however, although the skeletal muscle was obtained last, it did not exhibit such changes (Figure 2).

Based on the now established peak identity for each molecule and an optimal harvesting/extraction protocol for mouse heart tissue (Figure 3(a)), concentrations of the redox coenzymes, NAD^+, NADH, $NADP^+$ and NADPH, were measured using Chenomx software. Simultaneously, concentrations of ATP, ADP and AMP were also measured using the same spectra. Typical concentrations thus obtained for mouse heart tissue are shown in Figure 4. Next we employed mouse models with disturbed NAD(H) redox balance to test the efficacy of this approach. Cardiac-specific *Ndufs4* knockout (cKO) mice present inhibited mitochondrial Complex I activity.[31] We observed an increase in NADH level and NADH/NAD^+ ratio with little change in the NADH/NAD^+ pool in cKO hearts compared to wild-type (WT) (Figure 5). In contrast, the transgenic mice that overexpress nicotinamide phosphoribosyltransferase (cNAMPT) only in hearts[32] exhibited elevated NAD^+ levels and NAD(H) pool size. In addition, cKO mice with cNAMPT expression showed higher NAD^+ levels as well as NAD(H) pool size but lower NADH/NAD^+ ratios than those in cKO mice (Figure 5b). These changes are illustrated in Figure 5a as portions of representative NMR spectra highlighting the NAD^+ and NADH peaks for different genetic variants and the corresponding concentrations shown in Figure 5b. The results from cKO and cNAMPT hearts are consistent with the literature[31, 32] and indicate that the new approach will be a useful tool for investigating numerous diseases.

More generally, this approach is applicable for all tissue types and enables absolute quantification of the seven coenzymes including the NAD(H) and NADP(H) redox couples in a single experiment, which is important to assess the biological significance of their levels in health and disease. In contrast, the established enzymatic assays increase the likelihood of errors due to the requirement of separate sample preparation steps for their individual measurement.

Further, because the NMR approach offers the ability to see each coenzyme peak with naked eye, it offers a new avenue to simultaneously evaluate extraction quality, which is critical considering the sensitivity of many coenzymes to the extraction protocols (Figure 3).

Using the NMR approach, the time and temperature dependences of the coenzymes were evaluated to assess their stability in solution. The results show that apart from small chemical shift changes, the coenzymes did not show any effect of temperature in the range 280-298 K. Hence, 298 K was chosen for investigations in this study. Time dependent analysis, however, showed that the levels of the reduced forms of the coenzymes, NADH and NADPH, decreased with time and the levels of their oxidized forms, NAD^+ and $NADP^+$, increased, proportionately. Over a period of 24 h after preparation of the solutions, roughly 50% or more of the NADH and NADPH levels were reduced (Supplementary Figure S5). Interestingly, however, degassing the NMR solvent and flushing the sample tube with helium gas, followed by sealing the tube with Parafilm prevented this change (Supplementary Figure S6). These results indicate the somewhat unstable nature of NADH and NADPH in solution in the presence of oxygen, and highlight the need to analyze the samples as soon as the solutions are made, or otherwise degas the solvent and the sample tube using an inert gas.

In this study, about 5 to 80 mg tissue was used to develop the NMR method for simultaneous analysis of the coenzymes within a 10 to 15 min analysis time. The phosphorylated redox coenzymes $NADP^+$ and NADPH, which are generally found at much lower concentrations (a few ng/mg tissue) compared to the other coenzymes, benefit from using large amounts of tissue. Based on the results, however, the other coenzymes with larger signals (typically 10-fold, Figure 4) can be quantified using <10 mg tissue (Supplementary Figure S7). Utilizing sensitivity enhancement approaches, such as with additional signal averaging or utilizing micro-coil probes, the detection limit can be reduced further to enable the analysis of smaller biological samples (<5 mg) for absolute concentrations of all the coenzymes.

In conclusion, we demonstrate a simple method for the simultaneous quantification of the major coenzymes of cellular energy and redox reactions: NAD^+, NADH, $NADP^+$, NADPH and ATP along with ADP and AMP using ^1H NMR spectroscopy. Considering that the balance between the redox coenzymes play critical roles in various cellular functions, their involvement in electron shuttling in oxidation reduction reactions[5] and the challenges associated with the established analysis methods, the ability of an NMR method to visualize cellular levels of the coenzymes represents a significant step for mechanistic understanding of cellular metabolism in health and disease. A one step detection of the coenzymes is demonstrated for different types of mouse tissue with the goal of evaluating the utility of the method for a wide range of biological specimens. As an example of the utility of this method, the sensitivity of coenzymes NAD^+ and NADH to different mouse tissue genotypes is demonstrated. Experimental protocols along with the annotated spectral fingerprints of the coenzymes provided here enable their easy identification and simultaneous quantification using a single internal reference. An added advantage of this method is that it not only enables analysis of the coenzymes, but also enables analysis of a large number of other small molecule metabolites, simultaneously, from the same NMR data without the need for additional sample or experiments (Supplementary Figure S8) as we have demonstrated recently for human blood.[26] The time dependent studies indicate the gradual oxidation of NADH and NADPH to NAD^+ and $NADP^+$, respectively, in solution at room temperature, which points to the need to analyze them as soon as the solutions are made. Alternatively, degassing the NMR solution and flushing the NMR tubes using an inert gas such as helium, followed by sealing the tube can provide for reliable quantification. This is the first successful effort providing the absolute quantification of major coenzymes of cellular redox reactions and cellular energy, simultaneously, and this approach is anticipated to find widespread utility for investigations of cellular function.

4.5 Figures

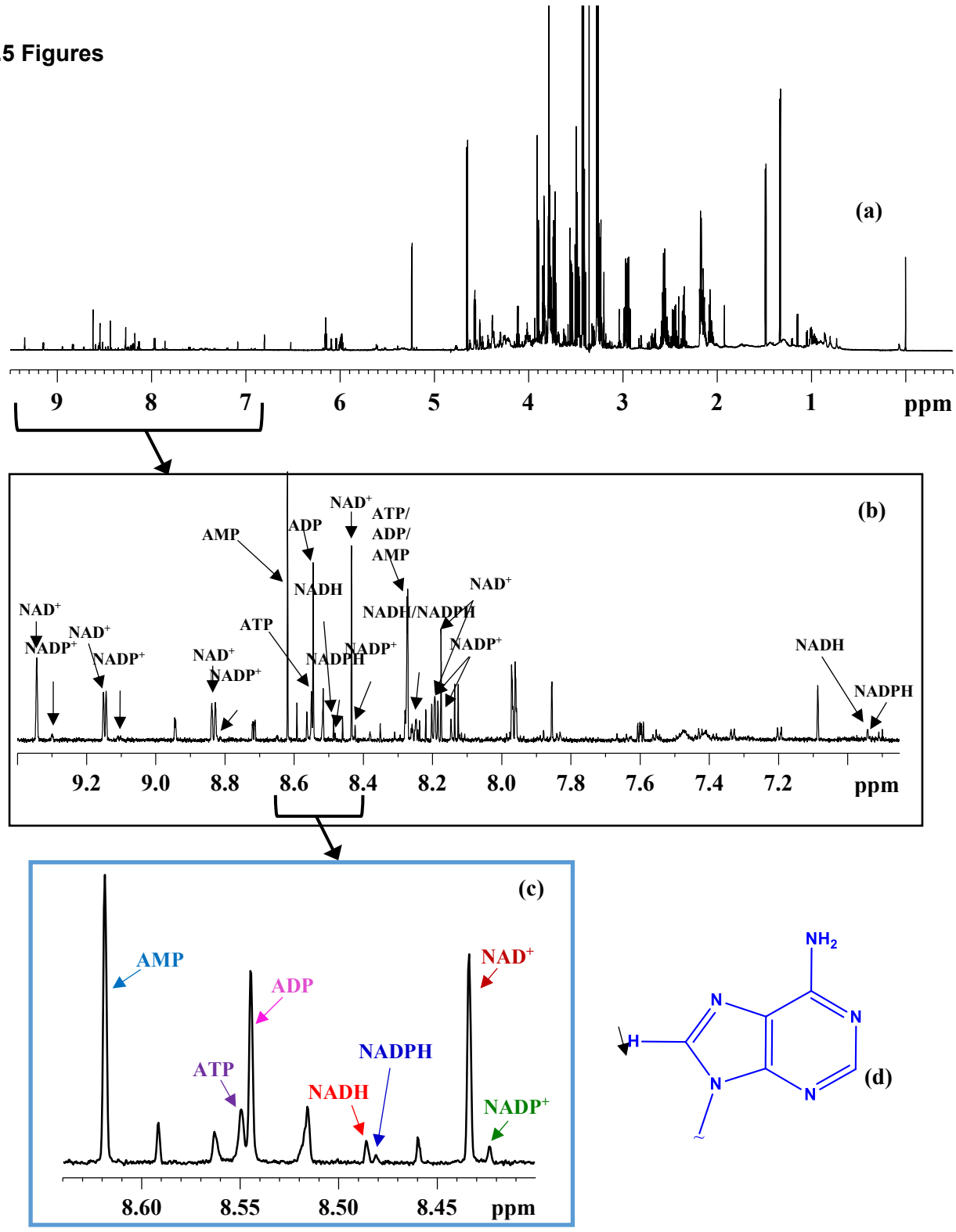

Figure 1. (a) Typical 800 MHz ^{1}H NMR spectrum of a mouse liver tissue obtained using 5 mm sample tube; (b) expanded spectral region with annotations for peaks for oxidized nicotinamide adenine dinucleotide (NAD^+), oxidized nicotinamide adenine dinucleotide phosphate ($NADP^+$), reduced nicotinamide adenine dinucleotide (NADH), reduced nicotinamide adenine dinucleotide phosphate (NADPH), adenosine triphosphate (ATP), adenosine diphosphate (ADP) and adenosine monophosphate (AMP); (c) expanded spectral region showing the characteristic fingerprint of the redox and energy coenzymes; and (d) adenine moiety with the lone hydrogen atom on the five membered ring indicated by an arrow; all peaks in the fingerprint region shown in (c) arise from this hydrogen atom (see also Supplementary Figure S3).

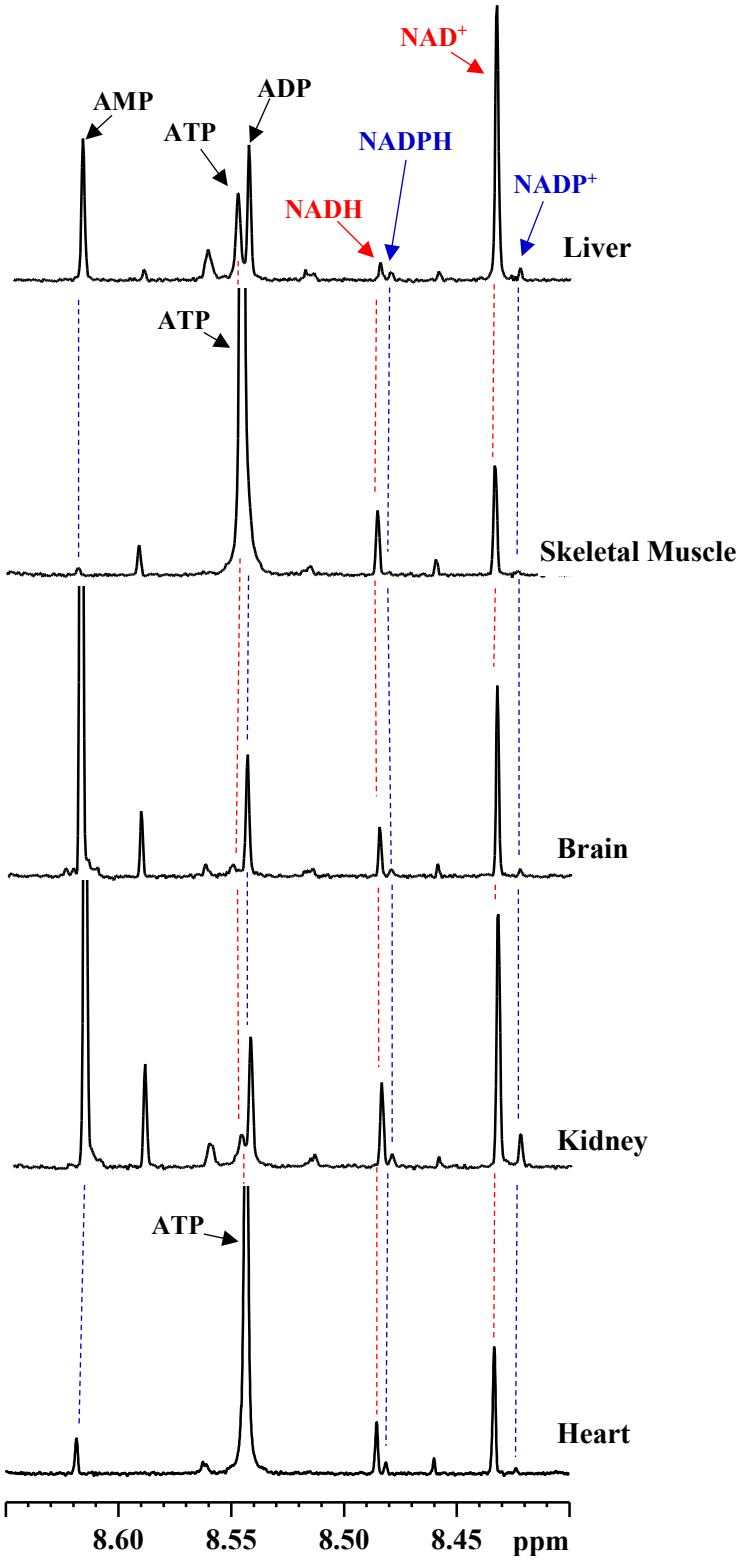

Figure 2. Characteristic annotated fingerprint regions of 800 MHz ^{1}H NMR spectra of a mouse heart, kidney, brain, skeletal muscle and liver tissue extracts for visualization and simultaneous quantification of the coenzymes. 3 mm sample tube was used for the heart tissue and 5 mm sample tubes were used for others.

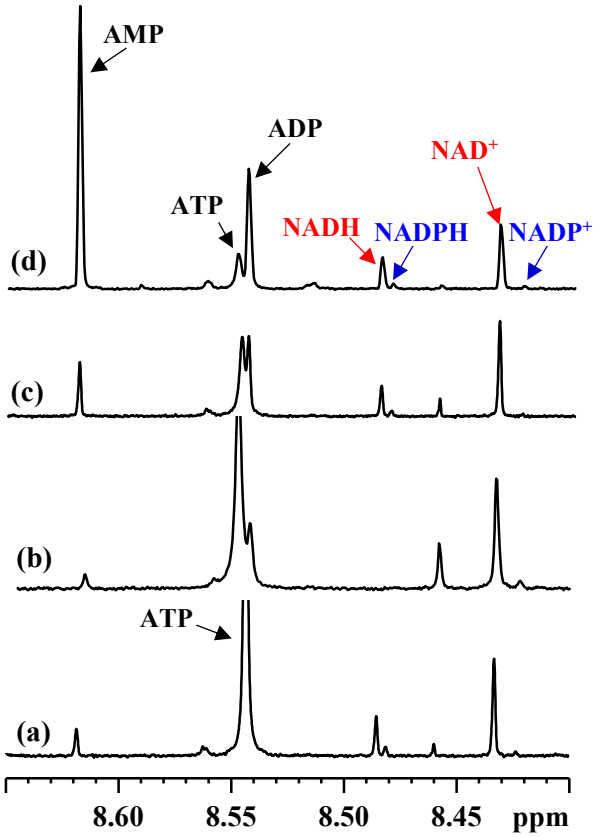

Figure 3. Portions of 800 MHz ^{1}H NMR spectra obtained using 3 mm sample tubes highlighting the sensitivity of coenzyme levels to tissue harvesting/extraction protocols: (a) mouse heart harvested, washed with glucose/pyruvate solution and freeze clamped, followed by extraction using methanol-chloroform mixture; (b) mouse heart harvested, perfused with glucose/pyruvate solution and freeze clamped, followed by extraction using methanol-chloroform mixture; (c) mouse heart freeze clamped *in vivo*, followed by extraction using methanol-chloroform mixture; and (d) mouse heart harvested, washed with PBS and freeze clamped, followed by extraction using methanol-water mixture. Of the prominent changes are the missing NADH/NADPH peaks in (b) and diminished ATP and enhanced ADP/AMP in (b-d).

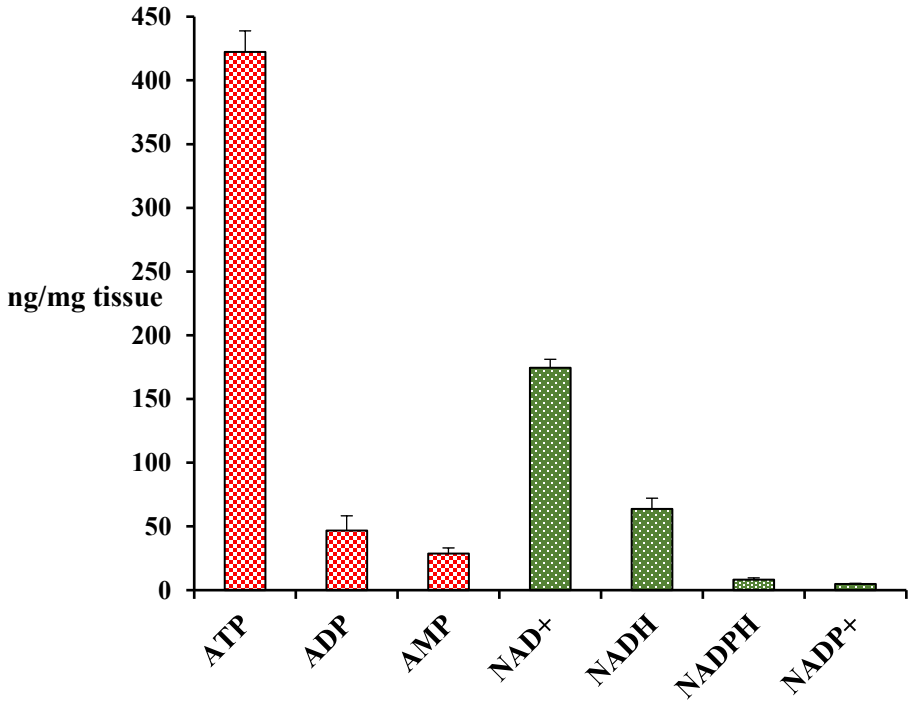

Figure 4. Absolute concentrations for ATP, ADP, AMP, NAD^+, NADH, $NADP^+$ and NADPH in heart tissue of wild type mice (n=6) obtained in a single step using the ^1H NMR spectroscopy method.

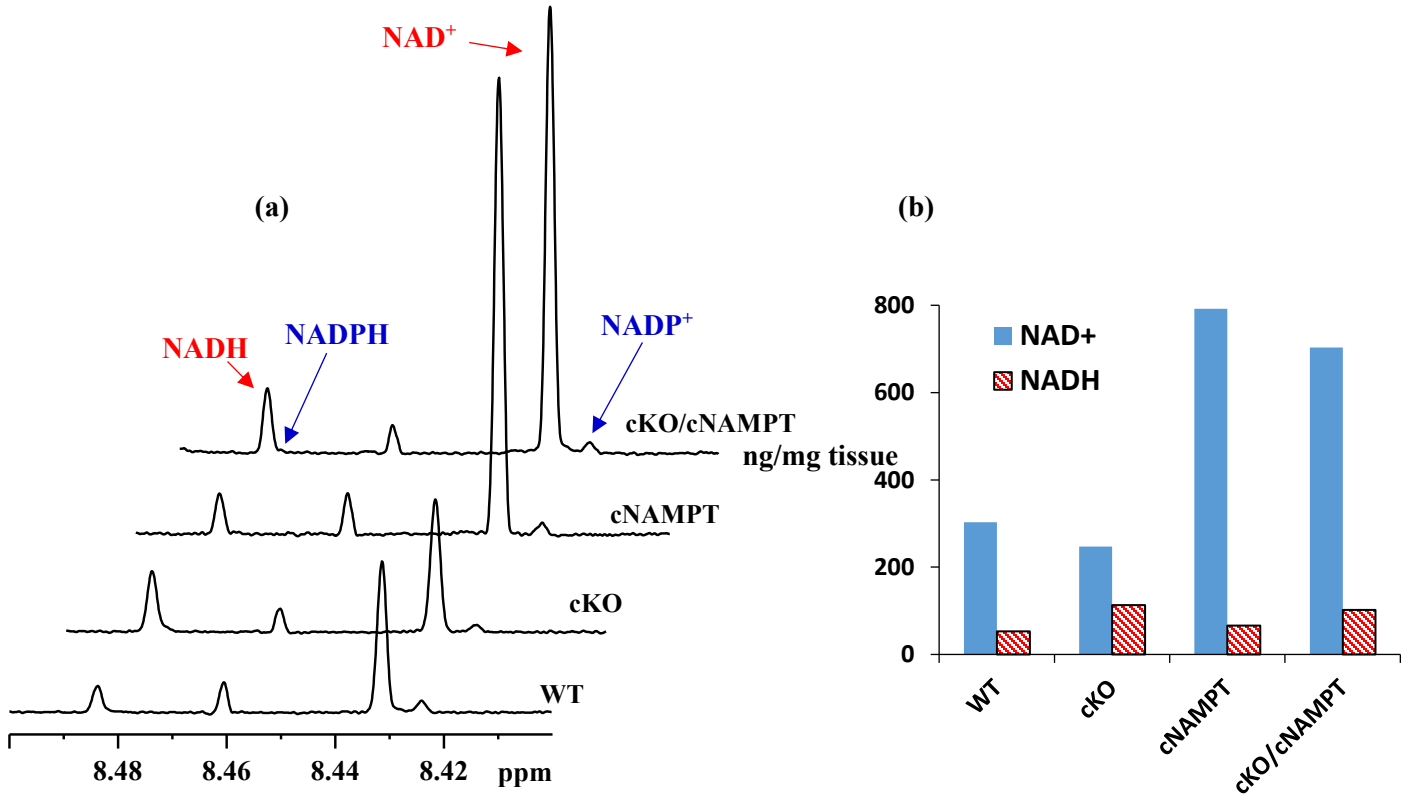

Figure 5. (a) Portions of typical 800 MHz NMR spectra of heart tissue extracts obtained using 3 mm sample tubes highlighting the changing NAD^+ and NADH peaks' intensity in WT, cKO, cNAMPT and cKO/cNAMPT mice and (b) the corresponding concentrations (ng/mg) in the cardiac tissues shown in (a).

Table 1: ^{1}H NMR Chemical Shifts (in ppm) and *J* couplings (in Hz) for the coenzymes/metabolites of redox reaction and cellular energy.

Coenzyme/Metabolite	Mouse heart/kidney/brain/liver/skeletal muscle	Authentic compounds[b]
Nicotinamide adenine dinucleotide, oxidized (NAD^+)	4.371 (m); 4.387 (m); 4.429 (m); 4.487 (t, J= 5.213); 4.515 (m); 4.545 (m); **6.041** (1H, d, J=6.042); **6.093** (1H, d, J=5.482); **8.174** (1H, s); **8.193** (1H, dd); **8.434** (1H, s); **8.832** (1H, d, J=7.992); **9.147** (1H, d, J =6.158); **9.344** (1H, s)	4.191-4.291 (m); 4.369 (m); 4.386 (m); 4.430 (m); 4.488 (t; J=5.196); 4.514 (m); 4.546 (m); 6.042 (d, J=6.089); 6.092 (d, J=5.510); 8.176 (s); 8.193 (dd); 8.435 (s); 8.833 (d; J=8.032); 9.148 (d; J= 6.138); 9.344 (s)
Nicotinamide adenine dinucleotide phosphate, oxidized ($NADP^+$)	6.101 (d); **8.146** (1H, s), **8.424** (1H, s); **9.104** (1H, d); **9.300** (1H, s)	4.181-4.236 (m); 4.284-4.342 (m); 4.377 (m); 4.411 (m); 4.461 (t; J=5.286); 4.503 (m); 4.617 (t, J=4.990); 4.968 (m); 6.037 (d; J=5.560); 6.101 (d, J=4.969); 8.146 (s); 8.168-8.199 (m); 8.423 (s); 8.818 (d, J=8.008); 9.106 (d; J = 6.259); 9.299 (s)
Nicotinamide adenine dinucleotide, reduced (NADH)	6.137 (d); **6.942** (1H, s); **8.247** (1H, s); **8.486** (1H, s)	2.669 (br. d, J=17.976); 2.793 (br. d, J=17.976); 4.082 (br. m); 4.097 (br. m) 4.169-4.289 (br. m); 4.389 (br. m); 4.512 (t, J =4.448); 4.709 (t, J =5.272); 5.980 (d, J=8.424); 6.138 (d, J=5.479); 6.943 (s); 8.248 (s); 8.487 (s)
Nicotinamide adenine dinucleotide phosphate, reduced (NADPH)	6.216 (d); **6.936** (1H, s); **8.481** (1H, s)	2.737 (br. d, J=18.093); 2.838 (br. d, J=18.093); 4.044 (br. m); 4.066 (br. m); 4.154-4.236 (m); 4.285-4.325 (br. m); 4.390 (br. m); 4.597 (t, J=5.049); 4.950 (m); 5.963 (d, J=8.363); 6.216 (d, J=4.597); 6.935 (s); 8.246 (s); 8.481 (s)
Adenine triphosphate (ATP)	4.410 (m); 4.621(m); 6.155 (d); 8.274 (s); **8.549** (1H, s)	4.192-4.233 (m); 4.278-4.318 (m); 4.392-4.421 (br. m); 4.620-4.648 (m); 6.153 (d, J=5.974); 8.274 (s); 8.557 (s)
Adenine diphosphate (ADP)	4.387 (m); 4.621(m); 6.155 (d); 8.273 (s); **8.544** (1H, s)	4.187-4.219 (m); 4.244-4.283 (m); 4.377-4.398 (br. m); 4.611-4.634 (m); 6.156 (d, J=5.383); 8.273 (s); 8.547 (s)
Adenine monophosphate (AMP)	4.014 (m); 4.372 (m); 4.515 (m); 6.147 (d); 8.271 9(s)**; 8.619** (1H, s)	3.995-4.026 (m); 4.359-4.383 (br. m); 4.501-4.526 (m); 6.148 (d, J=5.965); 8.272 (s); 8.620 (s)

[a]Chemical shifts for characteristic peaks of metabolites that provide unambiguous information for identification and quantification using 1D ^{1}H NMR are shown in bold. Chemical shifts for authentic compounds are also shown separately for comparison. [b]Spectra for the authentic compounds were obtained near their physiological concentrations (100 □M) in D_2O buffer at pH 7.45 at 298 K. Abbreviations: br. broad; s, singlet; d, doublet; dd, doublet of doublets; t, triplet; m, multiplet.

4.5 References

1) Kilfoil, P. J.; Tipparaju, S. M.; Barski, O. A.; Bhatnagar, A. Circ. Res. 2013, 112 (4), 721−41.
2) Koch-Nolte, F.; Haag, F.; Guse, A. H.; Lund, F.; Ziegler, M. Sci. Signaling 2009, 2 (57), mr1.
3) Ying, W. Antioxid. Redox Signaling 2008, 10 (2), 179−206.
4) Engel, P. C. Neurochem. Res. 2014, 39 (3), 426−32.
5) Nakamura, M.; Bhatnagar, A.; Sadoshima, J. Circ. Res. 2012, 111 (5), 604−10.
6) Oka, S.; Hsu, C. P.; Sadoshima, J. Circ. Res. 2012, 111 (5), 611− 27.
7) Nelson, D. L.; Cox, M. M. Lehninger Principles of Biochemistry, 6th ed.; Freeman & Company, W. H.: New York, 2012.
8) Bar-Or, D.; Bar-Or, R.; Rael, L. T.; Brody, E. N. Redox Biol. 2015, 4, 340−345.
9) Du, J.; Cleghorn, W.; Contreras, L.; Linton, J. D.; Chan, G. C.; Chertov, A. O.; Saheki, T.; Govindaraju, V.; Sadilek, M.; Satrústegui, J.; Hurley, J. B. Proc. Natl. Acad. Sci. U. S. A. 2013, 110 (46), 18501− 18506.
10) Santidrian, A. F.; Matsuno-Yagi, A.; Ritland, M.; Seo, B. B.; LeBoeuf, S. E.; Gay, L. J.; Yagi, T.; Felding-Habermann, B. J. Clin. Invest. 2013, 123 (3), 1068−1081.
11) Anderson, R. M.; Bitterman, K. J.; Wood, J. G.; Medvedik, O.; Cohen, H.; Lin, S. S.; Manchester, J. K.; Gordon, J. I.; Sinclair, D. A. J. Biol. Chem. 2002, 277, 18881−18890.
12) Smith, J. S.; Brachmann, C. B.; Celic, I.; Kenna, M. A.; Muhammad, S.; Starai, V. J.; Avalos, J. L.; Escalante-Semerena, J. C.; Grubmeyer, C.; Wolberger, C.; Boeke, J. D. Proc. Natl. Acad. Sci. U. S. A. 2000, 97, 6658−6663.
13) Sporty, J. L.; Kabir, M. M.; Turteltaub, K. W.; Ognibene, T.; Lin, S. J.; Bench, G. J. Sep. Sci. 2008, 31 (18), 3202−3211.

14) Evans, C.; Bogan, K. L.; Song, P.; Burant, C. F.; Kennedy, R. T.; Brenner, C. BMC Chem. Biol. 2010, 10, 2.

15) Trammell, S. A. J.; Brennera, C. Comput. Struct. Biotechnol. J. 2013, 4, No. e201301012.

16) Nagana Gowda, G. A.; Zhang, S.; Gu, H.; Asiago, V.; Shanaiah, N.; Raftery, D. Expert Rev. Mol. Diagn. 2008, 8 (5), 617−633.

17) Larive, C. K.; Barding, G. A., Jr; Dinges, M. M. Anal. Chem. 2015, 87 (1), 133−46.

18) Halouska, S.; Fenton, R. J.; Barletta, R. G.; Powers, R. ACS Chem. Biol. 2012, 7 (1), 166−171.

19) Clendinen, C. S.; Lee-McMullen, B.; Williams, C. M.; Stupp, G. S.; Vandenborne, K.; Hahn, D. A.; Walter, G. A.; Edison, A. S. Anal. Chem. 2014, 86 (18), 9242−9250.

20) Ellinger, J. J.; Chylla, R. A.; Ulrich, E. L.; Markley, J. L. Curr. Metabolomics 2012, 1 (1), 28−40.

21) Nagana Gowda, G. A.; Raftery, D. J. Magn. Reson. 2015, 260, 144−60.

22) Zhu, X. H.; Lu, M.; Lee, B. Y.; Ugurbil, K.; Chen, W. Proc. Natl. Acad. Sci. U. S. A. 2015, 112 (9), 2876−2881.

23) Ingwall, J. S. ATP and the Heart; Kluwer Academic Publishers: Norwell, MA, 2002.

24) Bottomley, P. A. NMR Spectroscopy of the Human Heart. In Encyclopedia of Magnetic Resonance; Harris, R. K., Wasylishen, R. E., Eds.; John Wiley: Chichester, U.K., 2009.

25) de Graaf, R. A.; Behar, K. L. NMR Biomed. 2014, 27, 802−809.

26) Nagana Gowda, G. A.; Gowda, Y. N.; Raftery, D. Anal. Chem. 2015, 87 (1), 706−715.

27) Kolwicz, S. C., Jr.; Tian, R. J. Visualized Exp. 2010, 42, 2069.

28) Wishart, D. S.; Jewison, T.; Guo, A. C.; Wilson, M.; Knox, C.; Liu, Y.; Djoumbou, Y.; Mandal, R.; Aziat, F.; Dong, E.; Bouatra, S.; Sinelnikov, I.; Arndt, D.; Xia, J.; Liu, P.; Yallou, F.; Bjorndahl, T.; Perez-Pineiro, R.; Eisner, R.; Allen, F.; Neveu, V.; Greiner, R.; Scalbert, A. Nucleic Acids Res. 2013, 41, D801−D807.

29) Ulrich, E. L.; Akutsu, H.; Doreleijers, J. F.; Harano, Y.; Ioannidis, Y. E.; Lin, J.; Livny, M.; Mading, S.; Maziuk, D.; Miller, Z.; Nakatani, E.; Schulte, C. F.; Tolmie, D. E.; Kent Wenger, R.; Yao, H.; Markley, J. L. Nucleic Acids Res. 2007, 36, D402−D408.

30) Agar, N. S.; Rae, C. D.; Chapman, B. E.; Kuchel, P. W. Comp Biochem Physiol B 1991, 99 (3), 575−597.

31) Karamanlidis, G.; Lee, C. F.; Garcia-Menendez, L.; Kolwicz, S. C., Jr; Suthammarak, W.; Gong, G.; Sedensky, M. M.; Morgan, P. G.; Wang, W.; Tian, R. Cell Metab. 2013, 18 (2), 239−50.

32) Hsu, C. P.; Oka, S.; Shao, D.; Hariharan, N.; Sadoshima, J. Circ. Res. 2009, 105 (5), 481−91.

CV and Publications

Lauren Emily Abell

3906 1st Ave NE Apt A, Seattle, WA, 98105
(310) 941-4681
leabell@uw.edu

RESEARCH EXPERIENCE

University of Washington, Seattle, WA
Graduate Researcher, Department of Pathology
9/2013-Present

- Designed and executed novel biochemical experiments to test the link between defective branched chain amino acid catabolism and glucose homeostasis in the mouse.
- Built and executed methods on GCMS and LCMS in collaborations with the Northwest Metabolomics Core and UW Mass Spectrometry Center.
- Performed statistical analysis on data sets using Excel, R Statistics, and Prism GraphPad.

Research Adviser: Rong Tian

National Institutes of Health, Bethesda, MD
Post-baccalaureate Intramural Research Training Award (IRTA) Fellow
9/2011-7/2013

- Designed and investigated photoactive crosslinkers to elucidate transcriptional activation mechanism and regulation in bacteriophage T4 middle promoters.
- Investigated the mechanisms of transcription initiation in *Bordatella pertussis* virulence gene promoters.

Research Adviser: Dr. Deborah Hinton

Institute for Collaborative Biotechnologies, UCSB, Santa Barbara, CA
Center for Energy Efficient Materials Undergraduate Research Internship
11/2010-6/2011

- Conducted research on the development of more efficient positive thermal coefficient of resistivity (PTCR) composite materials for internal battery safety devices.

Research Adviser: Dr. Daniel Morse

Northrop Grumman Space Technologies (NGST), Manhattan Beach, CA
Organic Chemistry Laboratory Intern
6/2010-9/2010 and 6/2008-9/2008

- Developed a quantitative method of FTIR for unknown sample analysis. Additional responsibilities included a variety of chemical analyses using FTIR, GC-MS, ICP-MS, and IC.

Inorganic Chemistry Laboratory Intern
6/2009-9/2009

- In collaboration with NGST Airborne Laser Program, I constructed and tested an apparatus designed for measuring the decomposition rate of chemical components within an airborne chemical laser device.

Destructive Analysis Laboratory Intern
6/2007−9/2007

- Conducted an internal research project on the bond strength of several composite materials. Prepared and tested newly imported and shelf-worn materials for viability.

LEADERSHIP EXPERIENCE

South Lake Union Group, UW
Co-Chair
2014-2016

- Led organization of annual UW-SLU research symposium and poster session, quarterly career workshops, monthly trainee research seminars, and quarterly social events.
- Organized and lead volunteer workshops at the Pacific Science Center.

Undergraduate Research Mentor¸ UW
2017-2018

- Provided mentorship and training in proper scientific technique, animal handling, genotyping, and biochemical assays.

Expanding Your Horizons, Seattle, WA
Committee Member
2014-2017

- Assisted in the organization of a conference aimed at connecting middle-school aged girls with women in STEM fields.
- Recruited and organized presenters with leadership roles in academia, biotech and medicine for workshops.

NIH Postbaccalaureate a cappella group, *Nerds In Harmony*
Director
2011-2013

- Composed music, lead rehearsals, organized recitals and events.

EDUCATION

University of Washington
Seattle, WA
PhD Candidate in UW Medicine Department of Pathology, GPA: 3.6
Expected June 2019
University of California, Santa Barbara (UCSB)
Santa Barbara, CA
College of Creative Studies
Class of 2011
Bachelor of Science degree in Chemistry/Biochemistry, GPA: 3.61

PUBLICATIONS

Abell L, Kolwicz SC, Shao D, Raftery D, Tian R. *In preparation*. Defective branched chain amino acid catabolism impairs exercise capacity in mice.
Miklas J, Hofsteen P, Robitaille A, Levy S, **Abell L**, et al. *In preparation*. Amino acid priming of mTOR is essential for heart regeneration.
Lee CF, Caudal A, **Abell L**, et al. *Submitted* Targeting NAD+ Metabolism as Interventions for Mitochondrial Disease, *Scientific Reports*
Gowda, N; **Abell L**; Rong T. (2018) Extending the Scope of 1H NMR Spectroscopy for the Analysis of Cellular Coenzyme A and Acetyl Coenzyme A. *Analytical Chemistry*
Li T, Zhang Z, Kolwicz SC, **Abell L**, et al. (2017) Defective Branched-Chain Amino Acid Catabolism Disrupts Glucose Metabolism and Sensitizes the Heart to Ischemia-Reperfusion Injury. *Cell Metabolism*
Gowda, N, **Abell L**, et al. (2016) Simultaneous analysis of major coenzymes of cellular redox reactions and energy using ex vivo (1) H NMR spectroscopy. *Analytical Chemistry*
James TD, Cardozo T, **Abell L**, et al. (2016) Visualizing the phage T4 activated transcription complex of DNA and E. coli RNA polymerase. *Nucleic Acids Research*

AWARDS and HONORS

- Bioengineering Cardiovascular Training Grant, UW
- Best Presentation, UW Medicine Department of Pathology Retreat, UW
- Phi Lambda Upsilon Award, National Honorary Chemical Society, UCSB
- Undergraduate Research Internship with the Center for Energy Efficient Materials, UCSB